Foundation Technologies for Offshore Deep Water Renewable Energy

Lieselot Vantomme

Thesis to obtain the Master of Science Degree in Civil Engineering

Masters in Civil Engineering

Supervisor: Prof. Peter John Bourne-Webb

Examination Committee:

Chairperson: Prof. Jaime Alberto dos Santos

Supervisor: Prof. Peter John Bourne-Webb

Members of the Committee: Prof. Alexandre da Luz Pinto

June 2015

Acknowledgements

I would like to thank everyone who helped me to achieve this master dissertation.

First of all I would like to thank Dr Peter Bourne-Webb to gave me the possibility to write this master dissertation. He encouraged me to pursue this master disertation, was always available to discuss several parts of this thesis and to help me simulating the models with Abaqus. Furthermore he gave me the opportunity to improve my English.

A special thank to my partents for their guidance, encouragement and understanding, not only the last semester but throughout all my years of studying. They also allowed me to make my master dissertation abroad.

Finally, I would like to thank my colleague Matthias Laga. We were helping each other where we could, especially to learn the program Abaqus.

Lieselot Vantomme,
June 14, 2015

Abstract

Floating platforms for bearing offshore wind turbines are fast becoming required to produce renewable energy from the wind capacity in the Atlantic, Mediterranean and deep North Sea. These platforms can be attached by way of mooring lines and anchors embedded in the seabed. The purpose of this study was to investigate the reaction of the soil on different types of pile anchors. A numerical study of anchor piles was performed by using the finite element software Abaqus. Several two-dimensional and three-dimensional models were simulated with different pile lengths and embedded in soils with different failure criteria. First, an elastic behaviour for the pile and soil was simulated. After, the analysis focused on the reaction of undrained, clayey soil with the failure criterion of Tresca. As well as axial, lateral and combined loads were examined. The effect of the pile length to diameter ratio was analysed in an undrained soil with constant and with varying cohesion.

Keywords

pile anchor; finite elements; geotechnical; Tresca failure criterion

Table of Contents

List of figures

List of tables

List of Acronyms

OWT = Offshore Wind Turbine

EWEA = European Wind Energy Association

TLP = Tension Leg Platform

VLA = Vertically Loaded Anchor

SEPLA = Suction Embedded Plate Anchors

DPA = Deep Penetrating Anchor

hmpe = high modulus polyethylene

MBL = Minimum Breaking Load

ULS = Ultimate Limit State

ALS = Accidental Limit State

SLS = Serviceablity Limit State

FEA = Finite Element Analysis

2D = two-dimensional

3D = three-dimensional

CC = concequence class

List of symbols

λ = wave length

T = wave period

H = wave heigth

A_c = crest heigth

f = friction coefficient between the mooring line and the seabed

l = length of the mooring line lying on the seabed

w = unit length of the mooring line in water

$\Delta\sigma$ = changes in the total pressure

$\Delta\sigma_K$ = changes in the pore pressure

$\Delta\sigma_W$ = changes in the water pressure

$T_{c\text{-}mean}$ = characteristic mean line tension due to pretension of the steel and the environmental loads.

$T_{c\text{-}dyn}$ = characteristic dynamic line tension due to oscillatory low-frequency and wave-frequency effects.

γ_{mean} = load coefficient for mean line tension due to pretension of the steel and the environmental loads

γ_{dyn} = load coefficient for dynamic line tension due to oscillatory low-frequency and wave-frequency effects

T_d = design mooring line tension

R_d = design anchor resistance

R_K = characteristic resistance

γ_m = material coefficient

ζ = soil shear strength

c' = apparent cohesion

σ' = effective stress

φ = effective angle of shearing resistance

$\in_p$ = plastic strain

c_u = undrained shear strength

P_u = ultimate pile capacity in compression

P_{pu} = ultimate pile tip capacity

P_{si} = skin resistance developing simultaneously with ultimate tip resistance P_{pu}

T_u = ultimate pullout capacity

W = weight of pile being pulled

P_{si} = skin resistance developing simultaneously with ultimate tip resistance P_{pu}

q' = γL = vertical stress (at pile point)

N_i = the bearing capacity factors

s_i = the shape factors

d_i = the depth factors

i_i = inclination factors

g_i = ground factors

b_i = base factors

A_p = the area of pile point

P = the perimeter of the pile

ΔL = length of the segment of the shaft passing through a particular layer

f_s = unit skin friction in each layer

α = an adhesion coefficient that depends on the pile type (displacement/replacement) and the undrained shearing resistance

$s_{u,avg}$ = the average undrained shear strength in a particular layer

K_S = a coefficient that defines the horizontal effective stress acting on the pile shaft, and depends on the pile type (displacement/replacement)

σ'_v = the vertical effective stress

δ = the pile-soil interface friction angle

E = the soil modulus of elasticity

V = the Poisson's ratio

$(EI)_f$ = the bending stiffness of the foundation

B = the width of the foundation or the diameter of the pile

f_y = the specified minimum yield stress

S_e = the elastic section modulus

d_1 = the inner diameter of the hollow steel pile

d_2 = the outer diameter of the hollow steel pile

ρ = density

Chapter 1

Offshore wind turbines

In this chapter, general aspects of offshore wind turbine technology will be discussed. First the importance of offshore wind energy today, especially offshore wind turbines in Europe is outlined. Then, the components of the wind turbine are enumerated, some statistics relating to foundation types used for offshore wind turbines are given, the types of loading taken into account for the design of these structures are detailed, and specifics relating to floating wind turbines are discussed.

1.1 Introduction: Offshore Wind Turbines

The use of renewable energy is one of the most crucial issues of our time. This is a consequence of global climate change (pollution, global warming,...). There are a lot of different forms of renewable energy. Figure 1 shows that following hydropower (64%), wind power (20%) was the second most used form of renewable energy at the end of 2013. That is why the wind energy market will be one of the key markets in the renewable energies sector in the future [1].

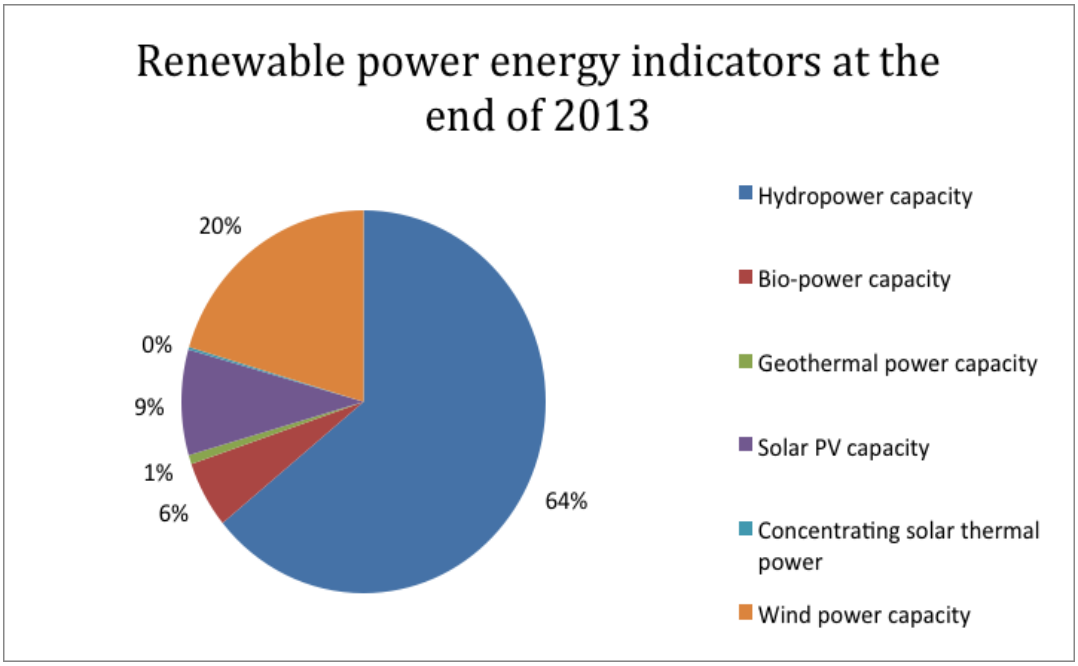

Figure 1 - The distribution of the different kinds of renewable energy at the end of 2013 [1]

The advantage of offshore wind turbines (OWTs) is that offshore wind has a higher wind resource than onshore wind. There is also less turbulence offshore in comparison with onshore, which is better for the wind turbine. Another benefit is that 70% of the earth consists of water, which means a lot of available space for OWTs. Finally, good locations for onshore wind turbines are becoming scarce [3].

Figure 2 shows the expected annual installed capacity of onshore and OWTs and the expected cumulated capacity until 2030 [2]. It is apparent that the rate of growth for onshore developments is in decline while offshore growth is steady.

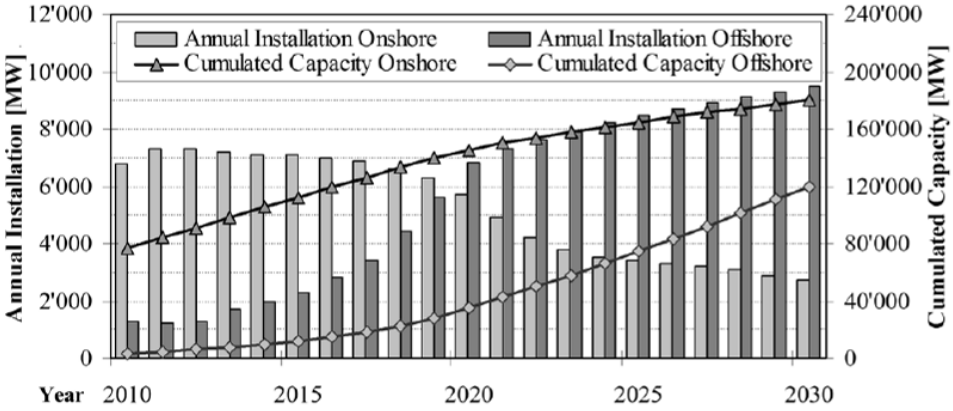

Figure 2 - Expected annual and accumulated capacity of onshore and OWTs from 2010 to 2030 [2]

Following these trends, it can be seen that by around 2020 the annual installation of OWTs will exceed the annual onshore installation. That confirms that the OWTs will become an important issue in the future [2]. This evolution can be confirmed by the data from the European Wind Energy Association (EWEA). During 2014, seventeen new offshore wind farms were built in Europe. There were ten in Germany, five in the UK, one in Belgium, and another one in the Netherlands. Figure 3 shows the water depth and the distance to shore for OWTs built in 2014. The average water depth in 2014 was 22.4 m, an increase of 10% on the average 20 m water depth in 2013. Also, the average distance to shore in 2014 increased by about 10% in comparison with 2013 from 30 km to 32.9 km. This is a trend that will likely continue in the future [4].

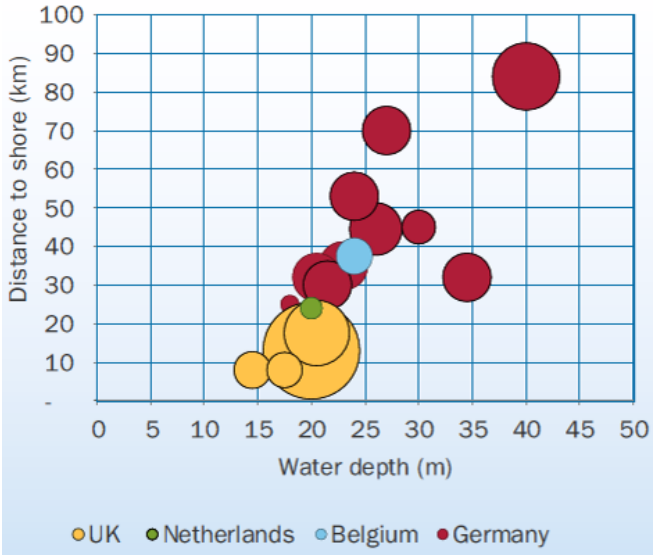

Figure 3 - Water depth (in m) and the distance to shore (in km) of offshore wind farms installed in Europe in 2014 [4]

At the end of 2014, the UK had the most OWTs in Europe. The UK is followed by Denmark, Germany, Belgium, the Netherlands, Sweden, Finland and Ireland, Figure 4 [4].

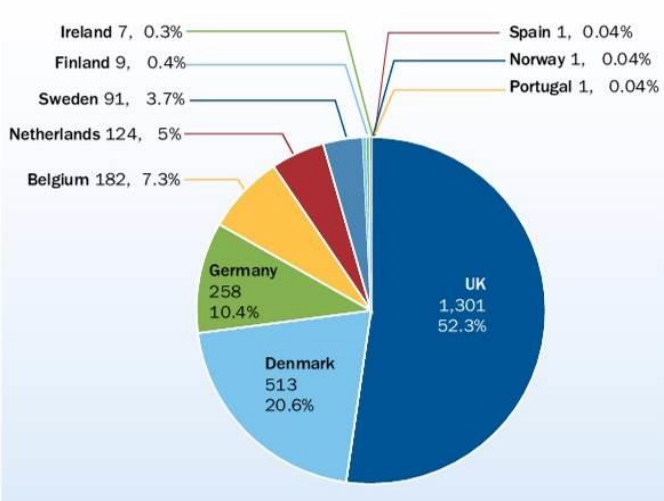

Figure 4 - The distribution of the wind turbines installations among the European countries [4]

Worldwide, the wind energy market is led by Asia because of China who has the most wind turbines in the world. Asia is followed by the EU and North America [4].

1.2 Wind turbine components

A wind turbine converts kinetic energy from wind into electrical power. Although vertical axis wind turbines also exist, today most wind turbines have a horizontal axis due to its greater electricity production. The upper parts of the wind turbine are shown in Figure 5 [5].

The tower (3) is a hollow (or steel lattice) structure usually made of concrete, steel or a combination of both. The tower encloses an access ladder (4) and cables to connect to the electrical grid. The foundation system (not in the figure) and support structure are used to keep the turbine in position while being exposed to external natural conditions.

The nacelle (6) transfers the loads originating from the blades to the tower. It also contains the key components of the wind turbine, including the brake, gearbox, generator and the control system. In case of emergency or for maintenance, the brake (9) is used to block the rotor. The anemometer and wind vane (8) measures the wind direction and wind speed. This information is sent to the control system and the yaw control (5) turns the nacelle in the optimal wind direction. The gearbox (10) converts the rotation speed of the blades to a much higher one that matches the speed of the generator. The electrical generator (7) is the unit that transforms the mechanical energy into electric power.

The rotor includes the hub (13) that is at the junction of the blades (11). To optimize the efficiency and reduce the loads, the blades can vary their angle of incidence to the wind. The pitch control (12) can capture more or less wind by rotating the blade around its longitudinal axis.

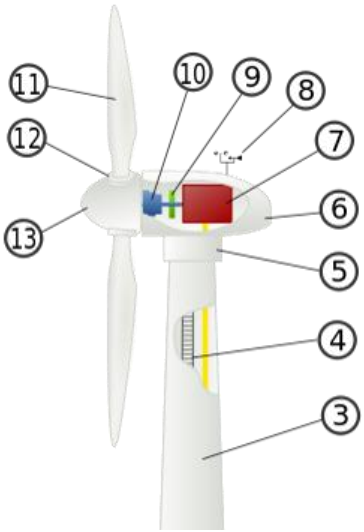

Figure 5 - Wind turbine components [5]

1.3 Offshore Wind Turbine support structures

At the end of 2014, a total of 2920 support structures were fully installed in European offshore wind farms. In Figure 6, the proportion for each type of support structure is shown. The most common were monopiles: 2301 monopiles were installed at the end of 2014 (78.8% of all installed foundations). Gravity based foundations were the second most common type with 303 units installed (10.4%), followed by jacket foundations (137 units: 4.7%), tripods (120 units: 4.1%) and tri-piles (55 units: 1.9%), Figure 7and Figure 8. Two full-scale floating structures were already in the water in 2014 [4].

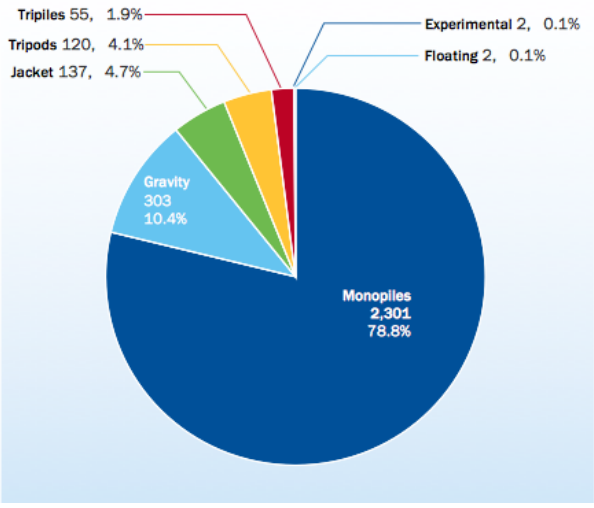

Figure 6 - Share of support structures for online wind turbines in Europe [4]

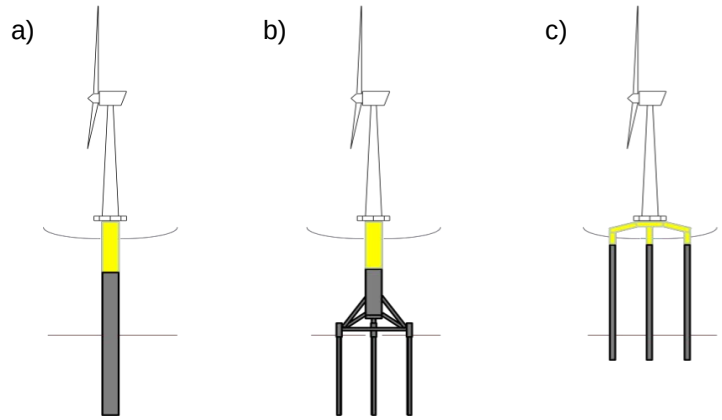

Figure 7- Support stuctures: a) monopile, b) tripod, c) tri-pile [45]

Figure 8- Transportation of the jacket structure [45][4]

1.4 Foundation modelling

1.4.1 Design loads

There is much experience designing foundation structures within the oil and gas industry. However, compared to OWTs, these structures are large and therefore more exposed to dynamic excitation. OWTs are characterised by small gravity loads, large horizontal loads, large bending moments at the seabed and strong cyclic loading, originating from extern environmental conditions [6].

1.4.1.1 Permanent loads

The permanent load of the OWT is the overall self-weight of the structure, including [6]:

- Rotor, nacelle, tower, support structure and foundation (mass of structure);
- Equipment and permanent ballast, or attachments which are permanent;
- Hydrostatic pressure on the support structure and foundation below the waterline.

All these permanent loads are taken into account in the design of the foundation.

Table 1 presents typical OWT permanent loads.

Table 1 - Permanent loads for OWTs [6]

Power (MW)	3.0	3.6	5.0	7.5
THH* (m)	80	80	90	100
Self-weight Tower + Nacelle + Rotor (ton)	± 260	± 290	± 700	± 1000

*THH = Turbine Hub Height

The characteristic value of these loads is defined as the expected value based on accurate data of the unit, the mass and the volume of the material [43].

1.4.1.2 Variable loads

Variable loads are loads that affect the structure and vary in magnitude, position and direction during the normal use and operations of the structure. They include [6]:

- Ship impacts from maintenance vessels, loads from fendering, crane operational loads and also actuation loads due to operation and maintenance of the OWT;
- Variable ballast on access platforms and ladders in the internal structure;
- Loads due to turbine operation such as centrifugal and Coriolis forces due to rotation; and gyroscopic forces due to yaw;
- Loads during fabrication, installation and transportation of the OWT;
- Aerodynamic drag forces on the tower and nacelle.

Accidental loads such as explosions or ship collisions are not excludable but are not taken into account in this dissertation work.

1.4.1.3 Environmental loads

Environmental loads are site-specific design loads and will therefore form a part of a cost-optimal design process. For design of the foundation, it will always have to be site-specific because it needs to be designed for the prevailing local soil conditions [6]. Environmental loads on the foundation including loads from wind, wave, current and ice are more uncertain and time dependent. The analysis of these loads is based on the longest possible time period for the relevant kind of load [7].

Each type of environmental load will be characterized by an intensity parameter. For example for wind is that the 10-minute mean wind speed, for waves the significant wave height, for current the mean current,… [43].

a) Wind Loads

For the design of a wind farm, site-specific wind data has to be collected over a sufficiently long period. It is an important issue to collect wind statistics in order to find the most suitable site. The data contains the wind speed at different heights, a standard deviation and a distribution for this parameter. When all data is used to calculate the loads on the OWT, it is important to keep in mind a few factors that may influence the wind conditions and the magnitude of the loads [6].

- Tower shadow and tower stemming, i.e. the disturbances of the wind flow owing to the presence of the tower;
- Wake effects wherever the wind turbine is to be located behind other turbines, e.g. in wind farms;
- Misalignment of wind flow relative to the rotor axis, e.g. owing to a yaw error.

b) Hydrodynamic Loads

Waves are caused by wind so both data should correlate. However, it is also preferable to collect wave data over a sufficient long period. These data will be determined by analysis based on model test or full scale measurements. To reduce uncertainties associated with loads and their effect, full-scale measurements will be better than model scale measurements. The measurements will be done by wind tunnel tests to check the influence of the wind on hydrodynamic loads, by proof tests to confirm assumptions made in the design, etc. Besides this data, the theoretical models for the calculation of from icebergs or drift ice and hydrodynamic loads on appurtenances will be taken into account [7].

Structures with a quasi-static response on the wave loads are analysed using the deterministic regular waves characterized by wave length, λ, wave period, T, wave height, H, and crest height (the distance from the still water level to the crest, Ac). These parameters, shown in Figure 9 will be predicted by statistical methods. Structures with a dynamic response will use a stochastic modelling of the waves. A sea state is determined by a wave frequency spectrum, a wave height, a representative frequency, a mean propagation direction and a spreading function. Usually, the sea state is assumed to be a

stationary random process. The standard time between two different sea states is three hours, but this period of stability can vary between 30 minutes and 10 hours [8].

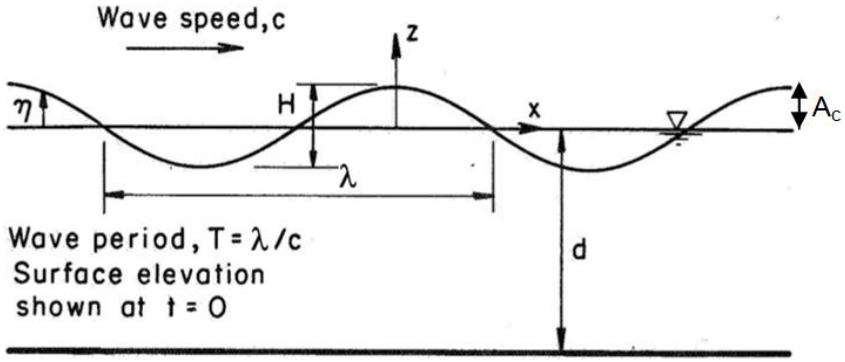

Figure 9 - Wave properties [8]

Wave conditions can be divided in two classes: wind seas and swells. Wind seas are generated by the extern local wind, while swell have no relationship with local wind [8].

c) Current Loads

Wind-generated current is caused by wind stress and atmospheric pressure throughout a storm, while tidal currents are more regular, following the astronomical motions of the moon and planets. Near the shoreline, in shallow waters, currents are more significant than in deep water. They also have the potential to create seabed scouring around the foundation of bottom-mounted structures and have a great influence on the wave height and wave period [8].

d) Seismic Loads

When an OWT is located in a seismic area it has to be designed in order to withstand the earthquake loads. Normally, a pseudo response spectrum is developed for displacement, velocity and acceleration of the structure. It is important to analyse the OWT in one vertical and, if necessary, in two horizontal directions. A simplified analysis of the OWT is done with a concentrated mass at the top of the tower representing the nacelle, rotor and hub. If not much vertical motion is expected, buckling analyse in the tower is conducted with the loads from maximum vertical acceleration caused by an earthquake [8]. The seismic loads will not have a lot of impact on the floating structures except when the ground will fail due to the seismic loads.

e) Other loads

Other environmental loads that play a minor role in the foundation design of OWTs are [8]:

- Temperature;
- Airtightness;
- Humidity;
- Radiation and UV radiation;
- Rain, snow and hail.

1.4.2 The dynamic characteristics of foundations

Studies highlight the importance of the dynamic behaviour in the design of offshore wind foundations. Dynamic behaviour can be interpreted as the free vibration response of the system and its relationship to the forcing frequencies applied to the system. They are crucial for the long-term performance of the OWT [9].

First, based on the Joint European North Sea Wave Project (JONSWAP) spectrum, cyclic loading from waves typically occurs with a peak at 0.1 Hz. Secondly, frequency distributions for wind loadings are usually less than 0.1 Hz [9].

When a standard 5 MW wind turbine rotates, the blades create a certain level of vibrations. It has been shown that the tower resists peak forces at frequencies of 1P and 3P, where P is the frequency of the blades passing. The 3P-frequency lies in the range of 0.345-0.6 Hz, in Figure 10, 1P-frequency lies in the range of 0.115-0.2 Hz. Therefore, to avoid system resonance and increased fatigue damage, OWT (nacelle, blades, tower, support structure and foundation) have to be designed with a system frequency (the global frequency of the overall OWT foundation), which stays outside the range of the 1P and 3P frequency ranges [9].

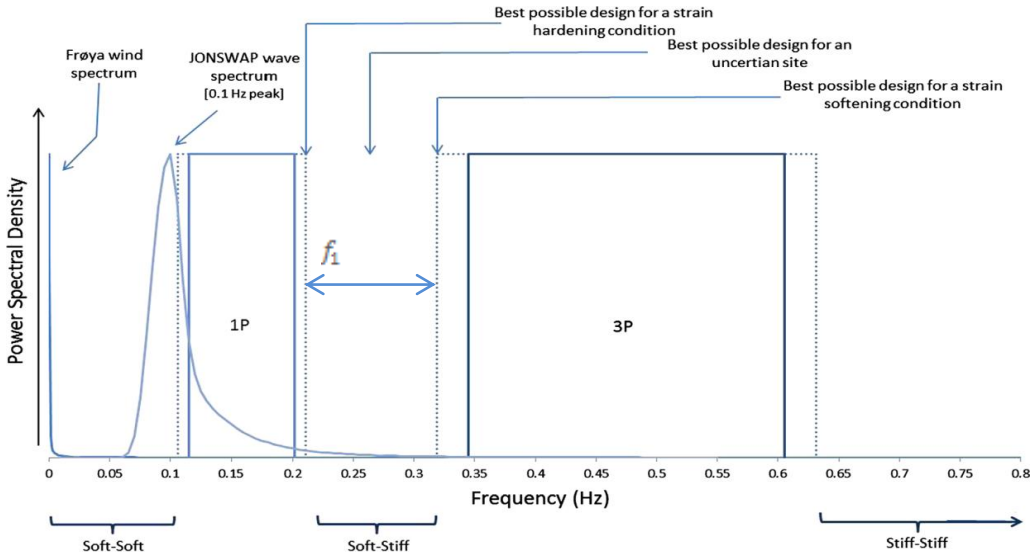

Figure 10 - Frequencies plotted against the power spectral densities for a three blades standard 5 MW OWT [9]

The choice of the frequency range for the overall system frequency is an indication of the required stiffness of the foundation. As seen in Figure 10, there are three types of design possibilities according the first natural frequency, f_1 [9]:

1. A “soft-soft” structure with f_1 below 1P frequency range. This indicates a very flexible structure where less steel is required and a smaller diameter is necessary. However, this type is almost impossible to design due to the fatigue or ultimate capacity issues;

2. A “stiff-stiff” structure with f_1 above 3P frequency range. This indicates a very stiff and thus massive structure and foundation that would seem the safest solution regarding the system frequency. However, from an economical point of view these structures are very expensive due to high material, transportation and installation costs;

3. Today, all OWTs are designed as a “soft-stiff” structure with the first natural frequency, f_1, in a range between at least ± 10% away from operational 1P and 3P frequencies as indicated in Figure 10. However, it has been proven that the system frequency changes with time due to the effect of dynamic soil structure interaction under cyclic loads.

    a. For strain-hardening sites (i.e. loose to medium dense sand), the system frequency increases because of an increase of stiffness of the soil under cyclic loads. The best possible design within these conditions is after the 1P +10% frequency indicated by the dotted line just above 0.2 Hz in Figure 10;

    b. For strain-softening sites (i.e. clay), the system frequency decreases because the stiffness of the soil decreases under cyclic loads. In contrast to strain-hardening sites, the best possible design within these conditions is before the 3P-10% frequency indicated by the dotted line just below a frequency of 0.35 Hz in Figure 10.

1.5 Floating wind turbines

1.5.1 Introduction

Sixty-three percent of the European OWTs are installed in the North Sea. 22.5% are situated in the Atlantic Ocean and the rest in the Baltic Sea [2]. The Atlantic, Mediterranean and deep North Sea waters have a large wind capacity but the problem is that water depths in these areas are too great to install fixed offshore foundations. Fixed structures are limited to water depths of 40 m to 50 m. Engineers are examining schemes with a potential to reach 80 m, but this depth is still not enough for deep water. That is why other new concepts are being developed that utilize floating support structures moored to the seabed [4].

The principle advantage of deep water sites is that higher wind resources and more stable winds are present in comparison with shallow water sites. Floating platforms do not require significant foundations (only the anchors of the mooring lines in the seabed) which means that nuisance from the installation of the foundations can be minimized and the structures are less dependent on the soil conditions. In addition, disturbance of sea life is reduced which is better in terms of potential environmental impacts [10].

A big advance in the development of the deep offshore wind energy in Europe was made between October 2011 and June 2012. Then, there was a Task Force, part of the EWEA, who had attention for

‘Deep offshore and new foundation concepts’. This research community included representatives from 16 leading European companies [4].

Working together during this period resulted in an instructive analysis. It was concluded that the electricity produced from wind turbines in deep water alone could meet the current European electricity consumption four times over. So, the evolution of the floating platforms for deep waters is a very important issue [4].

For the moment, there aren’t a lot of floating platforms installed. At the end of 2014 there were only two full scale floating wind turbines in the water in Europe, Hywind in Norway and WindFloat in Portugal.

1.5.2 The dynamic characteristics of the floating platforms

The dynamic characteristics of floating platforms are different to fixed structures. Floating wind turbines are more susceptible to wave effects than fixed structures. The waves will move the platforms significantly as a function of time. In the ocean, the waves can have a wavelength of 400 m. That is why it is not economical to make a platform that bridges a full wavelength [11].

Three main types of platforms have been demonstrated to be stable enough: the spar platform, semi-submersible platforms and tension leg platforms. These three options have the degrees of freedom of motion shown in Figure 11 and natural frequencies at very low frequencies [11].

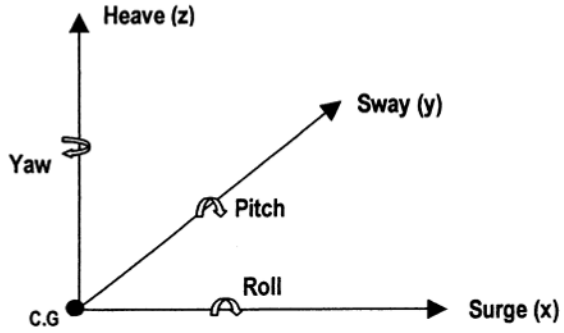

Figure 11 - The degrees of freedom of motion for a floating platform [12]

For floating wind structures, it is important to have good estimates of the low frequency part of the wind and wave effect, i.e. the pitch. For fixed structures, this is less important because these structures do not have natural frequencies in the low frequency range [11].

1.5.3 Main types of deep-water wind turbine platforms

A lot of useful offshore research has already been undertaken by the offshore oil industry. The results of this research can be used for the design of the foundations of the OWTs. Nevertheless, it is very important to examine the differences between offshore oil platforms and OWTs [4,13]. A big difference between the oil sector and the wind energy sector is that oil platforms are designed and built for a specific requirement and will be unique. In contrast, wind turbines are made in common production runs to reduce costs [11].

There are a lot of different platforms adapted from the oil industry. In this industry, floating platforms have existed for 30 years. Most of these platforms can be used for OWTs too. These types of platforms are divided into three groups: spar buoys, tension leg platforms and semi-submersibles, Figure 12. This subdivision is based on the way the platforms achieve stability [4,13].

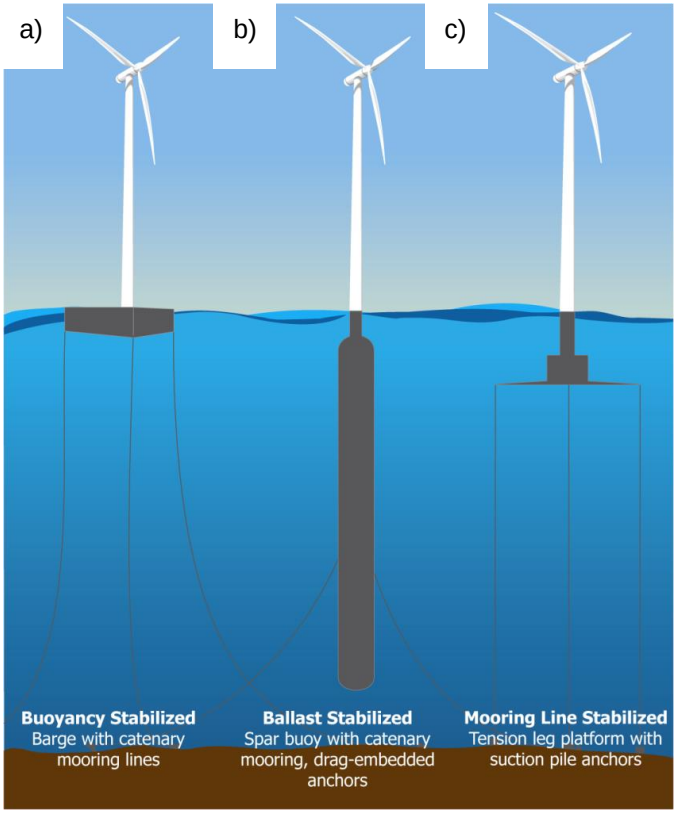

Figure 12 - The three main types of deep water wind turbine platforms: a) semi-submersible, b) spar buoy and c) tension leg platform [14]

1.5.3.1 Spar buoy (Ballast Stabilized)

This type of structure, Figure 12(b), achieves stability by ensuring that the lower part of the platform is heavy and the upper part is light. Because of the way it is ballasted, the centre of gravity is lower in the water than the centre of buoyancy. This results in a moment that keeps the spar straight [4].

In theory, a spar buoy would be able to keep straight the tower top using just the ballast and the buoy. In that case, the catenary mooring lines are only used to keep the platform on the right location. But in reality the buoy also needs the mooring lines to achieve stability [13].

1.5.3.2 Tension leg platform (TLP, Mooring Line Stabilized)

This type of platform, Figure 12(c), consists of a slender cylindrical buoy anchored to the seabed with taut leg mooring lines. The weight of water displaced by the buoy needs to be larger than the combined weight of the wind turbine and the buoy. Theoretically, the TLP would be able to hold in this way. However a reserve buoyancy is included to tension the mooring lines which are connected to anchors on the seafloor (see Section 2.1). During installation, the draft of the floater can be adapted by varying the water ballast [11, 16].

1.5.3.3 Barge (Buoyancy Stabilized)

The barge platforms, Figure 12(a), combine features from the two previous types. This platform contains a buoyancy tank that will hold the platform straight and mooring lines to anchor the platform in the seabed [4].

Chapter 2

Mooring systems

The different types of anchors are discussed in the first section where the anchor pile which is the focus of the thesis, is explained more extensively. The different mooring lines are explained in Section 2.3. Then the parameters of the holding capacity of the anchors, the different types of loading and the safety requirements are mentioned. Finally, soil classification and site investigation are clarified.

2.1 Anchors

Floating wind turbines can be anchored to the seabed by a number of methods. The choice of the anchor system depends on the size and nature of the OWT, the environmental conditions, the mooring system, the geotechnical properties of the seabed and any financial or installation limitations. There are two different main types of anchors: gravity anchors and embedded anchors. Before designing and optimizing the mooring and anchoring system, there has to be an analysis of the site and soil data [17].

2.1.1 Gravity or box anchors (dead weight)

This is the oldest form of anchor; the use of such anchors date back to at least 2000 BC when large stones, baskets of stones or blocks of wood were used to secure tethers. Now, in the offshore industry ballast comprising steel or concrete is used. Figure 13 shows that anchoring is provided partly by the weight of the ballast and partly by the friction that develops between the seabed and the dead weight [4].

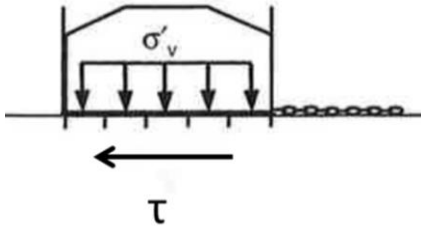

Figure 13 - Box anchors (gravity anchor) [16]

2.1.2 Embedded anchors

As shown in Figure 14 and Figure 15, the different types of embedded anchors are [4]:

- Piles anchors, Figure 14(a)
- VLA (vertically loaded anchors), Figure 14(b)
- Drag embedment and normal plate anchors, Figure 14(c)
- Suction anchor, Figure 14(d)
- SEPLA (Suction Embedded Plate Anchors), Figure 15

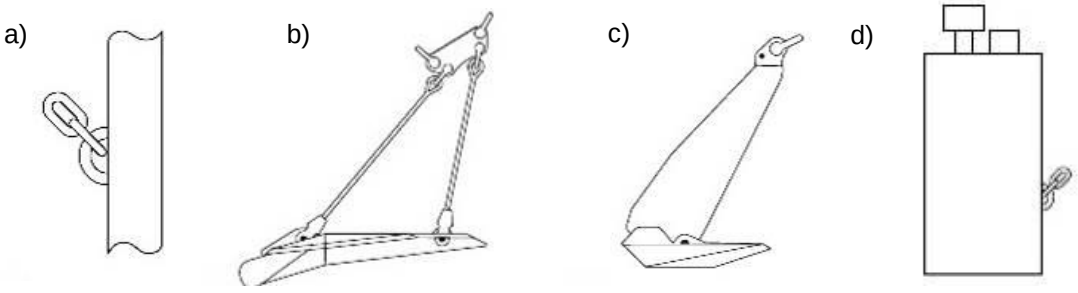

Figure 14 – a) anchor piles – b) VLA- c) drag anchors – d)suction anchor [17]

2.1.2.1 Anchor piles

This type of hollow steel pile is the subject of further analytical study in this thesis. The holding capacity is generated, just like a pile foundation, by the friction between the soil and the pile. To have enough holding capacity, the pile has to be installed at a sufficient depth below the seabed. The pile can withstand both horizontal and vertical loads [17].

2.1.2.2 VLA (vertically loaded anchors)

This anchor penetrates deep in the ground and the soil in front of the anchor generates the holding capacity. When the anchor is installed, it can withstand both horizontal and vertical loads [17]. The big problem with these anchors is to know exactly where they are in the soil. In theory, the depth can be determined by measuring the angle of the anchor line with the seabed and the length of wire in the soil, but in many cases the angle will not fit to reality [18].

2.1.2.3 Drag embedment anchors

This is the most common anchor, designed to penetrate partly or fully in the ground. In this case, the holding capacity of the anchor is also generated by the soil in front of the anchor. Most of the drag embedment anchors on the market cannot withstand vertical loads however being better suited to horizontal loading, these anchors are frequently used catenary mooring system [17].

2.1.2.4 Suction anchor

This is a hollow steel pipe with a typical diameter more than 5 meter which is more than the pile anchor. The suction caisson has a closed top with a connected temporary pump which creates a pressure difference in order to suck the pipe into the seabed. The holding capacity is granted by the friction between the soil and the pile, the weight of the plug of soil inside and the characteristic negative end-bearing resistance. To optimize the holding capacity, the mooring lines are attached to the side of the caisson [17,18].

2.1.2.5 SEPLA (Suction Embedded Plate Anchors)

Due to the positioning problems with the VLAs and plate anhors generally, a new system was developed achieving a more specific location below the seabed. SEPLA combines the advantages of a suction caisson and vertical loaded plate anchors. It consist of a suction caisson with an embedded plat anchor slotted vertically into its base [18].

Figure 15 shows the installation procedure of the SEPLA which starts with the penetration of the caisson under self-weight (1). Water will be pumped from the inside of the caisson to reach the pressure difference that sucks the caisson until the design embedment depth. After, the plate anchor mooring line will be disengaged from the caisson which will move upwards by pumping water into it (2). The mooring line attached to the plate anchor will be tensioned causing the rotation of the plate anchor in the direction of loading maximising the bearing capacity of the anchor (3 & 4) [19].

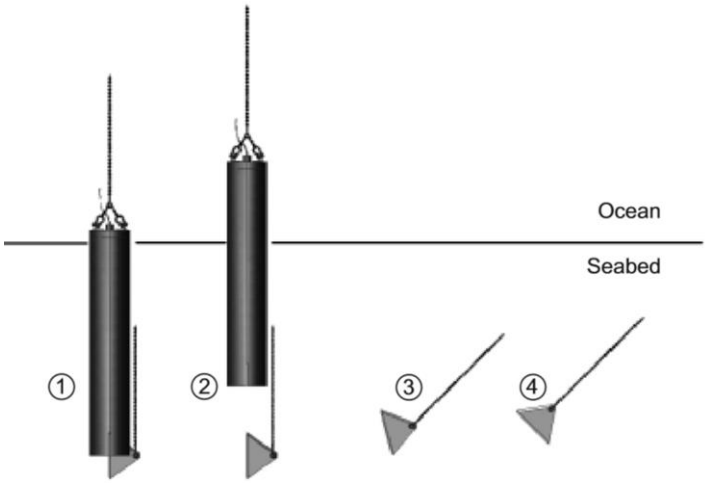

Figure 15 - SEPLA concept: 1 suction installation, 2 caisson retrieval, 3 anchor keying, 4 mobilised anchor [19]

2.2 Pile anchor

2.2.1 Driven and grouted pile anchors.

Pile anchors are typically hollow steel tubes which are attached with a mooring line in the seabed at some point below the mudline, Figure 16.

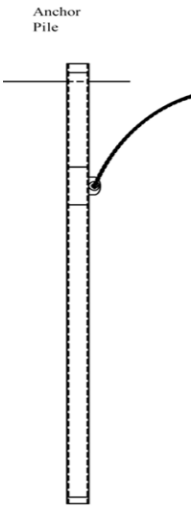

Figure 16 - Anchor pile [20]

According to the way the pile anchors are installed, there are two different kinds of anchors: the driven pile anchor and grouted piles. The driven pile anchor is the most commonly used anchor in the offshore oil production. This anchor is driven into the seabed by a large hammer, Figure 17. An advantage of adopting this type of anchor in the offshore wind industry is that the experience of the oil industry proves the reliability and the high load capacity of this anchor type. Another advantage is that the anchor can be installed very precisely [21].

Figure 17 - Driving hammer [16]

Grouted pile anchors are, for example, used in rocks due to the fact that this ground is too hard for driven piles. The only way to secure an anchor in rock is to drill an oversized hole and then grout the inserted pile, Figure 18 [16].

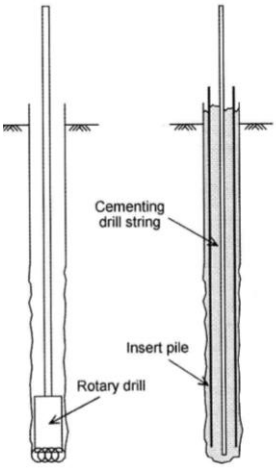

Figure 18 - The installation process for a grouted pile [16]

The pile anchor installation procedure employed depends on the site characteristics. The size and shape of pile anchors are similar and depends on the soil characteristics and the magnitude of design loads. Pile anchors are able to withstand horizontal and vertical loads. Due to this property, pile anchors are used in both catenary and taut leg mooring systems. The resistance to the applied loads is provided by the frictional resistance developed between the steel pile and the surrounding soil [20]. The most difficult soil to install a pile anchors will be the stiff and dense soils, while in the soft and loose soils, it will be difficult to gain resistance.

A disadvantage of pile anchors is that the installation costs are very high compared to other systems, due to the equipment required for installation [20].

2.2.2 Dynamically installed anchor piles

These types of anchor piles have differ in shape from the conventional cylindrical piles discussed above. They consist of a thick-walled, tubular steel shaft filled with scrap metal or concrete ballast with a conical or bullet shaped tip. Steel fins are attached to the shaft to improve the hydrodynamic stability and to increase frictional resistance. The anchor is installed in the seabed by dynamic self-weight penetration - they embed themselves by falling from a specified height above the seabed. Resistance to uplift loadings is provided by friction between the anchor and the soil. The final holding capacity is a function of the energy input (the drop height of the anchor) [22].

There are two types of dynamic anchors: the torpedo anchor and the Deep Penetrating Anchor (DPA). The installation costs are low relative to alternative systems because there is no external energy source or mechanical interaction required. Also, the installation costs are largely independent of the water depth. Once installed, they behave the same as normal pile anchors. They can withstand both horizontal and vertical loads and can be used in both catenary and taut-leg mooring systems.
A disadvantage of this kind of anchor is that there's a degree of uncertainty according to the embedment depth and subsequent capacity. These anchors may not be used in sandy soils [22].

2.2.2.1 DPA (Deep Penetrating Anchors)

Deep Penetrating Anchors are recently developed systems and have a shape similar to a rocket, Figure 19. They have a dry weight of 500-1000 kN and a length of 10 m to 15 m. These anchors are installed by dropping them from a certain height above the seabed (typically 20 m to 40 m) [22].

Figure 19 - Deep Penetrating Anchor [16]

2.2.2.2 Torpeo anchor

Torpedo anchors has almost the same shape as the DPA, except the tip is cone shaped rather than bullet shaped, Figure 20. The diameter of such an anchor is 0.76 to 1.07 m and the length is 12 to 17 m.The drop height above the seabed varies from 30 m to 150 m [23].

Figure 20 - Torpedo anchor [20]

2.3 Mooring lines and connections

There are two types of mooring systems: catenary mooring and taut leg mooring, Figure 21. Besides this classification, the mooring lines can also be distinguished by means of the materials they are made of.

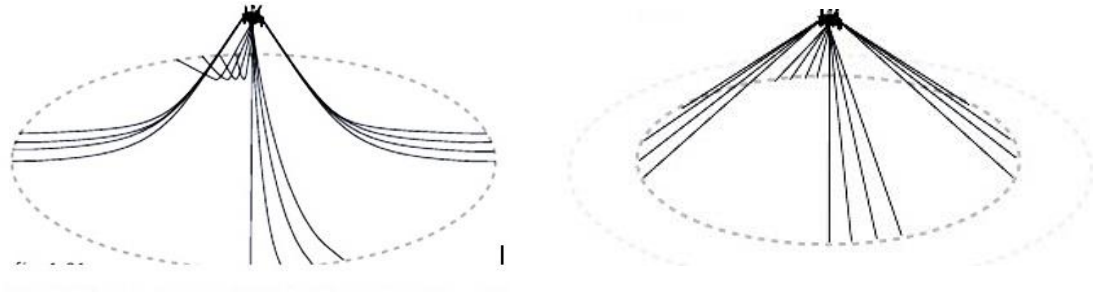

Figure 21 - Catenary system (left) and taut leg mooring [17]

2.3.1 Catenary mooring

This type of mooring system is mostly used in water depths under 1000 m. The mooring lines could be formed from either chains or wire rope. A significant length of the lines lies on the seabed, leading to the anchor being loaded in a horizontal direction. This type of mooring system is mostly combined with a conventional drag embedment anchor [17].

The holding capacity, P, of the mooring lines lying on the seabed is expressed by equation 2.1 [17]:

$$P = f * l * w \tag{2.1}$$

With,

f : Friction coefficient between the mooring line and the seabed

l : The length of the mooring line lying on the seabed (in m)

w : The unit weight of the mooring line in water (in t/m)

If the friction coefficient is not known, then the values of Table 2 can be used:

Table 2 - The friction coefficient of chains and wire ropes [17]

	Starting	**Sliding**
Chain	1.0	0.7
Wire rope	0.6	0.25

The values given under starting are used to calculate the holding capacity of the mooring line. The values under sliding are used to calculate the forces during the deployment of the mooring lines.

2.3.2 Taut leg mooring

In contrast to the catenary mooring, the taut leg mooring is mostly used in water depths deeper than 1000 m. At these depths, the weight of the mooring lines became a limiting factor in the design of the floater and has led to the development of synthetic ropes. The mooring lines make an angle with the seabed. In that way, no lines are lying down on the seabed. That is the reason the anchors of the taut leg mooring system are loaded in a vertical and horizontal direction. VLA are commonly used with this type of mooring system. The advantage of this type of mooring is that the footprint of the taut leg mooring is smaller than the footprint of the catenary mooring [17].

2.3.3 Types of mooring lines

There are three types of mooring lines: chains, wire ropes and synthetic fiber ropes. The most commonly used is chain. Two regularly used types of wire ropes in the offshore industry are spiral strand and six strands. The main disadvantage of using wire rope is that it is more sensitive to damage and corrosion than chain. The newest type of mooring line is the synthetic fiber rope. Typical materials are polyester and high modulus polyethylene (hmpe) [17].

In Figure 22 the weight of the three different types of mooring lines is related to its diameter. The synthetic fiber ropes are the lightest, followed by the wire ropes and the chains. Figure 23 gives the minimum breaking load (MBL) related to the diameter. Beside the largest weight, the chains also have the highest strength. Then, the wire ropes and the synthetic ropes have respectively a lower strength. The axial stiffness is the smallest for synthetic fiber ropes, than respectively wire ropes and chains [17].

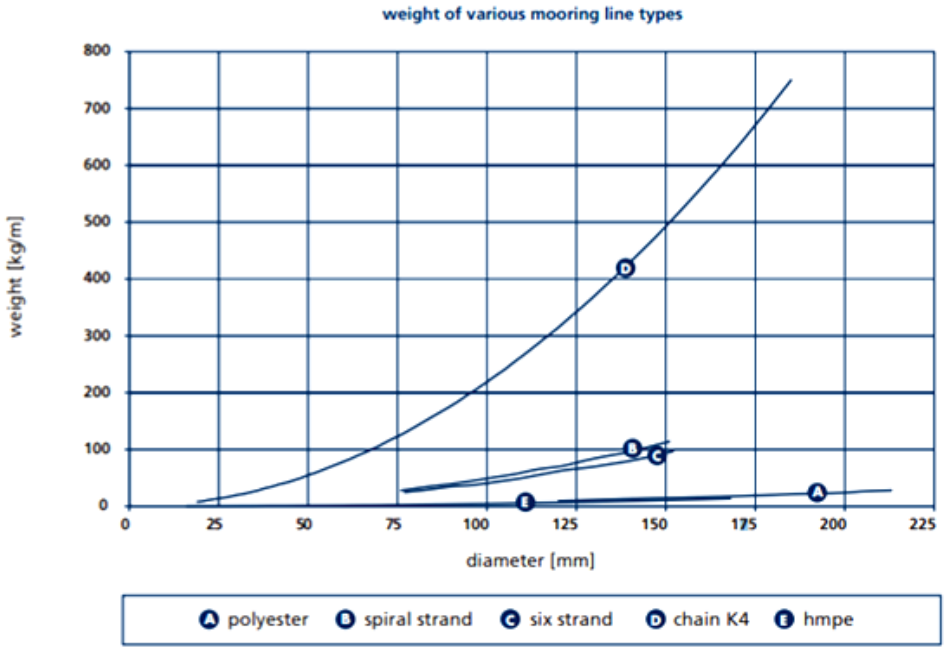

Figure 22 - Chart of the weight of various mooring line types as a function of the diameter of the mooring lines [17]

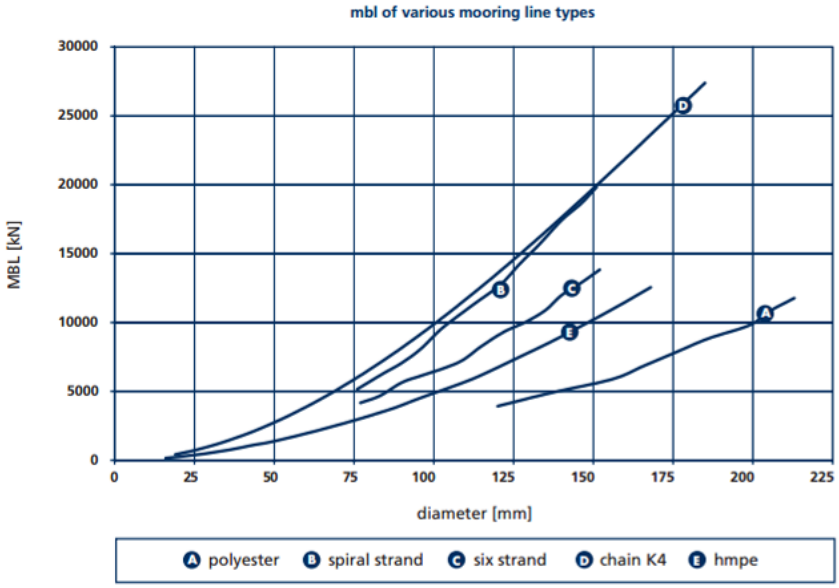

Figure 23 - Chart of the minimum breaking load (MBL) of various mooring line types as a function of the diameter of the mooring lines [17]

2.3.4 Connections

Another consideration is that here are different ways to connect the mooring lines to the anchors. Most often, the chains are attached on the side of the pile using a shackle system. A second method of connection is grouting the chains into the upper part of the pile [16]. Herefore the mooring shaft is screwed into the pile head and grout is extruded into the substrate wich encapsulate the steel screw mooring. In that way an incredibly strong mooring point is created [42].

The optimal attachment point for the anchor chain is below the mudline for both catenary and taut leg mooring system. The mooring system and the interaction with the soil will determine the angle of loading of the anchor [16]. In this thesis, the loads (axial, lateral and combined) were applied on the head of the pile.

2.4 Anchor holding capacity

Primarily, the anchor holding capacity depends on the type of soil, its shear strength profile and the type/geometry of the anchor. The newest anchor designs have a higher holding capacity more than 10 times that of older designs - in the range of 100 to 150 times the anchor weight compared to 7 to 20 times the weight of older types [17].

Next to it, a streamlined shape will penetrate deeper than a shape with protruding parts which will have much more soil resistance while penetrating in the soil (for the same fluke area). On the other hand, a rough surface will have a larger tension capacity than a streamlined shape due to the high friction. Also anchors with a larger fluke area will have a larger tension capacity because of the larger friction and weight [17].

Another parameter is the load inclination. When the load is close to a vertical load, the anchor will have tendency to move out of the ground. In this case, the shear stress along the length of the anchor will be activated. If the load is closer to the horizontal load, the resistance at the upper part of the pile will derive from passive and active resistance at the front and the back of the pile anchor respectively. Under combined loading, a combination of the mechanisms described above will develop [17].

2.5 Marine sediments

Generally, the sediments in world’s oceans are the thickest near continents and thinnest on newly formed mid-oceanic ridges. In some areas of the ocean, there are even no sediments due to strong bottom currents. In contrast, some areas have a continual rise which can reach up to 1.6 km thickness in places [35].

The marine sediments are made from land or the remains of marine organisms. The sediments can be classified as terrigenous (transported from land) and pelagic (sediments that settle through the water column). Because deposition of the pelagic sediments is very slow, coastal areas are full of

terrigenous sediments. Pelagic sediments are generally fine grained. There are two kinds of this sediment; organic derived from remains of marine organisms and lithogenous from particles transported by wind into the ocean. Besides these sediments, there are also sediments formed from biological and chemical reactions in the water or within sediments [35].

The stress state of the seabed can be normally consolidated, overconsolidated or incompletely consolidated. The sediments that deposit slowly and were not changed anymore since the deposition are normally consolidated. Overconsolidation can be a consequence of more recent events, such as erosion or a submarine slide. Incomplete consolidation occurs when excess pore pressures, due to a rapid deposition for example, have not had the opportunity to dissipate [35].

An important issue is that the depth of free water or changes in the depth do not affect excess pore pressure in the seabed because the water above the mudline contributes to the total stress and pore pressure such that the effective stress in the seabed remains constant. Only changes in the pore water or pore gas will affect the effective stress and so the shear strength and stability of the seabed [35].

The form of foundation system will depend on the soil conditions of the area. For example, in the ocean in West Africa, there will be soft, normally consolidated clays. The further from shore, the more fine-grained sediments will occur because they will transport further than coarse sediments [35].

2.6 Soil classification

Soils can be cohesive or cohesion-less. Cohesive soils, like clay, have very small flake like particles which can attract water. This kind of soil is examined in this thesis. On the other hand, cohesion-less soils do not stick to each other even with the help of water. Some examples of cohesion-less soils are gravel, sand and silt [25].

The classification of the soils can be made according to the particle size. Gravel are small pieces of rock with a grain size between 16 mm and 2 mm. Sand are small particles of quartz and feldspar with a grain size between 60 µm and 2 mm. The particles with a size between 2 µm and 60 µm are defined as silt, these particles are microscopic soil fractions of very fine quartz grains. Clay are flake-shaped minerals as mica, the particles has a grain size between 0.1 µm and 2 µm [17,25].

Clays are fond of water because the surface of a clay mineral has a net negative charge and water has a positive charge. These properties will bond the clay surface to water. According to applied loads, the water has a great effect on the clay. Very wet clay, in liquid state, should not withstand any type of loading in contrast to a potter's clay with a moderate amount of moisture. This clay is in plastic state, so when it's reformed it will not spring back as an elastic material. If this clay dries for a short time, it will lose its plasticity and reached the semisolid state. The solid state occurs when the clay is totally dry [25].

This thesis is concentrating on the failure mechanism of a loaded pile in clay. The caly is consdered to be undrained and the Tresca failure criterion was used. In general a clay soil has a cohesive, plasticity and slow-draining behaviour. If a soil has more than 25% of clay-sized particles, the clay properties will dominate the behaviour and it would be classified as clay [25].

While applying a load on a soil, the pressure within the soil will change. The changes in the total stress, $\Delta\sigma$, can be written as the sum of the changes in the effective stress, $\Delta\sigma_K$ and the changes in the water pressure, $\Delta\sigma_W$ [37] :

$$\Delta\sigma = \Delta\sigma_K + \Delta\sigma_W \tag{2.2}$$

When the stress increases in sandy soils, all compression, (except the creep) will take place directly due to the high permeability. The pore water will drain away immediately, so the external load will be totally carried by the soil skeleton. This is called a drained response [35]. The changes of the water and pore pressure are then equal to [37]:

$$\Delta\sigma_K = \Delta\sigma \tag{2.3}$$

$$\Delta\sigma_W = 0 \tag{2.4}$$

In clay, the compression states are more divided. Firstly, undrained compression will occur and then time dependent primary compression. There will be no immediate volume change, so the response is undrained [35]. The load will be carried by the pore fluid, not by the soil particles. In the moment the soil is loaded,the pressures can be written as [37]:

$$\Delta\sigma_K = 0 \tag{2.5}$$

$$\Delta\sigma_W = \Delta\sigma \tag{2.6}$$

After some time, depending on the permeability of the soil, drainage will occur and pore fluid will be driven out of the soil particles which will start compressing. This is called consolidation which is the time-dependent dissipation of excess pore water pressure in the soil skeleton due to the external load. It defines the transition from undrained to drained conditions. During consolidation, the soil decreases in volume as the pore water in the voids of saturated clay soils is squeezed out [35].

So the behaviour of clay can be described in three steps [35]:

Step 1: Initial undrained compression;

Step 2: Primary consolidation: the change in total stress caused by the loading transfers from the pore water to the soil skeleton (effective stress changes); with an associated change in volume with time;

Step 3: Secondary consolidation occurs after complete dissipation of the pore water pressure, some settlement of the soil will continue to take place due to the plastic behaviour.

The consequence is that for piles in sand (and gravel), the design is based on effective stress. For piles in clay, the total stress has to be taken into account [35].

Clay has generally an undrained shear strength, a submerged unit weight and plasticity parameters. The consistency of clays is related to the undrained shear strength. Table 3 summarises the undrained shear strength associated with clays of differing consistency [17].

Table 3 - The type of clay with the fitting undrained shear strength [17]

Consistency	Undrained shear strength
Soft clay	<25 kPa
Firm (medium) clay	25 kPa - 50 kPa
Stiff clay	50 kPa -100 kPa
Very stiff clay	100 kPa – 200 kPa
Hard clay	> 100 kPa

In Chapter 6.1 is mentioned which shear strength the models have.

2.7 Site investigation

Site investigation is a significant requirement before the installation of any OWT field. This examination will determine the foundation type, the dimensions and the installation procedure [27].

In the early stages, the gathered information should be enough to select the best site. In later stages, the investigation will expand in detail in order to design the OWT. The goal of the site investigation is to obtain a reliable model of the seabed including significant parameters of the soil layers [27].

For anchors, it is important that the soil stratigraphy and range of soil strength properties shall be considered per anchor location [7].

The offshore site investigation can be divided into three following steps [16]:

- Desk study
- Geophysical investigation
- Geotechnical investigation

The desk study implies the research of the existing data, such as the topography of the seabed on the site or nearby, the regional geology and previous experience with foundations in the area. This first step will also help to discover missing data [16]. Besides the technical data, for offshore wind farms it will be necessary to have information relating to the shipping movements, fishing activities and potentially military activities [27].

The second step is the geophysical investigation allowing the physical properties of the site to be evaluated, such as the nature or the characteristics of the seabed. This investigation includes the bathymetry (water depth) and an examination of the seabed floor to identify potential obstacles there [16]. With bathymetric mapping it is possible to make a 3D view of the seabed. The method commonly used for this technique is echo sounding. Obstructions on the seabed can be detected by sidescan sonar [16].

In the last step, the geotechnical investigation will take place after examining the results of the geophysical investigation. Therefore, the actual stress conditions in the soil has to be accounted and the cyclic loadings caused by the waves, wind and earthquakes shall be included [7]. The general objective of this research is the characterization of the soil properties by tests such as CPT (Cone Penetration Test) [16] and by soil sampling with subsequent laboratory testing [7].

It is possible that after the geotechnical investigation an additional geophysical survey may be required. The design of the OWT foundation depends strongly on the environmental loads: waves, wind, currents, ice sheets and earthquakes. To optimize the geotechnical investigation, it is important to have these loads quantified early in the site investigation program. In that way unexpected results can be avoided [27].

For clay the required basic soil parameters are [27]:

- General description
- Layering
- Grain size distribution
- Water content
- Total unit weight
- Atterberg (plastic and liquid) limits
- Remoulded shear strength
- Sensitivity
- Soil stress history and over-consolidation ratio
- Organic material content
- Elastic modulus

Table 4 will give some parameters to classify the soil and some test to achieve parameters according to the strength and the deformation of the soil.

Table 4 - Parameters for the classification and test to achieve parameters according to the strength and the deformation

Classification	• Grain size distribution • Water content • Total unit weight • Atterberg (plastic and liquid) limits
Strength	Field: • CPT • Field vane Lab: • Triaxial test • Direct shear test
Deformation	Field: • CPT Lab: • Oedometer test

Further, the variations in the vertical and horizontal direction have to be documented and the uncertainties in test results shall be described [7].

2.8 Safety requirements for anchor foundations

To assure the safety of the pile anchor, there are some safety requirements based on the limit state method of design. The analysis of anchor resistance shall be carried out for the ultimate limit state (ULS) and the accidental limit state (ALS). The ULS presents the ultimate resistance for the applied loads. The ultimate strength capacity and structural capacity will be checked for both yielding and buckling. In the case of an anchor, the mooring lines have to withstand extreme environmental conditions. It should also be ensured that the mooring system (with multiple lines) can hold the loads if either one mooring line or anchor fails for a reason outside the designers control. The ALS relates to the damage of a component of the structure due to an accident or an operational failure. Another limit state considered in the standard is the serviceablity limit state (SLS) which corresponds to the criteria applicable to normal use of durability. The load coefficeint according to this limit state is 1.0 for all load categories [7]. For the floating wind turbines, SLS will be not very important because the platforms will move a lot. This limit state will be more important for the fixed structures.

Next to the three different ultimate limit states, there are also two different consequence classes [7]:

- Consequence class 1 (CC1): Failure is unlikely to lead to unacceptable consequences such as loss of life, collision with an adjacent platform, uncontrolled outflow of oil or gas, capsize or sinking;
- Consequence class 2 (CC2): Failure may well lead to unacceptable consequences of the ULS and the ALS.

The method for anchor design is the partial coefficient method which will consider the strength and deformations of the foundation structure and soils. The load coefficients for the different consequence classes and different limit states are enumerated in Table 5 and Table 6. For mooring in water deeper than 200 m, a dynamic analysis is required because in this case the safety will be dominated by a mean mooring line tension component.

Table 5 - Load coefficients for ULS [7]

Consequence class	Type of analysis**	Υ_{mean}*	Υ_{dyn}*
1	Dynamic	1.10	1.50
2	Dynamic	1.40	2.10
1	Quasi-static	1.70	
2	Quasi-static	2.50	

* Υ_{mean} = load coefficient for mean line tension due to pretension of the steel and the environmental loads

Υ_{dyn} = load coefficient for dynamic line tension due to oscillatory low-frequency and wave-frequency effects

** Quasi-static loads are the loads due to the swell, wind, current and the frequency of the system. These quasi-static loads usually have a low frequency (periods between 140s and 200s). Besides the quasi-static loads, there are also individual wave forces that cause a high frequency resulting in dynamic shock loads with a period of 10s to 14s. The quasi-static loads and the individual wave forces together are called the total dynamic load, called 'dynamic' in the tables above [17].

Table 6 - Load coefficients for ALS [7]

Consequence class	Type of analysis**	Υ_{mean}*	Υ_{dyn}*
1	Dynamic	1.00	1.10
2	Dynamic	1.00	1.25
1	Quasi-static	1.10	
2	Quasi-static	1.35	

So the design mooring line tension, T_d, is equal to equation 2.7 [7]:

$$T_d = T_{c-mean} * \Upsilon_{mean} + T_{c\text{-}dyn} * \Upsilon_{dyn} \quad (2.7)$$

With,

$T_{c\text{-}mean}$ = the characteristic mean line tension due to pretension of the steel and the environmental loads;

$T_{c\text{-}dyn}$ = the characteristic dynamic line tension due to oscillatory low-frequency and wave-frequency effects.

The load coefficients for dynamic line tension are large in comparison with the load coefficients from Eurocode 7 (EC7). In EC7 the load coefficient for a perament load will vary between 1 and 1.35 and for a variable load between 1.3 and 1.5 [46].

Next to the load coefficients, there are also material coefficients to use in combination with the load coefficient. The soil material coefficients to be applied to the resistance of the pile anchor have to be more than [7]:

1.3 for ULS (CC1 and CC2)
1.0 for ALS (CC1 and CC2)
1.0 for SLS (CC1 and CC2)

The material coefficient applied on the resistance of the pile anchor of [7] is defined in Eurocode 7 [46] with the term γ_R, the partial resistance factor. The value of 1.3 of the ULS of [7] is equal to the partial resistance factor of a driven pile in EC7. The value for bored piles in EC7 is larger, 1.6.

Then the design anchor resistance R_d is defined as in equation 2.8 [7].

$$R_d = \frac{Rk}{\gamma m} \tag{2.8}$$

With,

R_K = characteristic resistance

Υ_m = material factor on the anchor resistance

For pile anchors where there are small possibilities for redistribution of loads from one pile to another, the material coefficient Υ_m should be more than 1.7 for ULS design. For laterally loaded piles, the materiald coefficient Υ_m has to be applied to the characteristic soil shear strength parameters and is reduced to 1.3 for ULS design [7].

Chapter 3

Geotechnical Models

Firstly, the Tresca failure criterion will be discussed. The ultimate capacity for axially loaded piles will be explained and applied. For the laterally loaded piles, there are the Broms method and the modified method to calculate the ultimate resistance.

3.1 Introduction

The focus of this thesis will be the failure of the soil-structure for lateral, axial and combined loadings. Using the program Abaqus, the response of the piles will be analyzed.

The geotechnical modelling in this thesis has been developed progressively, starting with an elastic pile with elastic soil around it. Subsequently, an elastic pile in a soil modelled as an elastic-plastic material was considered. Three elasto-plastic models were initially considered – Tresca, Mohr-Coulomb, and Drucker-Prager however severe difficulties were experienced in implementing the latter two and thus, the studies here only consider the Tresca model. The Tresca model can be used to simulate the undrained response of cohesive soil.

3.2 Strengths and Mohr's circles

The Tresca failure criterion can be considered as a particular case of the Mohr-Coulomb failure criterion. In Abaqus, the Tresca model has to be implemented as a Mohr-Coulomb model because Abaqus defines the Tresca model as a pressure-independent Mohr-Coulomb model with $\phi = 0°$ [28].

The Mohr-Coulomb criterion is widely used to simulate the inelastic behaviour of soils under drained conditions, i.e. in terms of effective stress. The limiting soil shear strength, τ defined by the model is described by equation 3.1:

$$\tau = c' + \sigma'.\tan\varphi' \tag{3.1}$$

With,

c' = apparent cohesion

σ' = effective stress

φ' = effective angle of shearing resistance

This equation can be illustrated by plotting the Mohr's circle, shown in Figure 24.

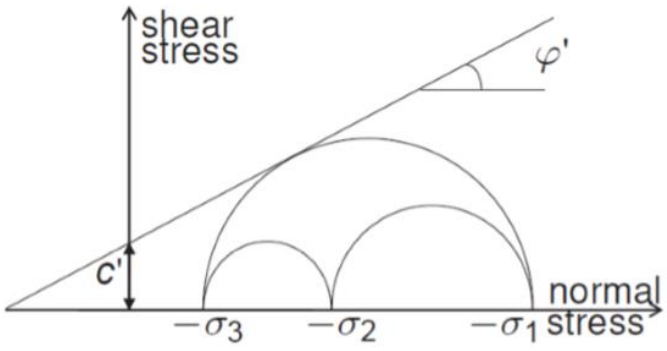

Figure 24 - Mohr-Coulomb criterion using drained (effective stress) strength parameters [29]

The Mohr's circle that touches the line defined by equation 3.1 represents the state of stress at yield or failure in the soil. The states of stress inside the yield surface are considered to be elastic. On the yield surface, hardening can occur which allows the yield surface to expand. In this thesis no hardening will be assumed, so the absolute plastic strain parameter, $\in_{p,}$ was set to zero. That means that the soil will be elastic-perfectly plastic. The parameters c' and ϕ' are not constant, and amongst other things they depend on the initial state of the soil and the applied loading [29].

In undrained analysis, the angle of shearing resistance of the soil is by definition zero and the Mohr-Coulomb criteria reduces to the special case of the Tresca model. In this model, the soil strength is described by the undrained shear strength, s_u or c_u, equation 3.2 [29]:

$$\tau = s_u \ (= c_u) \tag{3.2}$$

Another property of the undrained analysis is that the shear strength is independent of confining stress and the analysis is undertaken in terms of total stress. In undrained analysis, the pore water pressures are not known. Figure 25 represents the assumption made in terms of shear strength for an undrained analysis [29]. The failure envelope is determined by the cohesion only, which is equal to the undrained shear strength $s_{u.}$

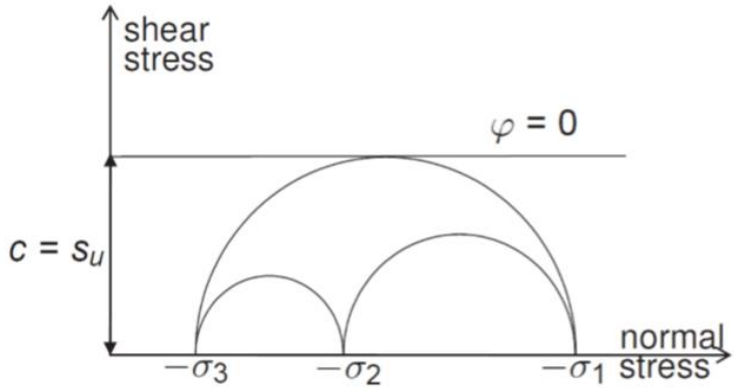

Figure 25 - Tresca criterion using undrained (total stress) strength parameters [29]

3.3 Ultimate capacity of a loaded pile anchor

The soil must be capable of carrying the loads applied on a pile anchor embedded in it without excessive deformation or shear failure. In this chapter, analytical methods for determining the bearing capacity of the soil under lateral or axial pile loads will be described and applied.

3.3.1 Ultimate bearing capacity: axial loaded pile anchor

For static axial pile capacity, a distinction can be made between end-bearing piles and floating piles. Floating piles effect the transfer of load to the ground primarily along the pile shaft, while for end-

bearing piles load is mostly transferred to the base. For the reason that a pile anchor is embedded in the soil, the floating piles are considered in this thesis.

Static pile capacity for compression loading can be defined by equation 3.3, Figure 26 [30]:

$$P_u = P_{pu} + \sum P_{si} \tag{3.3}$$

With,

P_u = ultimate pile capacity in compression

P_{pu} = ultimate pile tip capacity

P_{si} = skin resistance developing simultaneously with ultimate tip resistance P_{pu}

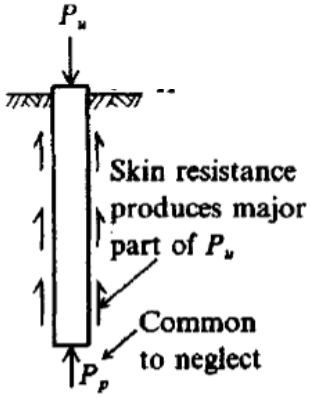

Figure 26 - Single pile 'floating' in soil mass [30]

Accordingly for a tension load like that shown in Figure 27, the following equation is obtained [30]:

$$T_u = W_p + \sum P_{si} \tag{3.4}$$

With,

T_u = ultimate pullout capacity

W = weight of pile being pulled

P_{si} = skin resistance developing simultaneously with ultimate tip resistance P_{pu}

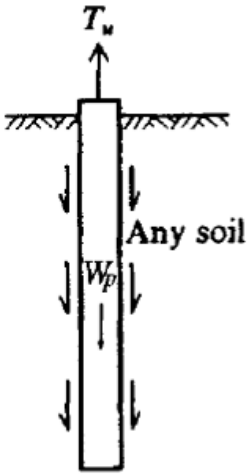

Figure 27 - Tension pile in soil mass [30]

The difference between compression and tension is that no base resistance is considered for tension capacity. Instead of the base resistance, the weight of the pile is taken into count in. The allowable anchor resistance is the characteristic anchor resistance at the pad eye divided by the material factor, equation 2.8, mentioned in Section 2.8.

3.3.1.1 Compression

a) Pile base resistance

The resistance mobilized at the pile base depends on the surrounding soil, the applied load, the length and the stiffness of the pile. There are numerous different methods to calculate the bearing capacity. Vesic [30] made a summary of the different theoretical solutions since 1940. Since that time the methods had several additional factors. One of the first bearing capacity equations was proposed by Terzaghi [30]. However, Terzaghi's bearing-capacity equations were intended for shallow foundations where the foundation depth, D is less than its breadth (width), B [30].

Then Meyerhof proposed a bearing-capacity equation similar to that of Terzaghi but included a shape factor s_q. He also introduced a depth factor and an inclination factor for inclined loads. So this method can be applied for deep foundations. Inclination factors cannot be used when $\phi = 0°$, because a base slip will occur. For a vertical load, the angle will be zero and all the inclination factors will be 1 [30].

Hansen modified the shape and depth factors. The Hansen equation can be used for shallow and deep foundations. Then Vesic gives almost the same equation like the Hansen equation. Some factors, like N_Y, are changed, but N_c and N_q stayed the same [30].

There are still other methods, but there's no special recommendation for the 'best' values to use. The end bearing capacity equations of Hansen can be written as [30]:

$$q_u = c\, N_c\, s_c\, d_c\, i_c\, g_c\, b_c + q'\, N_q\, s_q\, d_q\, i_q\, g_q\, b_q + 0.5\, \gamma B'\, N_\gamma\, s_\gamma\, d_\gamma\, i_\gamma\, g_\gamma\, b_\gamma \quad (3.5)$$

$$P_{pu} = A_p\, q_u \quad (3.6)$$

With,

c = the cohesion

q' = γL = vertical stress (at pile point)

N_i = the bearing capacity factors

s_i = the shape factors

d_i = the depth factors

i_i = inclination factors

g_i = ground factors

b_i =base factors

A_p = the area of pile point

For a pile, the N_γ factor is often neglected when the pile base is not too large. From the bearing-capacity examples in [30], it can be concluded that for a deep foundation in a cohesive undrained soil ($c = s_u$), for a pile with either a round or square base, the end bearing capacity is around nine times the cohesion. This value can change worldwide with local value from 7.5 to 11 [30].

The examples in [30] use either the Hansen or Vesic equations. The Terzaghi equation should give an end bearing capacity of 7.41 times the cohesion and Meyerhof's method should give a value of 25 times the cohesion. Clearly, this last method is not valid [30].

The calculations of the pile base resistance are given in Appedix A, Chapter 1.1.

b) Shaft resistance

The shaft resistance is calculated using either an effective stress or total stress approach based on the so-called β- and α-methods respectively. Broadly, the β-method can be used for granular soils and to a lesser extent clayey soils while the α-method is used for clayey soils alone. In all cases, the shaft resistance can be calculated as per equation 3.7 [30]:

$$P_{si} = \sum(P * (\Delta L) * f_s \quad (3.7)$$

With,

P = the perimeter of the pile

ΔL = length of the segment of the shaft passing through a particular layer

f_s = unit skin friction in each layer

Where, in the α-method,

$$f_s = \alpha s_{u,avg} \tag{3.8}$$

With,

α = an adhesion coefficient that depends on the pile type (displacement/replacement) and the undrained shearing resistance

$s_{u,avg}$ = the average undrained shear strength in a particular layer

And, in the β-method,

$$f_s = \beta.\sigma'_v = K_S.\sigma'_v.\tan\delta \tag{3.9}$$

With,

K_S = a coefficient that defines the horizontal effective stress acting on the pile shaft, and depends on the pile type (displacement/replacement)

σ'_v = the vertical effective stress

δ = the pile-soil interface friction angle

For this latter method, [30] makes the following assumptions:

- Soil remolding adjacent to the pile during driving reduces the apparent cohesion to zero;
- The effective stress acting on the pile surface after dissipation of excess pore pressures generated by volume displacement is at least equal to the horizontal effective stress ($K_{0.}\sigma'_v$) prior to pile installation;
- The major shear distortion during pile loading is confined to a relatively thin zone around the pile shaft, and drainage of this thin zone either occurs rapidly during loading or has already occurred in the delay between driving and loading.

Calculations for the shaft bearing capacity are given in Appendix A, Chapter A.1.2.

c) Total compression resistance

The total bearing capacity is equal to:

$$P_u = P_{pu} + P_{si} \tag{3.10}$$

With,

P_u = ultimate pile capacity in compression

P_{pu} = ultimate pile tip capacity

P_{si} = skin resistance developing simultaneously with ultimate tip resistance P_{pu}

The results of the total bearing capacity evaluation are given in Appendix A, Chapter A.1.3.

3.3.1.2 Tension

a) Shaft bearing capacity

The calculation of the shaft bearing capacity for tension is exactly the same as for compression [30]. Only the direction of loading will be different.

The results of the shaft bearing capacity are given in Appendix A, Chapter A.1.2.

b) Weight of the pile

The weight of the pile is calculated by equation 3.11:

$$W_P = \rho * \pi * r^2 * L * g \tag{3.11}$$

The results of the shaft bearing capacity are given in Appendix A, Chapter A.2.2.

c) Total static bearing capacity for tension

The total static bearing capacity is equal to:

$$T_u = W_p + \sum P_{si} \tag{3.12}$$

With,

T_u = ultimate pullout capacity

W = weight of pile being pulled

P_{si} = skin resistance developing simultaneously with ultimate tip resistance P_{pu}

The results of the total bearing capacity are given in Appendix A, Chapter A.1.3.

3.3.2 Ultimate static bearing capacity: lateral loaded pile anchor

The ultimate capacity of a laterally loaded pile can be calculated using the traditional technique of limit analysis. This technique is only possible within a nonlinear relationship between the soil resistance and the pile deflection along the length of the pile. The resistance of the soil along the pile depends on the settlement of the pile and is needed to solve the relevant equations. So iteration is needed to solve the equations [24].

Horizontally loaded piles can be defined as being actively or passively loaded. An active pile has most of the loads on its top, for example a pile supporting a bridge. Thereby the soil will resist the load. A passively loaded pile is a pile where the load imparted on the pile derives from the soil moving relative to the pile [24,31].

3.3.2.1 Reaction modulus

An important parameter from the soil around a laterally loaded pile is the reaction modulus, k. This parameter is defined as the ratio of the resistance from the soil at a point along the pile, p (kN/m) to the deflection, y (m) of the pile at the same point, equation 3.13 [24]:

$$k = p/y \tag{3.13}$$

Figure 28 (a) shows a section through a laterally loaded pile with a horizontal load p_t, deflection y_1, and depth below ground level, z_1. In Figure 28 (b) and (c) the horizontal stresses in the layer of the soil situated at a depth z_1 are shown for the situation before and after applying the lateral load respectively.

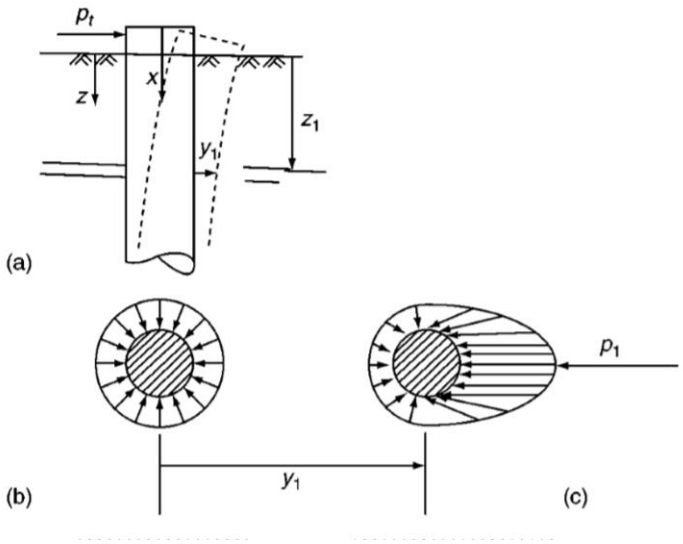

Figure 28 - A laterally loaded pile and the distribution of the unit stresses before and after applying the lateral load [24]

While applying a lateral load, the horizontal stresses on the side where the load is situated will decrease. The stresses on the other side will increase. The integration of the unit stresses will result in a reaction, p_1 (Figure 28 (c)) with an associated deflection y_1. p_1 is defined as the load per length along the pile which unit is N/m. y_1 stands for the deflection and is expressed in m. The slope of the secant of a p-y curve can be used to define the reaction modulus, Figure 29.

Between a and b in Figure 29 (a), the soil resistance is increasing at a decreasing rate while the deflection is increasing. This part of the curve represents the nonlinear portion of the in situ stress-strain curve. After this part, there is a linear near-horizontal curve where the soil resistance is fully mobilized and deflection increases dramatically. This part can be assumed to be perfectly plastic and can be used to calculate the ultimate resistance of the pile depending on the dimensions of the pile and the properties of the soil.

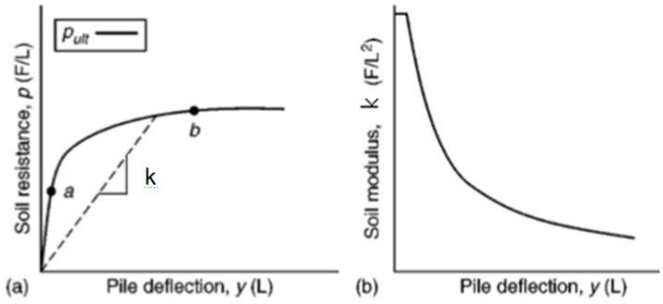

Figure 29 - Typical p-y curve and the resulting reaction modulus [24]

Figure 29 (b) illustrates the relationship between the reaction modulus k and the lateral deflection y. The reaction modulus k is constant at very small deflections however at larger defections the value of k steadily decreases.

In practice, the reaction modulus changes along the length of the pile. Compatibility between the pile deflection and the soil resistance will appear after iteration and will depend on the selected p-y curves, the dimensions of the pile and the properties of the soil [24].

3.3.2.2 Elastic models used for the analysis of lateral loads

Terzaghi [24] calculated deflection and bending moment using the subgrade modulus. According to the approach of Terzaghi, the calculation could not be used for lateral loads that result in a mobilized soil resistance of more than half of the bearing capacity of the soil [24].

Later, Poulos [24] has developed further the equations of a laterally loaded pile using the elastic model and some variations of it. Solutions have been obtained for different types of loading of single piles. This solution can't be used for larger deformations [24].

3.3.2.3 Plastic models used for the analysis of lateral loads

Broms [32] integrated a model with a rigid pile and plastic soil based on the ultimate bending moment. The ultimate lateral bearing capacity can be calculated by the equations of statics for the ultimate resistance. These equations are mentioned later in this chapter. The method of Broms can be used for piles with constant dimensions and soils with uniform characteristics. Engineers use this procedure to estimate the size and length of the pile [24].

Duncan et al. [24] developed the characteristic-load method for different soils with a nonlinear p-y curve and for different pile-head conditions. This method gives a fast solution of the response of piles under lateral loading. Both ground-line deflections and maximum moments can be calculated by this method [24].

3.3.2.4 Broms method for the analysis of laterally loaded piles

Broms method assumes that the pile is embedded in homogeneous soil. So the analysis does not allow for layered subsoil. The method can be used for short and long piles, for restrained- and free-headed piles, and for cohesive and cohesion-less soils. In this thesis, an undrained, cohesive soil will be analyzed with a Tresca failure criterion. Therefore, only the ultimate lateral load for piles in cohesive soil will be considered [24].

The difference between short piles and long piles is shown in Figure 30 where free-headed piles are considered. The short pile will act as one unit when a lateral load is applied and failure is governed by the soil strength. In contrast, the long pile will fail structurally through the formation of a plastic hinge with perhaps some local soil yield only. When a pile is defined as ‘restrained’, the head of the pile is considered to be fixed to prevent rotation [24].

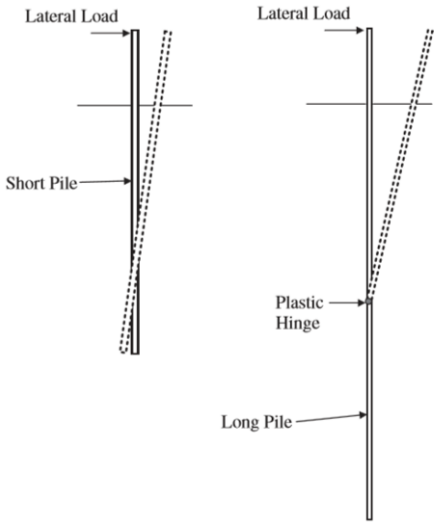

Figure 30 - The difference in behaviour between short and long laterally loaded piles [25]

A way to define the relative stiffness of the pile-soil systems is the classical Winkler solution. Therefore the reaction modulus of soil, k has to be calculated, e.g. by using equation 3.14 [30].

$$k = 0.65 \sqrt[12]{\frac{E\,B^4}{(EI)_f}} * \frac{E}{(1-\nu^2)} \tag{3.14}$$

With,

E = the soil modulus of elasticity

ν = the Poisson's ratio

$(EI)_f$ = the bending stiffness of the foundation

B = the width of the foundation or the diameter of the pile

The distinction between flexible, semi-flexible and rigid for a free-headed pile in uniform soil is determined by the parameter λL, equation 3.15 [30].

$$\lambda = \sqrt[4]{\frac{k}{4(EI)_f}} \tag{3.15}$$

A pile with λL larger than 3 is defined as a flexible, long pile, between 1 and 3 as a semi-flexible pile and smaller than 1 as a rigid pile. The calculations are given in Appendix B, Chapter B.1.

For a free-headed pile in a soil with a modulus of reaction increasing with the depth ($k = n_h x$), the distinction is determined by the parameter ηL, with η defined by equation 3.16 [30]:

$$\eta = \sqrt[5]{\frac{n_h}{E_p I_p}} \tag{3.16}$$

A pile with ηL larger than 4 is defined as a flexible, long pile, between 1.5 and 4 as a semi-flexible pile and smaller than 1.5 as a short, rigid pile. Also this calculations are given in Appendix B, Chapter B.1.

Another manner to know if the pile has to be defined as a long or short pile for soil with constant undrained shear stress is to compute the maximum moment (if it's considered a short pile) and the yield moment (if it's considered a long pile). If the resulting maximum moment is larger than the yield moment, the pile can be considered as a long pile. These calculations are given in Appedix B, Chapter 2.

If these two methods are compared, it is concluded that for both methods the piles with L/D-ratio 20 and 40 are long, flexible piles. The pile with a length of 10 m is a semi-flexible pile calculated with the first method and a short, rigid pile calculated with the second method because there is nothing defined between the short and long pile for the second method.

Broms states that for a pile in cohesive soil, static equilibrium can be demonstrated by accepting a uniform soil resistance along the length of the pile, p of $9c_ub$ (c_u is the undrained shear strength and b is the diameter of the pile). Near the surface, the soil resistance is ignored over a distance of 1.5b as shown in Figure 31. Because in that zone, the soil can move up and out when the pile is bending due to the lateral load. Therefore it would give no resistance anymore and can be ignored [24].

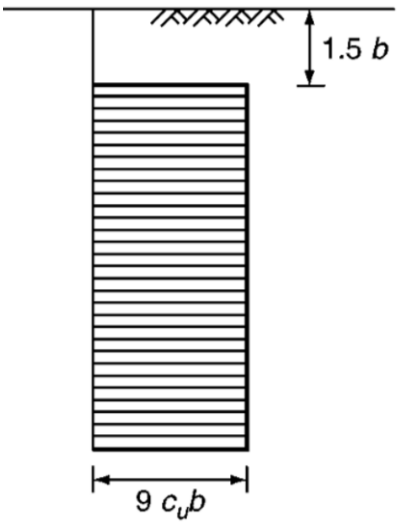

Figure 31 - Distribution of soil resistance along the pile in uniform cohesive soil [24]

Figure 32 presents the soil resistance, shear force and bending moments of a short free-headed pile:

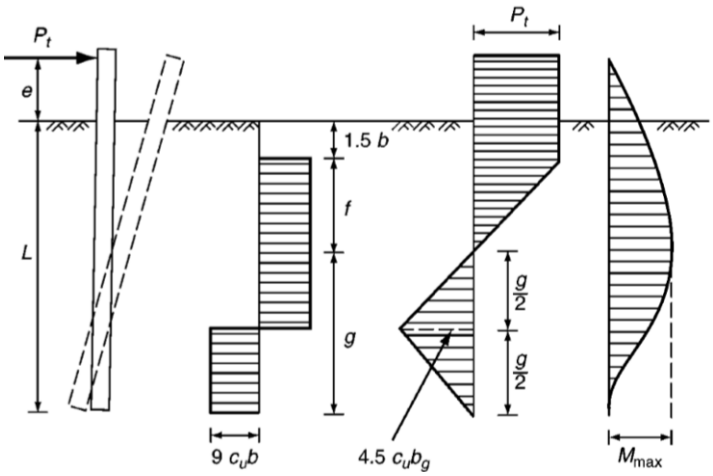

Figure 32 - Soil resistance, the shear and the moment of a short free-headed pile embedded in uniform cohesive soil [24]

Figure 32 shows that the shear force will reach a maximum at the depth where the cross-over point is situated in the failure state. At the depth where the shear force is zero, the bending moment will reach its maximum value. The maximum bending moment can be written by integrating the upper part of the shear diagram to the point where no shear force is, the point of the maximum moment [24]:

$$M_{max}^{pos} = P_t\,(e + 1.5b + f) - \frac{9\,cu\,b\,f^2}{2} \tag{3.17}$$

Another way to define the maximum moment is by integrating the lower part of the shear diagram to the point of zero shear force [24]:

$$M_{max}^{pos} = \frac{4.5\ cu\ b\ g^2}{2} \tag{3.18}$$

The distance f where the shear force is zero is calculated in 3.19 [24]:

$$Pt - 9\,c_u\,f\,b = 0 \tag{3.19}$$

$$f = \frac{Pt}{9\,b\,cu} \tag{3.20}$$

With this formulation of f, the first equation of the maximum moment can be written as [24]:

$$M_{max}^{pos} = P_t\,(e + 1.5b + 0.5f) \tag{3.21}$$

To obtain the ultimate lateral bearing capacity, the distance g has also to be rewritten in function of some known parameters, equation 3.22 [24].

$$g = L - 1.5b - f \tag{3.22}$$

For piles that can be considered to be long and flexible, at failure, a plastic hinge will occur at a depth of 1.5b+f as shown in Figure 33. The failure state occurs when the yield stress of the steel is reached over the entire cross-section.

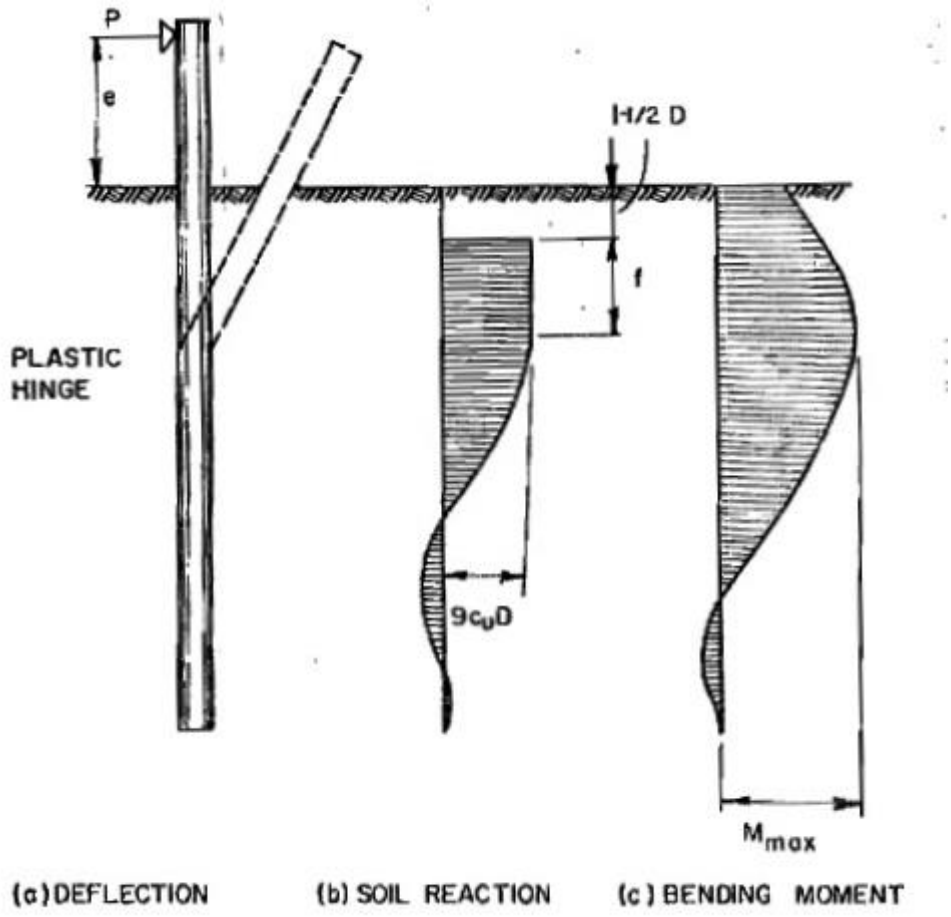

Figure 33 - The deflection, soil reaction and bending moment for long laterally loaded, free-headed piles in uniform cohesive soils [32]

The ultimate lateral load can be solved directly with equation 3.23 [24].

$$M_{max}^{pos} = P_t\,(e + 1.5b + 0.5f) \qquad (3.23)$$

The maximum moment in this equation is equal to the yield moment:

$$M_Y = f_y\,S_e \text{ and } S_e = \frac{\pi\,(d_2^4 - d_1^4)}{32\,d_2} \qquad (3.24)$$

With,

f_y = the specified minimum yield stress = 355MPa (HS: high strength steel) [7]

S_e = the elastic section modulus

d_1 = the inner diameter of the hollow steel pile

d_2 = the outer diameter of the hollow steel pile

Figure 34 shows the graphs derived from the above relationships and used to get the ultimate lateral load for free-headed piles embedded in cohesive soil.

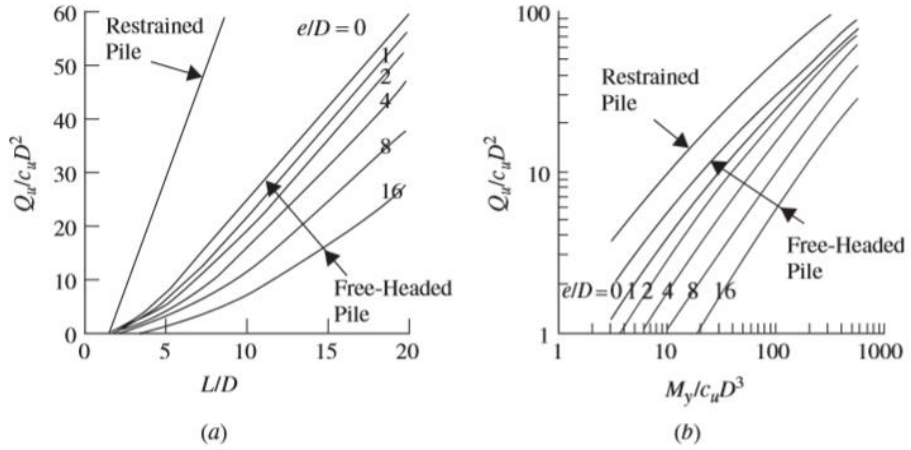

Figure 34 - Broms method solution for free-headed piles embedded in uniform cohesive soil: (a) short piles, (b) long piles [25]

In Figure 34 (a) the L/D-ratio is acting as a function of the normalized ultimate lateral force Q_u/c_uD^2 for different e/D-ratios. The ultimate lateral load of long piles can be derived from graph (b). This graph relates the normalized ultimate lateral force Q_u/c_uD^2 to the normalized yield moment of the pile M_Y/c_uD^3 for various e/D-ratios [25].

3.3.2.5 Modified method for the analysis of laterally loaded piles

In [31], another method to obtain the ultimate bearing capacity based on a modified version of Broms method is presented. The difference is that in the modified method, the distribution of soil resistance is defined in another way.

In Figure 35 the distribution of soil resistance for the Broms method is presented in blue. The black striped area shows the modified distribution with soil resistance that increases from $2c_u$ at the ground surface to $9c_u$ at a depth of three times the pile diameter, d. Figure 36 shows the soil resistance according to the modified method for short and long piles.

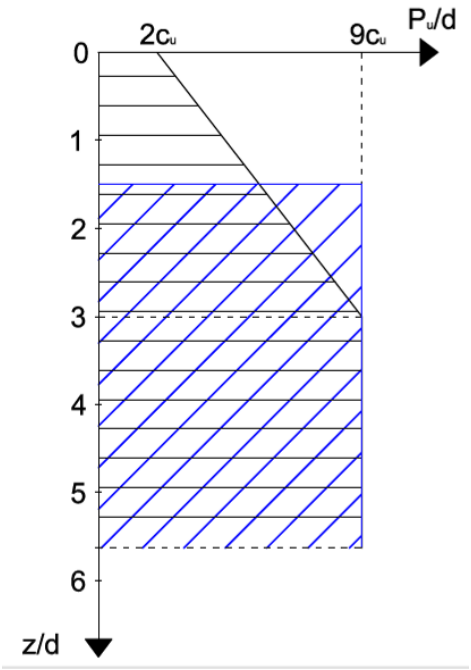

Figure 35 - The distribution of the soil resistance of the Broms and the modified method

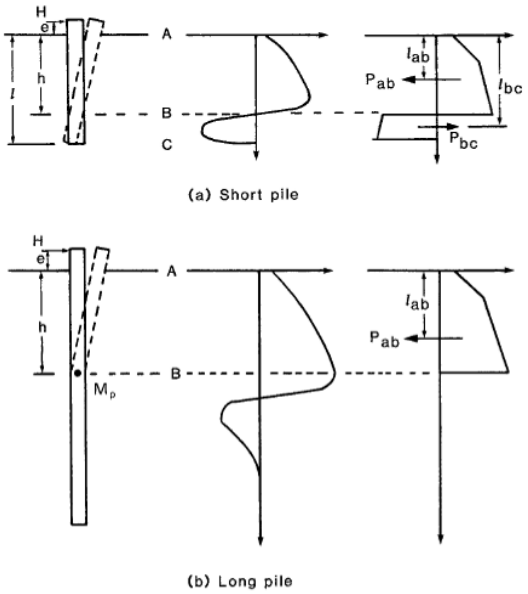

Figure 36 - The soil resistance for short and long piles according to the modified method [31]

As in Broms method, the short piles and piles with a large plastic moment are considered as a rigid body. Passive pressure will occur in front of the pile above the plastic hinge. In contrast, below the plasic hinge, passive pressures will develop behind the pile. For a long pile, only the upper part will be affected by displacements [31].

To calculate the ultimate bearing capacity, only the part above the plastic hinge of the long pile will be considered. That's why only the upper part is idealized for the calculations. The limiting pressure goes from the full limiting pressure just above the plastic hinge to zero just below it. For short piles it goes from the full limiting pressure in front of the pile to the full limiting pressure behind the pile. According

to Figure 36, the horizontal equilibrium, equation 3.25, and moment equilibrium, equation 3.26, at point B for short piles can be written as [31]:

$$H_f = P_{ab} - P_{bc} \tag{3.25}$$

$$H_f\,(e+h) = P_{ab}\,(h-l_{ab}) + P_{bc}\,(l_{bc}-h) \tag{3.26}$$

By these two equations, the ultimate lateral bearing capacity H_f can be found. In contrast with the method of Broms, the plastic hinge will be considered at the point of maximum bending moment and zero shear stress which is point B in Figure 36 [14].

To calculate the bearing capacity for the long piles, the moment in point B should be set equal to the yield moment of the piles section. The pressure under the plastic hinge can be ignored. So the horizontal equilibrium, equation 3.27, for long piles is equal to [14]:

$$H_f = Pab \tag{3.27}$$

The moment in B is:

$$H_f\,((e+h) - (h-l_{ab})) = H_f\,(e+ l_{ab}) = M_{\gamma} \tag{3.28}$$

Chapter 4

Simulations Abaqus

The numerical simulation of the pile anchors was carried out using the finite element program Abaqus. In this chapter, several parameters are defined from the soil and the steel of the pile. After, the kind of interaction between the two is explained. Finally, the boundary conditions and the mesh of the two-dimensional and the three-dimensional model are mentioned.

4.1 Introduction

The aim of this thesis is to analyze the reactions of the soil on a pile anchor for a floating OWT using finite element analysis (FEA). The structure will be simulated as an elastic steel pile.

As a verification study, an elastic model of the pile was analyzed – this enabled the application of the software to be understood and allowed the results to be compared with some theoretical results to check the validity of the computational model. Subsequently, the response of the pile was examined allowing soil plasticity to occur Chapter 5.

The numerical simulation was carried out using the finite element program Abaqus Version 6.14 [28]. This is a tool that can be used to calculate forces, deformations, stresses and strains of a structure.

For the analyses undertaken for this thesis, both two-dimensional (2D) and three –dimensional (3D) piles with different dimensions were simulated. The dimensions of the pile are expressed in terms of the length to diameter ratio, L/D. The L/D-ratios considered here are 10, 20 and 40. Since the diameter of the pile is constant and equal to 1 m, the length of the pile was defined by the L/D-ratio.

Generally, the wall thickness of a pile will vary along its length [36]. The pile should be thicker near where the bending moments reach their maximum. A typical pile diameter, d, to wall thickness, t, ratios vary from 30 to 50 [36]. In this thesis, the smallest thickness, 20 mm, is used for the pile. That results in a d/t-ratio of 50.

In reality, anchor piles are hollow steel piles situated in the seabed. To make the simulation easier, the piles were represented by solid elements with stiffness properties of the solid elements adjusted in order to provide a similar bending stiffness to a hollow steel pile. The calculation of this effective E-modulus is described in Section 4.2. In addition, an effective density of the model pile was also evaluated and is described in Section 4.2.

2D axi-symmetric elements can be used when the geometry and the loads have rotational symmetry such as was the case for axial compression and tension loading of the pile. To create the 3D models used in this thesis, the 2D model was revolved around the symmetry axis.

Except for angles and rotations, the units in Abaqus are not defined. That means that the units have to be determined and have to fit with each other. In these simulations, the International System of units (SI) has been used, Table 7.

Table 7 - SI-units used in the Abaqus-simulations

Quantity	SI	Quantity	SI
Length	m	Force	N
Mass	Kg	Time	s
Stress	Pa (N/m^2)	Density	kg/m^3

4.2 Steel parameters

As mentioned in Section 4.1, the model pile consisting of solid elements has to have the same bending stiffness as the hollow anchor pile it represents, Figure 37. The stiffness of the pile depends on the flexural stiffness EI where E is the elastic (Young's) modulus and I the geometrical moment of inertia, also called the second moment of area. The second moment of area is a geometrical property of a section which shows how its shape is distributed with respect to an arbitrary axis.

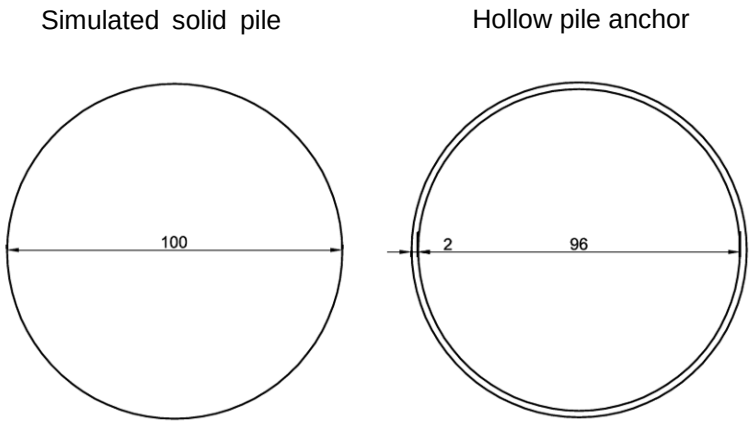

Figure 37 - The dimensions of the simulated solid pile and the hollow pile anchor

The flexural stiffness EI of a hollow anchor pile:

$$E_h = 210 \text{ GPa} = 210 \text{ kN/mm}^2 = 210 * 10^9 \text{ N/m}^2 \quad (4.1)$$

$$I_h = \frac{\pi (D^4 - d^4)}{64} = \frac{\pi ((1)^4 - (0.96)^4)}{64} = 0.0074 \text{ m}^4 \quad (4.2)$$

$$EI = 210 * 10^9 \text{ N/m}^2 * 0.007395 \text{ m}^4 = 1.55 * 10^9 \text{ Nm}^2 \quad (4.3)$$

Calculation of the Young's-modulus for the solid pile to obtain the same stiffness as the hollow anchor pile:

$$I_s = \frac{\pi D^4}{64} = \frac{\pi (1)^4}{64} = 0.049 \text{ m}^4 \quad (4.4)$$

$$E_s = \frac{Eh\ Ih}{Is} = \frac{1.55*10^9}{0.049} = 3.16 * 10^{10}\ N/m^2 \quad (4.5)$$

There has to be mentioned that also the axial stiffness, EA will be difference for the solid pile. For the hollow steel pile the axial stiffness, E_hA_h will be 1.65 * 10^{11} and for the solid pile, the axial stiffness E_sA_s will be equal to 1.95 * 10^9.

Besides the Young's-modulus, the steel is defined by another parameter, Poisson's ratio, ν. This parameter describes the expansion of material in two directions when it is compressed in the third direction. So it is the ratio of relative contraction to relative longitudinal extension in the direction of stretching force. This value is defined between -1 and 0.5. The value used for the steel in the models presented in this thesis is 0.2.

The last parameter for the steel pile is the density. The density of steel is generally 7850 kg/m³. To simulate the hollow steel pile with the soil inside, the density of the solid steel pile in Abaqus was changed. The density is calculated as following:

$$\rho = \frac{\rho steel * Vsteel + \rho soil * Vsoil}{Vsolid} \quad (4.6)$$

With,

ρ_{steel} = 7850 kg/m³

ρ_{soil} = 2000 kg/m³

V_{steel} = the volume of the hollow steel pile

V_{soil} = the volume of the soil in the hollow steel pile

V_{solid} = the volume of the solid simulated pile

$$\rho = \frac{7850\ (\pi\ (0.5)^2 - \pi\ (0.48)^2\ )10 + 2000\ \pi\ (0.48)^2\ 10}{\pi\ (0.5)^2\ 10} = 2459\ kg/m^3$$

4.3 Pile-soil interaction

To define the interaction between the soil and the pile, within Abaqus there are two different modules: the interaction module and the constraint module. Both of these modules use the master-slave-principle for the contact definition. That means that in the analyses, the master surface can penetrate unhindered in the slave surface but the slave surface is not able to penetrate in the master surface.The master surface of a surface-to-surface contact is the largest of two deformable surfaces. If that distinction cannot be made, then the master surface is the surface of the stiffer body. In the case of the pile and the soil, the pile was considered the master surface [28].

4.3.1 The interaction module

The first and most commonly used module is the interaction module. This module defines different types of interaction. In this model, the surface-to-surface contact is used. This contact interaction describes contact between two deformable surfaces, like the soil and the pile.

An interaction property is a set of data that is referred to by an interaction, but it is independent of the interaction. There are also different types of interaction properties. In this case, the contact interaction is defined. Within this property, there are different behaviours to define. For the two models the tangential behaviour and the normal behaviour are defined [28].

In the elastic and Tresca model, the friction formulation is rough. This formulation specifies an infinite coefficient of friction that prevents all the relative sliding motion between the contacting surfaces. The normal behaviour can be hard, soft or damped contact. For the entire model, the normal behaviour is defined by hard contact which means that the penetration of the slave surface into the master surface is minimized at the constraint locations [28].

4.3.2 The constraint module

The other module that is able to define interactions is the constraint module. With this module, the degrees of freedom between regions can be constrained. Within this module there are different types of constraint. The most common one is the tie constraint. With this type, two surfaces are tied together so that there is no relative motion between them. As a result, this type of interaction is similar to the interaction defined by the interaction module with a rough contact. The similarity is proven in Chapter 5.

4.4 The boundary conditions

The 2D model has two different boundary conditions as presented in Figure 40. The first one is situated on the bottom of the mesh, where movement in the x- and y-direction is constrained. On the side boundary, only the degree of freedom from the x-axis is set to zero.

For the 3D model, the boundary conditions are similar. Movement of the bottom is fixed in all directions, the x-, y- and z-direction. On the side that represents the lateral extent of the model, the degrees of freedom of the x- and z-direction are zero. Finally, the symmetry of the half of the cylinder has to be defined. As Figure 41 shows, the model is z-symmetric. Therefore the displacement in the z-direction and the rotation in the x- and y-direction will be prevented.

4.5 Meshing the structure

The element type for the soil in the 2D simulation, Figure 40, was first chosen to be CAX4R. Where the C stands for continuum stress/displacement, AX for axi-symmetric, 4 for the number of

nodes and R for reduced integration. Later, a quadratic element (CAX8R) was used because these elements gave a better result, Figure 38.

Figure 38 - The difference between linear and quadratic elements [28]

A linear (4-node) element uses first-order interpolation while quadratic (8-node) elements use second-order interpolation. In first-order elements, a constant volumetric strain is considered throughout the element. This option prevents mesh 'locking' when the material response is incompressible. The second-order elements have a higher accuracy when the problem doesn't involve a lot of distortion [28]. This option is better for modelling geometric features because you can model a curved surface with fewer elements. Finally, second-order elements are more effective to simulate bending moments [28].

The element type used for the 3D simulations is C3D8R, as in Figure 39. This code is standing for a 3D continuum element with 8 nodes and reduced integration.

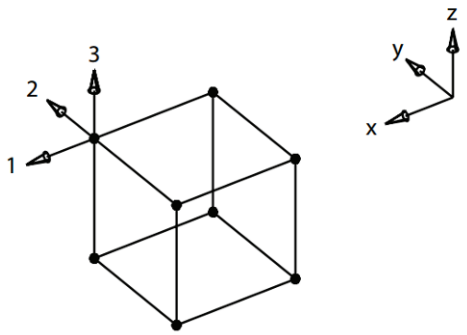

Figure 39 - C3D8-element with degrees of freedom and global coordinate system [33]

In a 3D model, each node has three degrees of freedom. These are shown in Figure 39 together with the global coordinate system (x,y,z). Elements with 8 nodes, have nodes only at their corners. They use linear interpolation in each direction and are often called linear elements or first-order elements like the 4-node elements in the 2D model [28]. These linear elements are used for the 3D models instead of the quadratic element because they give faster run times.

Solid elements are the standard elements of Abaqus, they can be used for both linear and complex nonlinear analyses involving contact, plasticity, and large deformations. The reduced integration option uses a lower-order integration to model the element stiffness. Due to this, the run time is reduced.

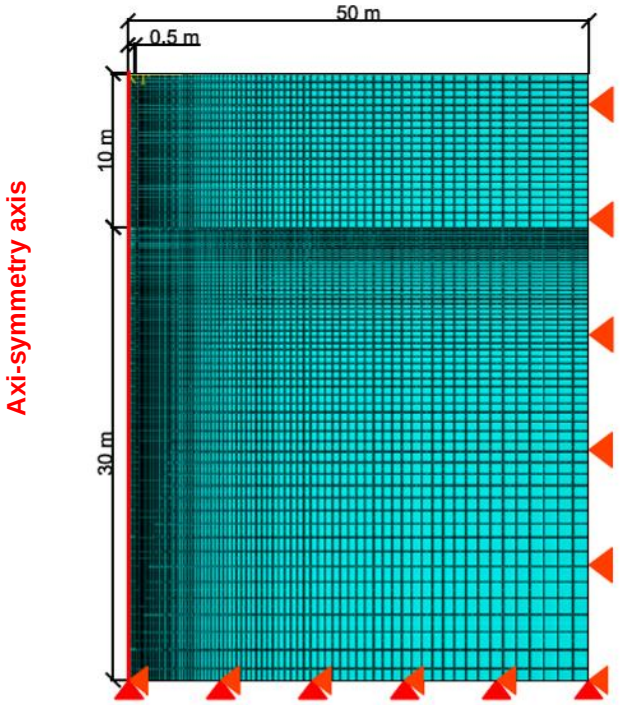

Figure 40 - The mesh of the 2D model with L/D-ratio 10

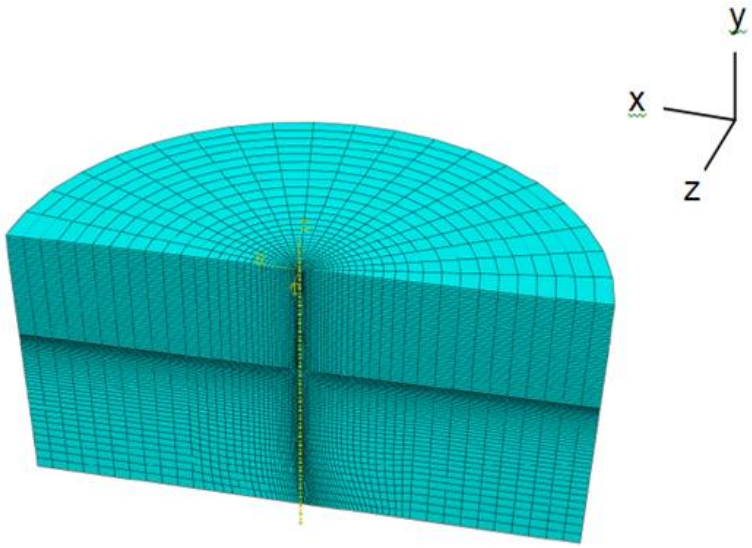

Figure 41- The mesh of the 3D model with L/D-ratio 20

Chapter 5

Elastic model

To verify the elastic pile model, the results of the elastic FEM are compared with the theoretical results from '*Pile foundation analysis and design'* [38]. Firstly this chapter provides an overview of the different parameters used for the elastic model, then the calculation of the theoretical settlement based on [38] is discussed and compared to the FEM results. Finally, a comparison between the constraint and the interaction contact definitions used to describe contact behaviour in Abaqus is made and discussed.

5.1 Parameters

In this part, an elastic model of a pile embedded in soil is simulated in Abaqus. This model is compared to a theoretical model [38]. To optimize the comparison, the parameters used in the FEM were chosen in order to minimize the interpolation needed within the graphs in [38].

5.1.1 Soil parameters

The soil is assumed to be elastic. The main property of an elastic model is that the stress is directly proportional to the strain. This is called Hooke's law. The elastic properties can be described by two parameters: the Young's modulus, E and the Poisson's ratio, ν. Hooke's law does not fit with the real behaviour of soil because soils are neither linear-elastic nor isotropic. Nevertheless, sometimes it can be useful to idealize soils as having a linear behaviour. In that way Hooke's law can be used to estimate the strains associated with the applied stresses.

A feature of this theory is that the principle of superposition is valid. Thus, if two or more loads are applied to the foundation, the stresses due to each load can be added. Finally, no gravity and no initial stress need be assumed [15].

After calculation with models of different dimensions, it was found that a distance from the pile toe to the bottom of the mesh representing the soil, of 30 times the pile diameter was enough to avoid a significant distortion of the calculation results. This was also the case for a mesh radius of 50 times the pile diameter. In Figure 42, the model is shown with these dimensions. Table 8 summarises the overall finite element mesh dimensions for each pile length to diameter ratio considered in this study. These dimensions are used for the 2D and 3D models for both the elastic and elasto-plastic analyses. The boundary conditions and the type of elements are discussed in Chapter 4.5 and 4.6.

Table 8 - Overall dimensions of finite elment mesh (soil part) used in the simulations

L/D-ratio	Length of the pile, L	Radius of the mesh	Depth of the soil (L + 30D)
10	10 m	50 m	40 m
20	20 m	50 m	50 m
40	30 m	50 m	60 m

The soil has to be an ideal homogeneous isotropic elastic continuum. The mass density of the soil, ρ, is defined 2000 kg/m³.

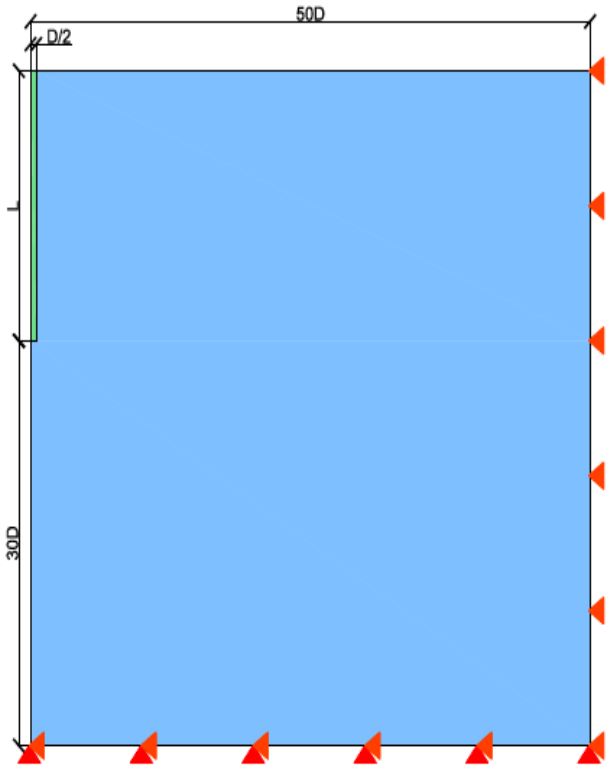

Figure 42 - Radial dimensions for 2D & 3D FE pile models

The Young's modulus of the soil is based on [39], Table 9.

Table 9 - Typical values of Young's modulus for clays [16]

Description	Soft (MPa)	Medium (MPa)	Stiff (MPa)	Hard (MPa)
Clays with low plasticity	1.5-6	6-10	10-30	30-60
Clays with medium-low plasticity	0.5-5	5-8	8-30	30-70
Clays with high plasticity	0.35-4	4-7	7-20	20-32

A value for the Young's modulus for the soil of 40 MPa was chosen for the analyses reported here. Therefore, arccording to Table 9, the model could be considered to be representative of a hard clay of low to medium plasticity. Poisson's ratio, v was assigned a value of 0.495. The theoretical meaning of the Poisson's ratio is explained in Chapter 4.2; a value of 0.5 means that the volume is unchanged during the deformation. The soil was assume to behave in an undrained manner however, to avoid numerical problems with a value slightly lower than 0.5, i.e. 0.495 is recommended.

5.1.2 Steel parameters

As mentioned in Section 4.2, all the simulations assume a solid steel pile with a diameter of 1 m and the length of the pile depends on the L/D-ratio. The effective density of the pile is 1458.64 kg/m³ and the Poisson's ratio is 0.2.

In the solution provided in [38], the parameter K is the pile stiffness factor and defines the relative compressibility of the pile with respect to the soil, equation 5.1.

$$K = \frac{E_p R_a}{E_s} \tag{5.1}$$

For a solid pile the area ratio, Ra is equal equal to 1. Based on the effective pile Young's modulus.

$$K = \frac{Ep\ Ra}{Es} = \frac{31.6 * 1}{40} = 790 \tag{5.2}$$

However, to reduce the possible errors deriving from interpolation of the graphs in [38], for this set of analyses E_p was increased to 40 GPa. Thus,

$$K = \frac{Ep\ Ra}{Es} = \frac{40 * 1}{40} = 1000 \tag{5.3}$$

5.1.3 Pile-soil interface

In an elastic model, no slip occurs at the pile-soil interface. The movements of the pile and the adjacent soil must be equal. Due to this fact, the pile-soil contact properties of the elastic model were selected as:

- Tangential behaviour: rough contact (no relative movement)
- Normal behaviour: hard contact (no separation)

The meaning of these properties was discussed in Chapter 4.4.

5.2 Calculation of the theoretical settlement of the pile

According to [38], in the calculation of the settlement of an incompressible pile there are two different cases to be considered: floating (or friction) piles and end-bearing piles. As mentioned in Chapter 3.2.1, this study considers a floating pile. Thus, from [38], the settlement of an elastic floating pile is calculated with Equation 5.4:

$$\rho = \frac{P\ I}{Es\ d} \tag{5.4}$$

With,

$I = I_0 R_K R_h R_v$ (5.5)

ρ = settlement of pile head

P = applied axial load

E_s = the Young's modulus of the soil

d = the diameter of the pile

I_0 = settlement-influence factor for incompressible pile in semi-infinite mass, for v_s= 0.5

R_K = correction factor for pile compressibility

R_h = correction factor for finite depth of layer on a rigid base

R_v = correction for soil Poisson's ratio v_s

h = total depth of soil layer

The comparison with the FE model was made with loads of 100 kN and 400 kN. The load was applied as a pressure acting across on the top surface of the pile. Thus, the applied pressures used in the 2D and 3D models were 127324 N/m^2 and 509297 N/m^2, respectively.

5.2.1 The settlement-influence factor, I_0

The parameter I_0 is obtained from Figure 43 [38] which suggests that for a pile of given diameter and all other things remaining equal, the settlement of a pile decreases as the length of the pile increases. An enlarged base will also decrease the settlement, although this effect is only significant for short piles (piles with low L/D ratios).

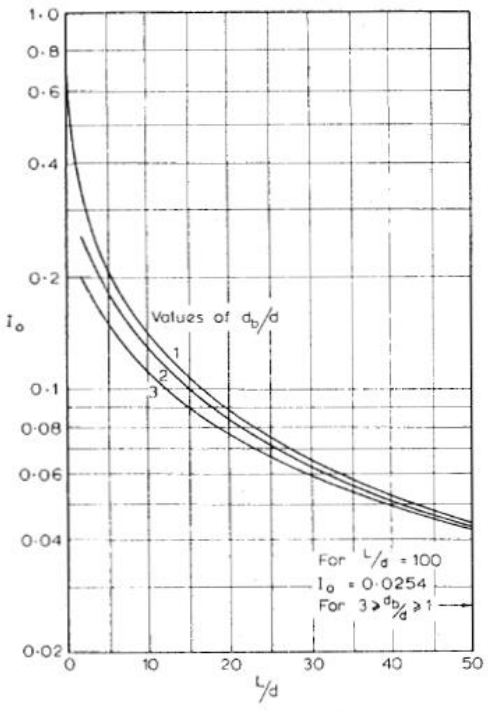

Figure 43 - Settlement-influence factor, I_0 [38]

In this chart, d_b presents the diameter at the base of the pile and in the elastic model the diameter is constant over the length of the pile, so the d_b/d ratio is 1. For each of the L/D ratios considered, the values for the influence factor I_0 in Table 10 were obtained.

5.2.2 Compressibility correction factor, R_K

The correction factor for pile compressibility, R_K is given by Figure 44 where it is clear that increasing pile compressibility and greater pile lengths, lead to an increase in the settlement at the pile head due to elastic shortening effects in the pile shaft.

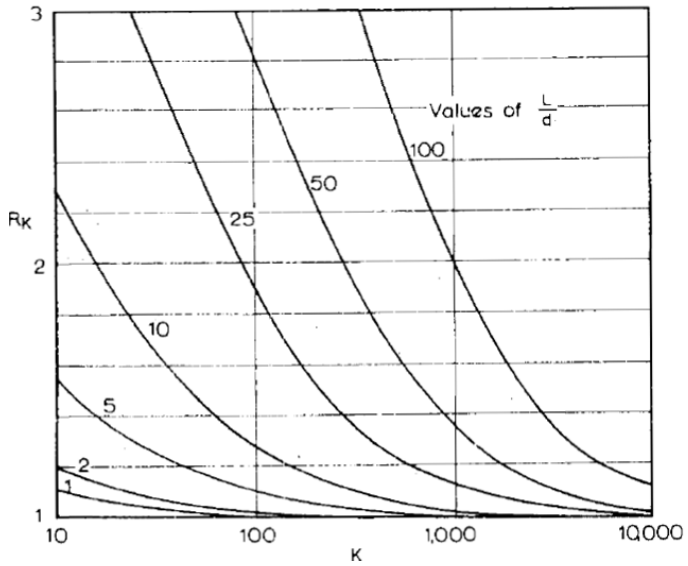

Figure 44 - Compressibility correction factor for settlement, R_K [38]

For the analyses undertaken here, the L/d-ratio varies and the stiffness of the pile was set to yield a value of K of 1000 (Section 5.1.2). Following Figure 44, the R_K- factors are as summarized in Table 10.

5.2.3 Layer thickness correction factor, R_h

The thickness correction factor, R_h given by Figure 45 is dependent on the L/d-ratio and the h/L or L/h-ratio where h is the total thickness of the soil layer. This correction implies that as the thickness of the soil layer reduces, the pile settlement will also reduce. Based on the parameters selected for this study and where h = (L + 30d), the values of R_h tabulated in Table 10 were obtained.

Table 10 - I_0, R_K and R_h for every L/D-ratio

L/D-ratio	I_0	R_K	h	L/h	R_h
10	0.1440	1.015	40	0.25	0.8920
20	0.0883	1.114	50	0.40	0.8460
40	0.0538	1.267	70	0.57	0.8460

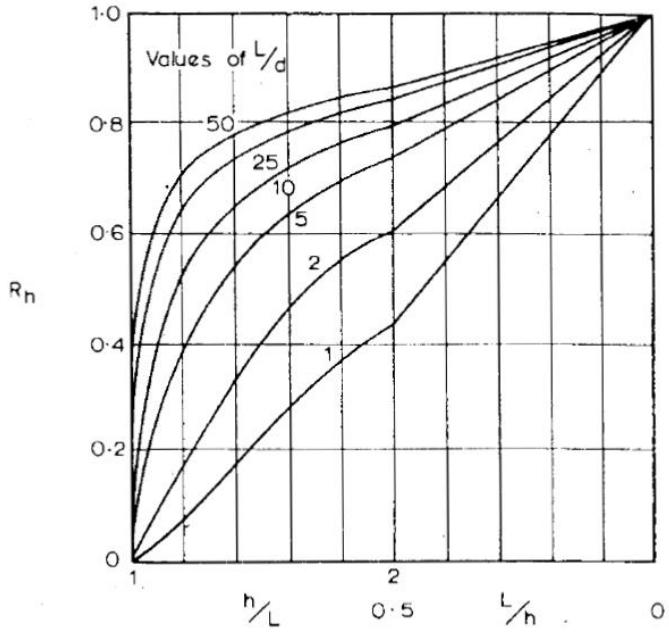

Figure 45 - Depth correction factor for settlement, R_h [17]

5.2.4 Poisson's ratio correction factor, R_v

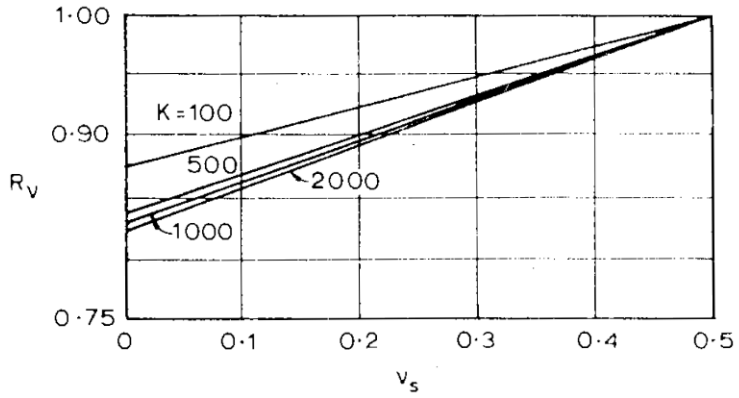

Figure 46 - Poisson's ratio correction factor for settlement, R_v [17]

For this set of analyses, with K equal to 1000 and v_s equal to 0.5, the correction factor R_v has a value of 1 for all the models, Figure 46. The figure implies that a decrease of the Poisson's ratio leads to a small decrease in the settlement.

5.2.5 The settlement of the pile head

With the various parameters for equation 5.4 defined it is now possible to evaluate the pile settlement according to [17], i.e. for an L/D-ratio of 10:

$$I = I_0 R_K R_h R_v = 0.144 * 1.015 * 0.892 * 1 = 0.1304$$

The settlement for a load of 100kN is:

$$\rho = \frac{P\ I}{Es\ d} = \frac{100 * 0.130}{40 * 1} = 0.3250 \text{ mm}$$

and for a load of 400kN, it will be:

$$\rho = \frac{P\ I}{Es\ d} = \frac{400 * 0.130}{40 * 1} = 1.300 \text{ mm}$$

The theoretical settlement for the all L/D-ratios considered is summerized in Table 11:

Table 11 - Theoretical pile settlement

L/D	I, -	Settlement, mm	
		100 kN	*400 kN*
10	0.1304	0.325	1.300
20	0.0832	0.208	0.832
40	0.0577	0.144	0.577

5.2.6 Comparison with the simulated elastic model

Because a uniform pressure was used to represent the load at the pile head, the settlement predicted at each node on the pile head differed slightly (at about the 6th or 7th decimal place) and so an average value of the vertical displacements (U2) is reported here. Table 12 provides a summary of the results in terms of the predicted settlements, the difference between the FEA and [38] and between the two types of FEA; 2D versus 3D.

Table 12 - Comparison of calculated pile settlements

Pile load, kN	L/D	Pile head settlement, mm (%-difference with [38])			%-difference 2D-3D
		[38]	2D-FEA	3D-FEA	
100	10	0.325	0.333 (+2.5%)	0.298 (-9.1%)	-11%
	20	0.208	0.213 (+2.4%)	0.214 (+2.9%)	+0.5%
	40	0.144	0.149 (+3.5%)	0.142 (-1.4%)	-4.7%
400	10	1.300	1.332 (+2.5%)	1.262 (-2.9%)	-5.3%
	20	0.832	0.854 (+2.6%)	0.854 (+2.6%)	0.0
	40	0.577	0.594 (+2.9%)	0.586 (+1.6%)	-1.3%

The difference between the FEA and [38] and between the 2D and 3D model can be declared by the type of elements used in the models. For the 2D model, there's used a quadratic element, in contrast to the 3D element which is linear. The difference between these two elements was explained in Chapter 4.6.

Another conclusion is that the smaller the elements, the better the results, however they lengthen the run time. A good equilibrium between the run time and the quality of the obtained values is a requirement. Taking these conclusions into account, the simulated models can be used further to analysis the reaction of the soil.

5.3 Comparison between rough contact and constraint

Within the interaction module with the contact interaction property, the tangential behaviour can be defined by a rough contact. This means that the adhesion is infinite, so there is no relative sliding motion between the two contacting surfaces.

It is also possible to define a tied contact in the constraint module. Due to this contact, two surfaces are tied together. Relative sliding motion between the two contacting surfaces is also impossible in this case.

To prove the similarity between these two kinds of interaction, there are created two different elastic models. The first is defined as a rough contact; the second one has an interaction defined by the tied contact of the constraint module.

The average settlement predicted by both approaches to define the pile-soil interface was equal and it was concluded that the interaction definitions are effectively equivalent. In this thesis, the rough contact was used.

Chapter 6

Tresca model

The Tresca failure criterion is widely used to simulate the undrained behaviour of soil. Since the beginning of the finite element method a lot of geotechnical analyses are carried out with this model. The first chapters explain the parameters assigned to represent the soil and the steel. After the load-displacement graphs are discussed. In Section 5, the laterally loaded piles are compared with theoretical methods. Finally, the combined loads are examined.

6.1 Soil parameters

For undrained clays, it is favourable to use the total stress analysis, for which the Tresca criterion could be used. This criterion is identical to the frictionless Mohr-Coulomb criterion. The Tresca failure criterion for a cohesive soil can be written in the form:

$$\tau = s_u \ (= c_u) \tag{6.1}$$

Where τ is the value of the shear stress on a failure plane and c_u is equal to the undrained shear strength.

In Abaqus, the Tresca failure criterion was implemented using the Mohr-Coulomb plasticity model with the angle of shearing resistance, $\varphi = 0°$, the dilation angel, $\Psi=0°$ and $c = c_u$ [28]. Two modelling assumptions were made regarding the vairation of undrained shear strength, c_u and Young's modulus, E_u as follows.

6.1.1 Soil Model 1: constant cohesion

In this model, the undrained shear strength of the soil is assumed to be constant and is equal to 60 kPa. In this model the density of the soil, Poisson's ratio and Young's modulus are the same as used in the elastic model presented in Chapter 5, 0.495 and 40 MPa respectively.

The value of the reaction modulus is calculated by the Vesic method and is equal to 20 MPa, Appendix B, Section B.1.1.

6.1.2 Soil Model 2: varying cohesion

In Soil Model 2, the undrained shear strength, c_u is assumed to increase with depth. At the ground surface, the undrained shear strength has a value of 5 kPa and it increases at a rate of 1.5 kPa/m with depth. In Abaqus, it isn't possible to enter a linear varying undrained shear strength and so the soil part was split into 5 m vertical intervals and for each layer, the average undrained shear strength has been assigned. In Table 13, the values of the undrained shear strength and Young's modulus, E_u assigned to each layer are presented. The Young's modulus has been assigned on the basis of the ratio $E_u/c_u = 500$. Soil density and Poisson's ratio again remain the same as used in the elastic model.

The value η is calculated from the slope of the reaction moduli and is for the L/D-ratio 10, 20 and 40 equal to 0.162, 0.203 and 0.243 respectively, Appendix B, Section B. 1.2.

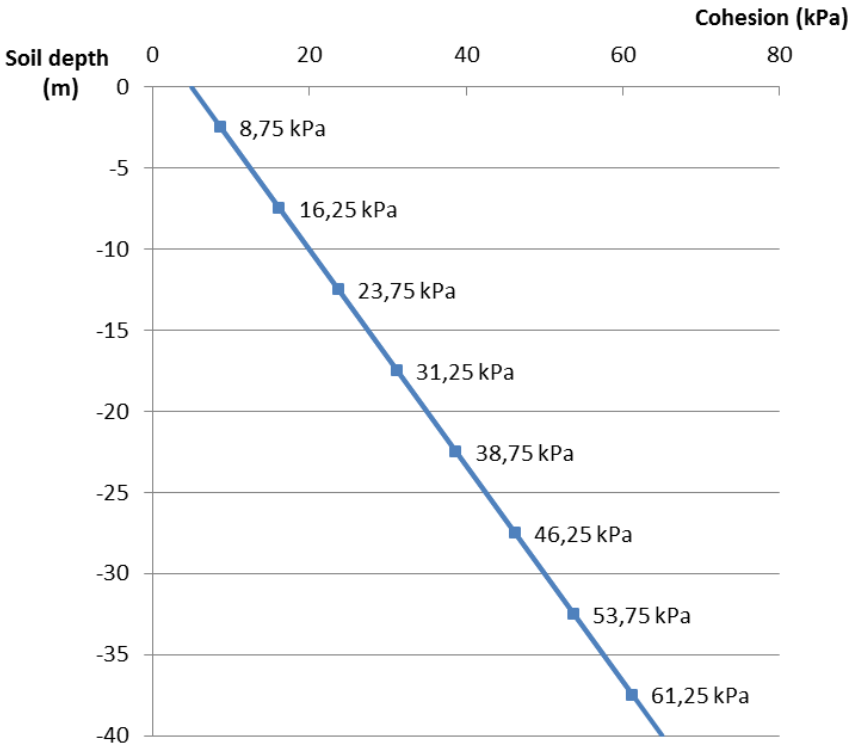

Figure 47 - The varying undrained shear strength depending on the soil depth

Table 13 - The undrained shear strength in the different layers of the soil

Depth (m)	Cohesion (kPa)	Young's modulus (kPa)
0-5	8.75	4375
5-10	16.25	8125
10-15	23.75	11875
15-20	31.25	15625
20-25	38.75	19375
25-30	46.25	23125
30-35	53.75	26875
35-40	61.25	30625
40-45	68.75	34375
45-50	76.25	38125
50-55	83.75	41875
55-60	91.25	45625
60-65	98.75	49375
65-70	106.25	53125

6.2 Load-displacement response of vertically loaded piles

6.2.1 Compression

The load-displacement response for the pile with an L/D-ratio of 10 shown in Figure 48 presents the displacement of the top of the pile if the load at the pile head increases and compares the results of 2D and 3D FEA, and the ultimate resistance estimated based on an analytical expression for pile capacity, Appendix A.1.3 and Table 14. Only this result is shown because similar behaviour was seen in all pile lengths analysed.

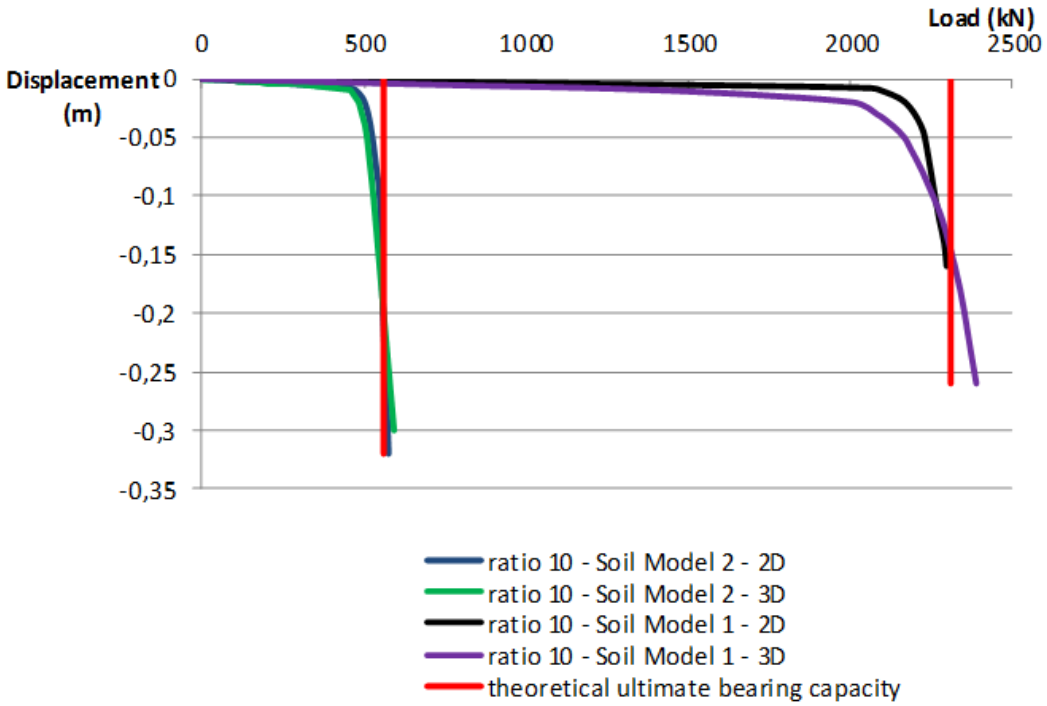

Figure 48 - Load-displacement graph of the 2D and 3D model with L/D-ratio 10

Table 14 - The theoretical ultimate bearing capacity of the simulated models

L/D-ratio	Soil Model 1 (kN)	Soil Model 2 (kN)
10	2309	561
20	4149	1531
40	7964	4884

The difference in the load-displacement curves between the 2D and 3D model can be explained by the kind of elements that were used in the mesh. In the 2D model, quadratic elements were used because they give better conditioned results. In the 3D model, linear elements were used because using quadratic elements lead to excessive run times for the analyses. Despite this, the 2D and 3D models are in close agreement with the theoretical ultimate bearing capacity (within 5.5%), and between each other.

When the ultimate load is reached, because the pile-soil interface is rough, the interface shear stress will be equal to the undrained shear strength of the soil. This can be seen in Figure 49 where the

shear stress along the length of the pile is presented for different displacements for Soil Model 1 where the undrained shear strength has a constant value of 60 kPa.

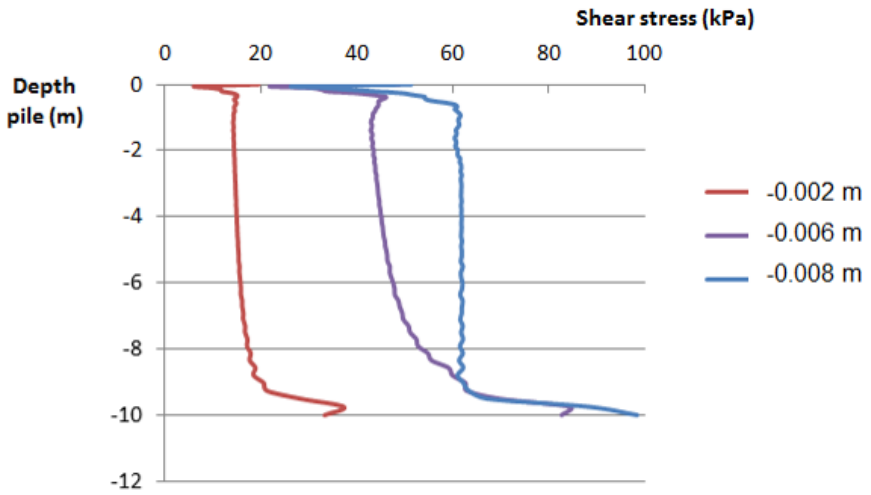

Figure 49 - Soil Model 1: interface shear stress of the 2D model with L/D-ratio 10

The mobilization of the interface shear stress for model 2 with varying cohesion is presented in Figure 50. These results confirm that the model is doing what it should on the pile-soil interface.

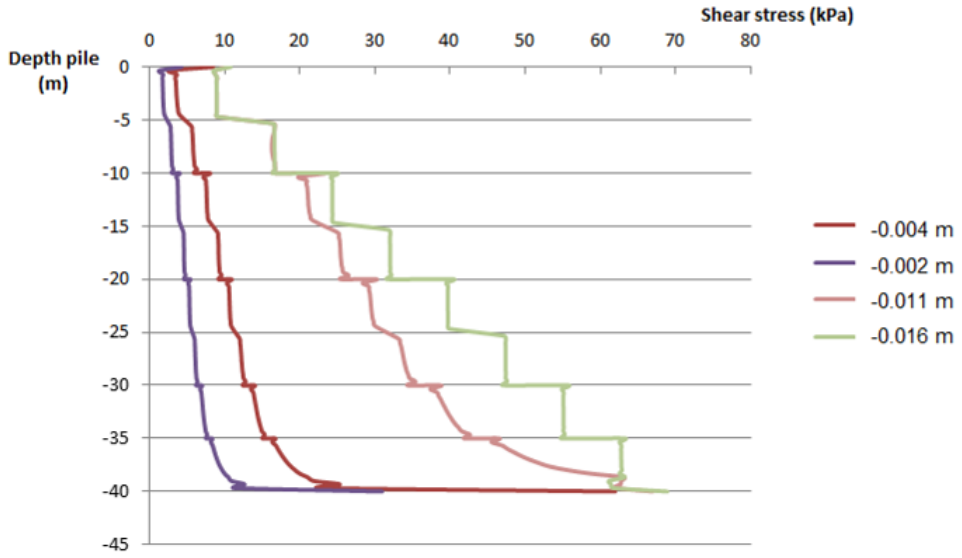

Figure 50 - Soil Model 2: interface shear stress of the 2D model with L/D-ratio 10

6.2.2 Tension

The load-displacement curve for tension loading applied to the pile with an L/D ratio of 20 is shown in Figure 51.

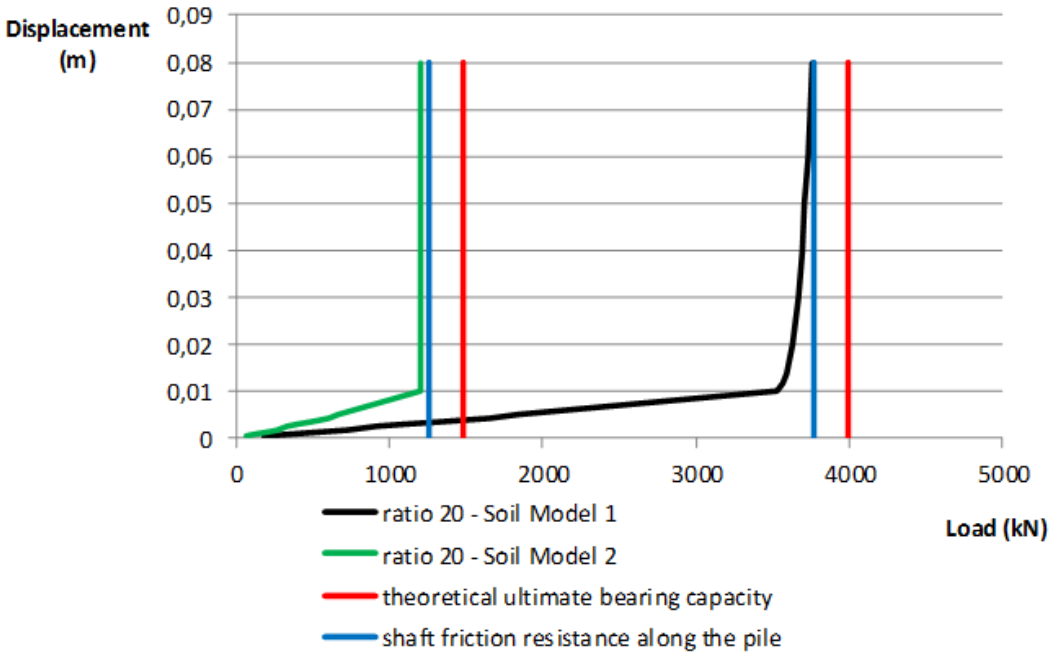

Figure 51 - Load-displacement graph of the 2D model with L/D-ratio 20

As the model used in this study was purely cohesive (strength independent of confining stress), it was not necessary to define an initial stress field or apply gravity body forces, and thus the pile has no weight. Therefore, the ultimate tension capacity only depends on the shaft friction resistance of the pile. The blue line in Figure 51 presents the shaft resistance along the pile which is also the predicted ultimate bearing capacity. The red line represents the theoretical ultimate bearing capacity that also includes the weight of the pile. If the pile should have a weight the green (Soil Model 2) and black curve (Soil Model 1) should move to the right. The analytical solution for the ultimate bearing capacity is mentioned in Section 3.2.1.2 and calculated in Appendix A, Section A.2.3.

6.3 The inverse slope as a prediction of ultimate bearing capacity of piles

In the previous chapter it was shown that the relationship between the load acting on the pile, P and the settlement for the pile, Δ is linear for very small displacements. Many soils have this linear behaviour at the initial values of loading. After this, the load-displacement response can be represented by a hyperbolic function. Due to this hyperbolic behaviour, a plot of Δ/P against an x-axis of Δ will be linear. The inverse slope of this line would therefore give the ultimate value of P [34].

When there is a high degree of linearity between the Δ/P and Δ, the inverse slope can give a close prediction of the observed failure load. This is primarily useful for load tests on a pile where the failure load of a pile can be predicted without extending the loading until failure.
The linear equation can be written as following [34]:

$$\Delta/P = m\Delta + c \quad (6.2)$$

This equation is confirmed by some pile load tests mentioned in the paper for both cohesive and cohesion-less soils. Normally there is an initial linear part of the load-settlement graph and these first few points on the load-displacement curve are not considered the regression used to determine the ultimate value of P.

In this study, not all the FEA terminated at the same displacement, so the above approach has been taken in order to provide a consistent value for the failure load of the model pile under both vertical, horizontal and combined actions. This will be seen in the extrapolated interaction diagrams presented later.

The results from the 2D model with an L/D-ratio of 10 are shown in Figure 52, a value for the slope m of 4.3179 $*10^{-4}$ (R^2 = 0.99989) was obtained for the slope of the line. Thus, the predicted failure load is the inverse of m, or 2316 kN which is similar to the 2303 kN predicted by the 2D model and the theoretical ultimate bearing capacity is 2309 kN which is also close to the predicted value. It is clear from this result and the load-displacement curve that the analysis terminated close to the asymptotic failure load.

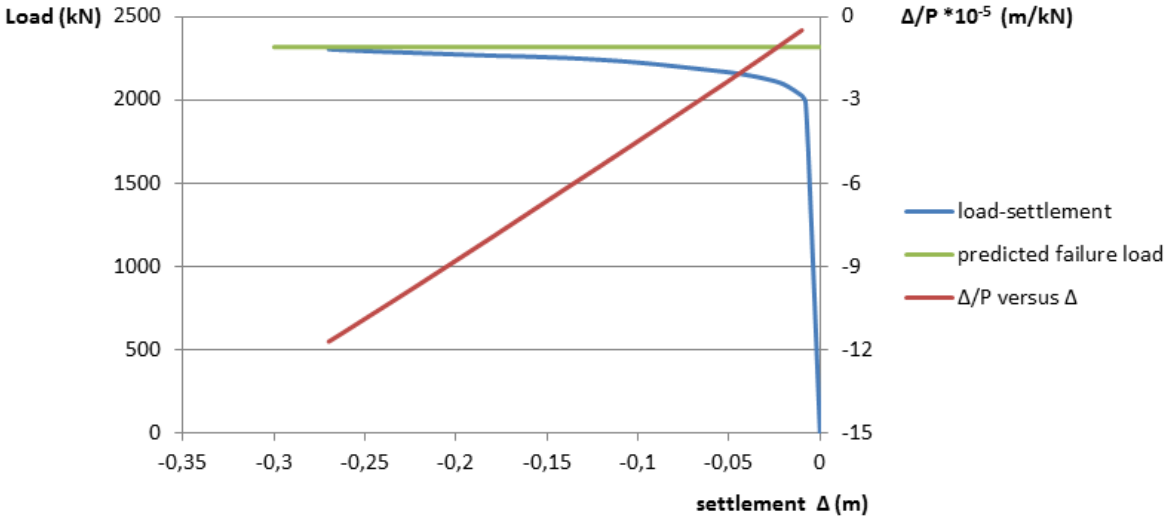

Figure 52 - Soil Model 1:The predicted ultimate bearing capacity for the L/D-ratio 10

The value of R^2 is very close to 1, which indicates a very high degree of linearity and confirms the hyperbolic relationship between P and Δ.

6.4 Laterally loaded piles

Pile anchors from OWTs (and other offshore structures) also have to support lateral loads and moments through the mooring lines. Some examples that cause lateral loads are: wind forces, force of water or lateral seismic forces from earthquakes. The behaviour of the laterally loaded pile anchors

depends on the mooring system, the stiffness of the pile and the soil, the mobilization of resistance in the surrounding soil, the boundary conditions and the duration and frequency of loading [30]. The laterally loaded pile can act like as though it is either a short rigid element or a long flexible element, or somewhere in between (semi-flexible), as discussed in Chapter 3.3.2.

6.4.1 Ultimate bearing capacity

The ultimate lateral load can be calculated in two different ways like mentioned in Chapter 3.3.2. The results of these two methods are shown in Table 15. The calculations are given in Appendix B, Chapter B.2. Further the ultimate bearing capacity of the FEA and the extrapolated value, calculated as discussed in Chapter 6.4, are given in Table 15.

Table 15 - Soil Model 1: lateral bearing capacity for piles

L/D-ratio	Type	Ultimate load, kN			
		Broms method	Modified method	FEA	Extrapolated
10	Semi-flex.	1512	1692	2900	3578
20	Flexible	1705	1892	4500	5036
40	Flexible	1705	1892	5100	5451

The ultimate lateral load resistance obtained from the simulations is much bigger than the Table 15 values. For the long piles this is because the theoretical solutions account for the moment resistance of the pile section whereas in the FEA, pile yield is not considered. For the pile with an L/D ratio of 10, the theoretical maximum moment is not limited by the yield moment and the lateral load of the final stage of the elastic pile analysis is still larger than the ultimate lateral load defined by the Broms method. This difference may be attributed to the contact definition between the pile and the soil which is completely rough, so the pile and the soil are not able to separate in contrast to what is assumed in the theoretical models, Figure 53. This will also enlarge the ultimate lateral load of longer piles.

The ultimate lateral loads obtained from the final stage of the elastic pile analysis in soil with varying undrained shear strength are shown in Table 16.

Table 16 - Soil Model 2: Ultimate lateral load of piles

L/D-ratio	Ultimate load (kN)
10	520
20	1700
40	2600

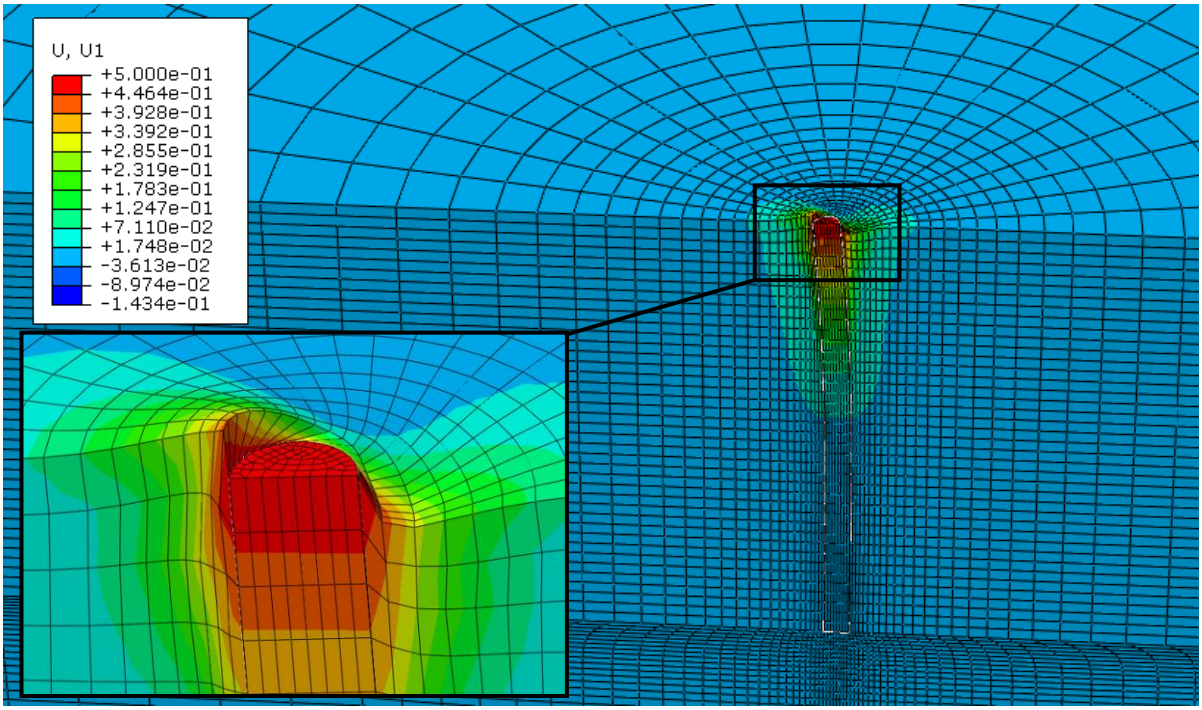

Figure 53 - The simulated contact between the pile and the soil from the pile with L/D-ratio 20 and constant cohesion

6.4.2 Deflection of the pile

In Figure 54, 55 and 56 the deflection graphs of all the FEA models are shown. The green curve (Soil Model 1) and brown curve (Soil Model 2) represent the deflection profile from the FEA at the stage when the maximum bending moment is mobilized approximately equal to the yield moment.

The blue curve shows the deflection profile for the piles in the soils with constant undrained shear strength (Soil Model 1) calculated by the Winkler equations [30] for the load that mobilizes the yield moment. Using these equations, the soil is idealized as a series of springs down the length of the pile. The Winkler method considers two different cases; the first is a uniform soil with a constant reaction modulus k (Soil Model 1) and the second is a layered soil with a reaction modulus which is varying linear with the depth (Soil Model 2). In the case of Soil Model 1, it is apparent that the deflections from the Winkler method are smaller than those suggested in the FEA. For Soil Model 2, only the deflection on the pile head is calculated by the Winkler method, these results are mentioned under the related figure below. Also in these models is the deflection determined by the Winkler equations smaller than the deflection of the FEA. The reason for this discrepancy is explained later in the thesis (Chapter 6.5.4).

The red and purple deflection curves show the displacement at the final stage of the elastic pile analysis for Soil Models 1 and 2 respectively.

Figure 30 compares schematically the deflection of a long and a short laterally loaded pile in a soil with constant cohesion. In Appendix B, the relative stiffness of the pile is determined by the λL-parameter

for piles in a uniform soil (Soil Model 1) and by the ηL-parameter for piles embedded in a soil with increasing undrained shear strength (Soil Model 2) In both cases, the pile with L/D- ratio 10 has to be considered as a semi-flexible pile. In Figure 54 it is apparent that the pile from Soil Model 1 is acting like a semi-flexible pile; the pile is neither acting as a rigid unit, nor a long flexible pile where the bottom of the pile doesn't move. In contrast, the pile from Soil Model 2 is clearly acting more as a short, rigid pile eventhough it was considered as a semi-flexible pile according to the ηL-parameter. The ηL-parameter of this pile was 1.62 where a pile with a ηL-value smaller than 1.5 can be considered as a short pile.

The pile with a length of 20 m should behave as a flexible pile in both cases. That can be confirmed by Figure 55. Also Figure 56 can confirm that the 40 m long pile is behaving as a long pile.

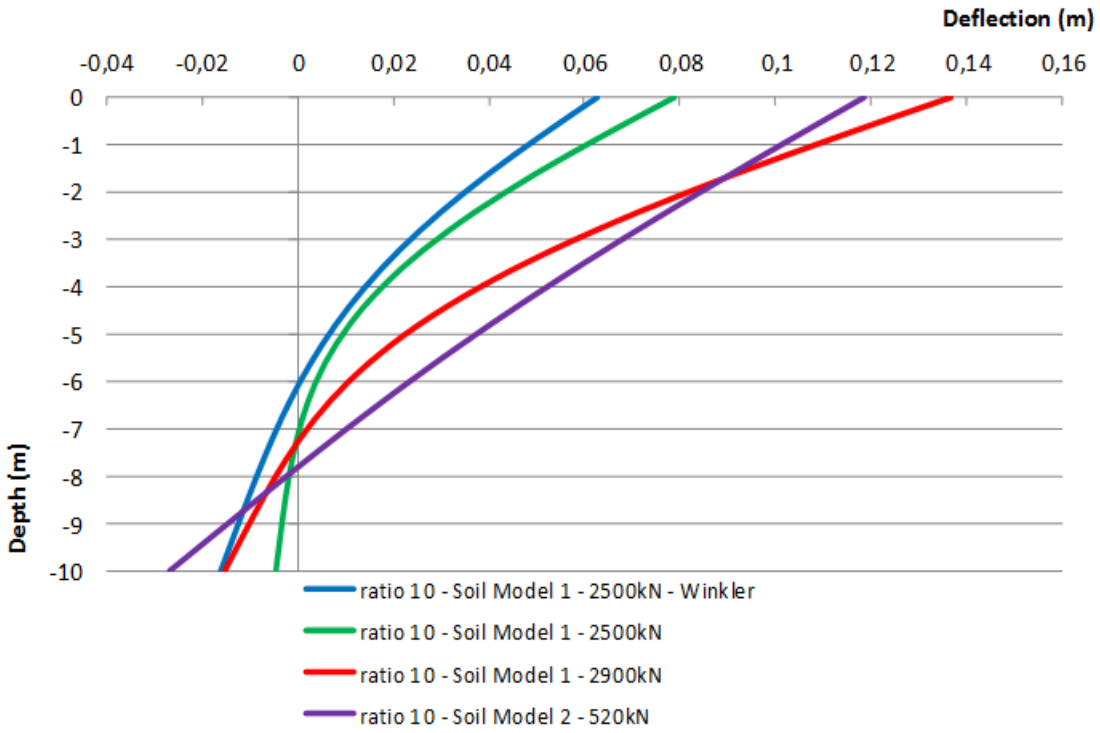

Figure 54 - Deflection curves of the laterally loaded pile with L/D-ratio 10

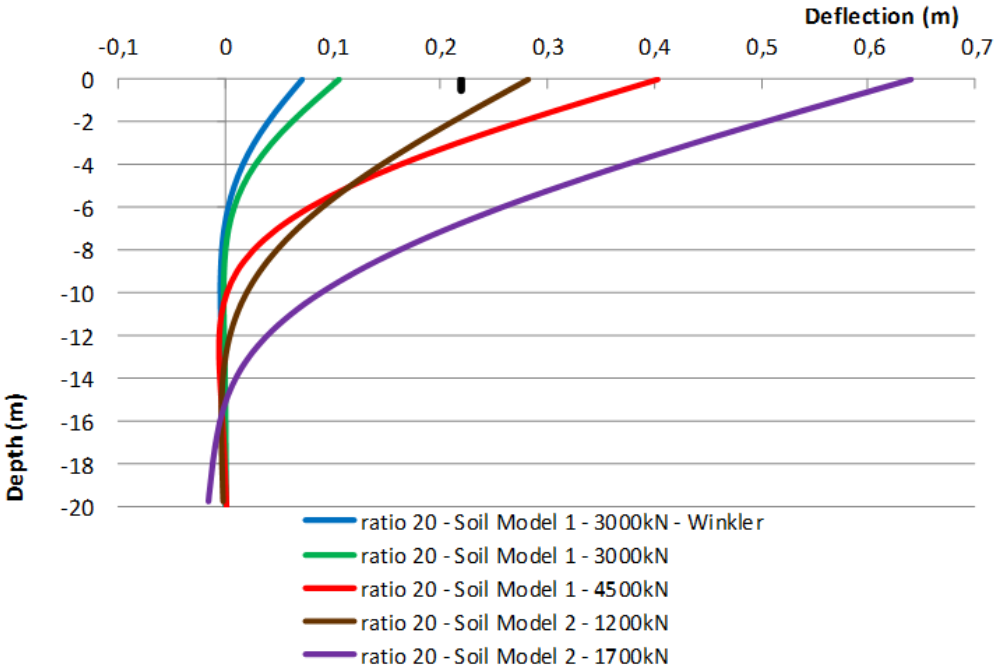

Figure 55 - Deflection curves of the laterally loaded pile with L/D-ratio 20

For the pile of Soil Model 2 and a lateral load of 1200kN, the deflection at the head of the pile is calculated by the Winkler equations: 0.22 m. This value, indicated with a black stripe in the graph, is smaller than the value obtained from the FEA (0.28 m), Figure 55.

The negative values of the purple curve can be explained by the fact that the flexible pile has a ηL-value of 4.07, which is near to the limit with the semi-flexible piles (ηL = 4).

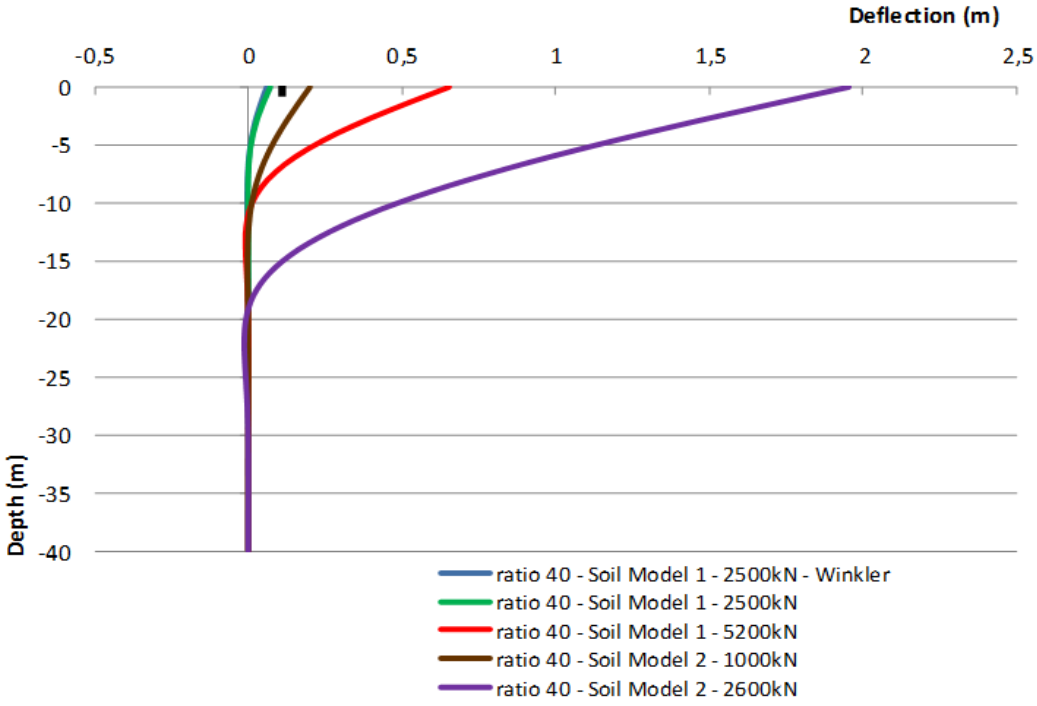

Figure 56 - Deflection curves of the laterally loaded pile with L/D-ratio 40

The deflection at the head of the pile obtained from the Winkler method is 0.11 m, as shown with the black stripe (1000 kN, Soil Model 2), which is less than the value from the FEA (0.19 m), Figure 56.

6.4.3 Bending moment of the pile

The bending moments shown in Figures 57 to 62 are derived from the second derivative of the deflection curves of the previous chapter. The red curves in the Figures 57 to 62 represents the bending moment of the final stage of the elastic pile analysis. They are bigger than the theoretical maximum bending moments, because the theoretical moments for long flexible piles are limited by the moment resistance of the pile section where in the FEA pile yield is not considered. For the semi-flexible pile (L/D =10) of Soil Model 1, the theoretical moments is not limited by the yield moment, still it is smaller than the maximum moment of the FEA. That can be declared by the contact definiton between the pile and soil, discussed in Chapter 6.5.1 which will gave also the long piles a bigger moment.

The stage from the FEA that is closest to the loading that mobilizes the yield moment (M_γ = 5250 kNm) is presented by the blue curve in the Figures 57 to 62.

The lateral loads that are mobilizing the maximum (yield) moments are enumerated in Table 17. The loads applied on the pile embedded in Soil Model 1 can be compared with the lateral loads of the Broms method. The loads of the FEA are still larger than the loads of the Broms method which can be explained by the fact that there will be more soil resistance because no gap formation has been modelled.

The loads from Soil Model 2 cannot be compared with the loads of the Broms method because the Broms method is only valid for uniform soils. Still the moments of the long piles will be limited by the yield moment of the pile. The loads that are mobilizing that yield moment are presented in Table 17. They are smaller than the lateral loads of Soil Model 1, so the yield moment will be reached faster. The load of L/D-ratio 10, for Soil Model 2 is not determined because the 10 m long pile will behave as a semi-flexible pile and in Figure 58 it is clear that at the end of the analysis, the mobilized maximum bending moment (1400 kNm) in the pile is well below the yield moment.

Table 17 - Lateral loads that mobilize the maximum moment

L/D-ratio	Broms method	Soil Model 1	Soil Model 2
10	1512 kN	2500 kN	-
20	1705 kN	3000 kN	1200 kN
40	1705 kN	2500 kN	1000 kN

Just like the deflection curves, also the bending moments will be compared with the Winkler method [30]. For Soil Model 1, the Winklers equations for a uniform soil with constant reaction modulus k will be considered. The bending moments, taking into account the lateral load where the theoretical maximum moment is about equal to the yield moment, are calculated by these Winkler equations.

They are presented by the green curves in Figures 57, 59 and 61 [30]. There can be concluded that the bending moments and the depths of the maximum moments obtained by the Winkler equations are smaller than those of the FEA.
For the Soil Model 2, the Winkler equations for a soil with a linear varying reaction modulus will be applied. Herefore the maximum moment and the depth of this moment were calculated. According to Figure 60 the maximum bending moment was calculated for a lateral load of 1200kN: 4545 kN at a depth of 6.39 m. According to Figure 62, the maximum bending moment for a lateral load of 1000 kN was 3170 kNm. This value was reached at a depth of 5.35 m. Also here can be concluded that the bending moments and the depths calculated by the Winklers method are smaller than those of the FEA. The reason for this will be explained in Chapter 6.5.4.

Comparing Figures 57 and 58 (L/D = 10), Figures 59 and 60 (L/D = 20) and Figures 61 and 62 (L/D = 40), according the shapes of the bending moments profiles it can be concluded that the pile embedded in a soil with varying undrained shear strength is less flexible than the pile in a soil with a constant cohesion. This statement is also confirmed by the deflection graphs, Figures 54 to 56.

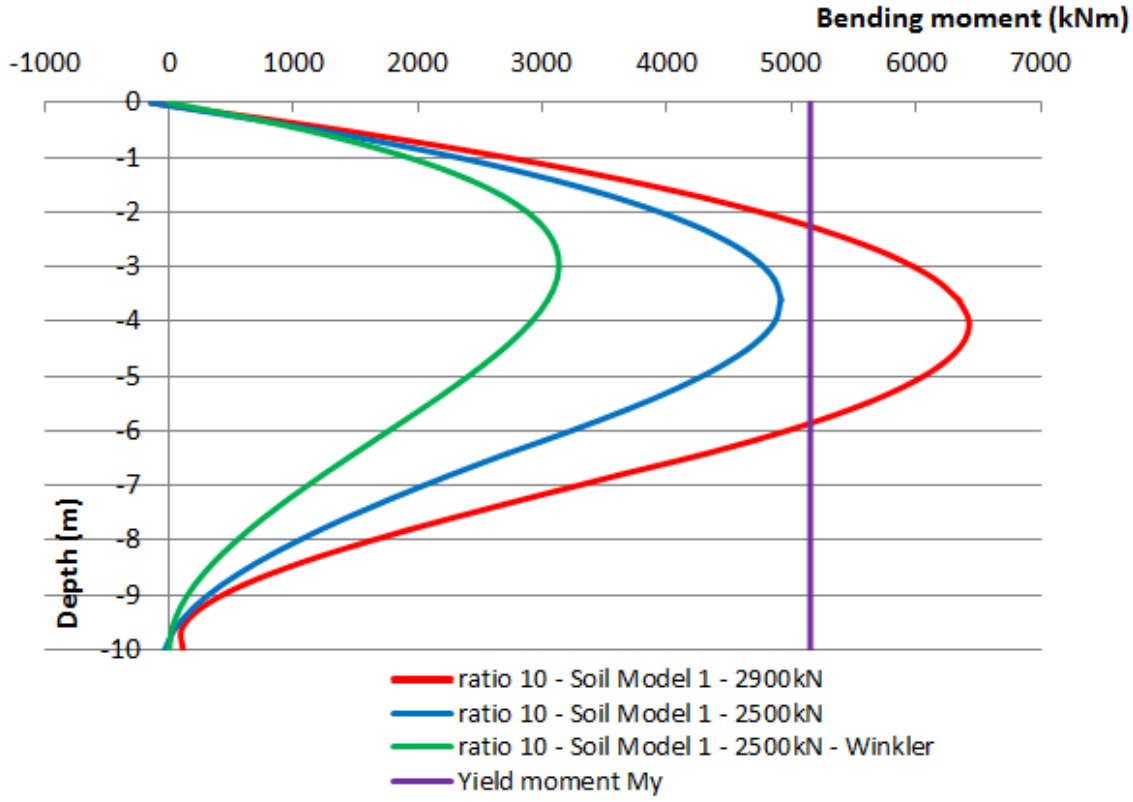

Figure 57 - Soil Model 1: bending moment of the laterally loaded piles for L/D-ratio 10

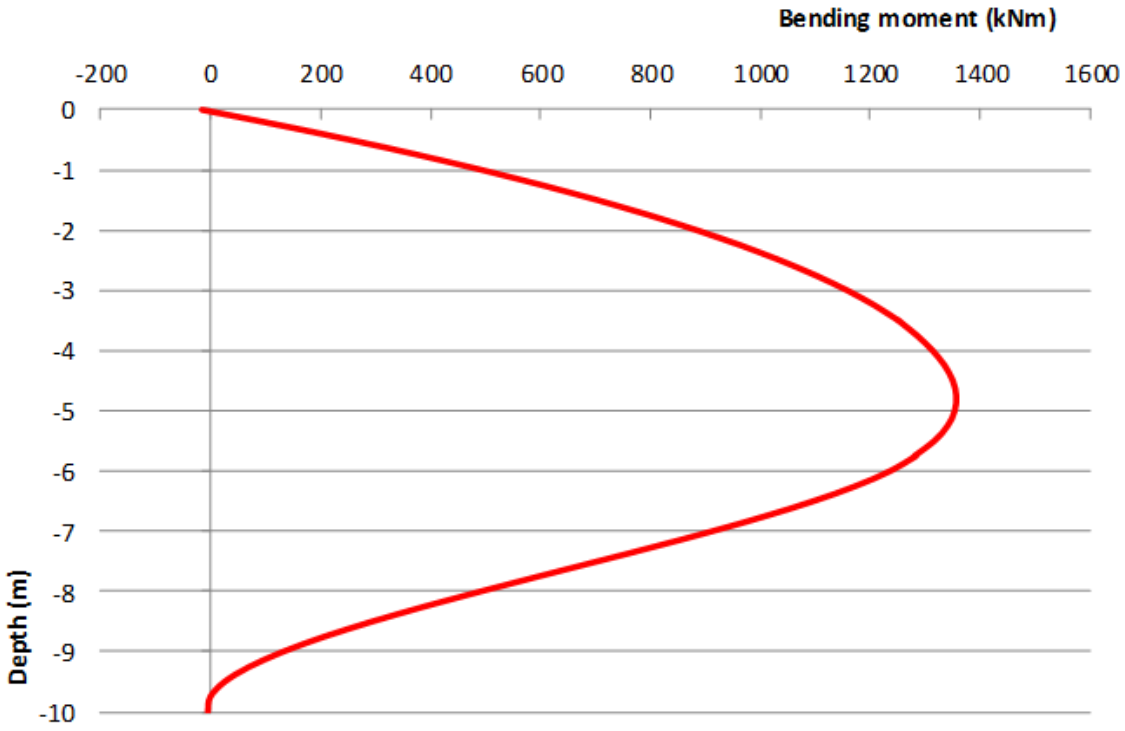

Figure 58 - Soil Model 2: bending moment of the laterally loaded piles for L/D-ratio 10

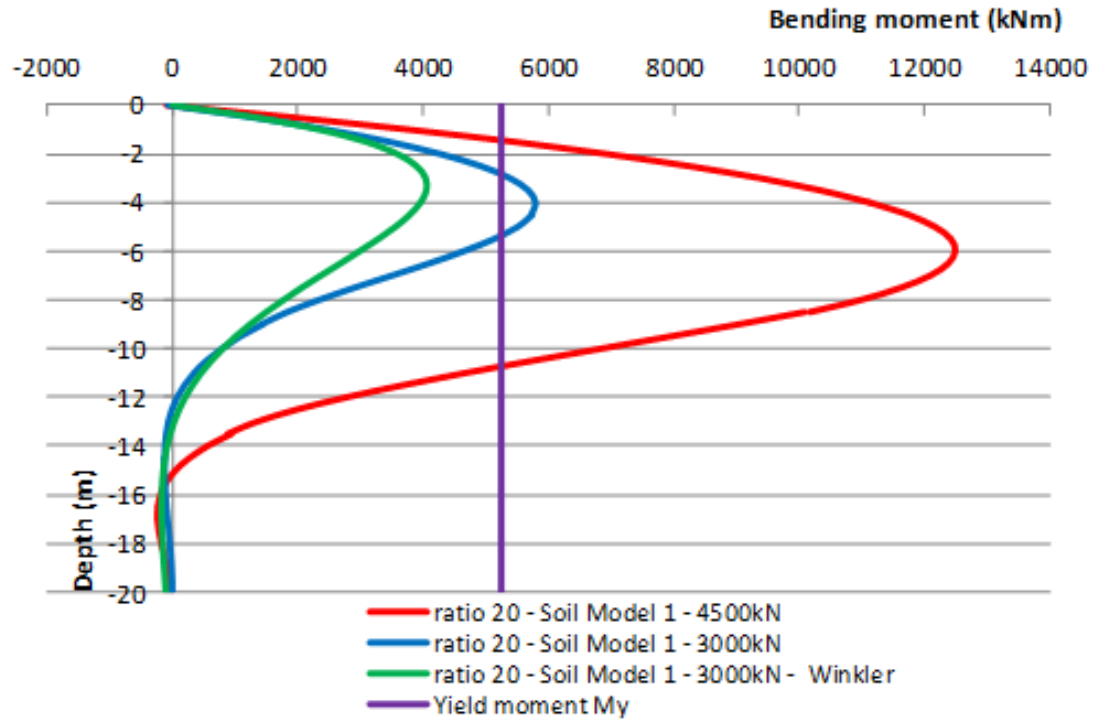

Figure 59 - Soil Model 1: bending moment of the laterally loaded piles for L/D-ratio 20

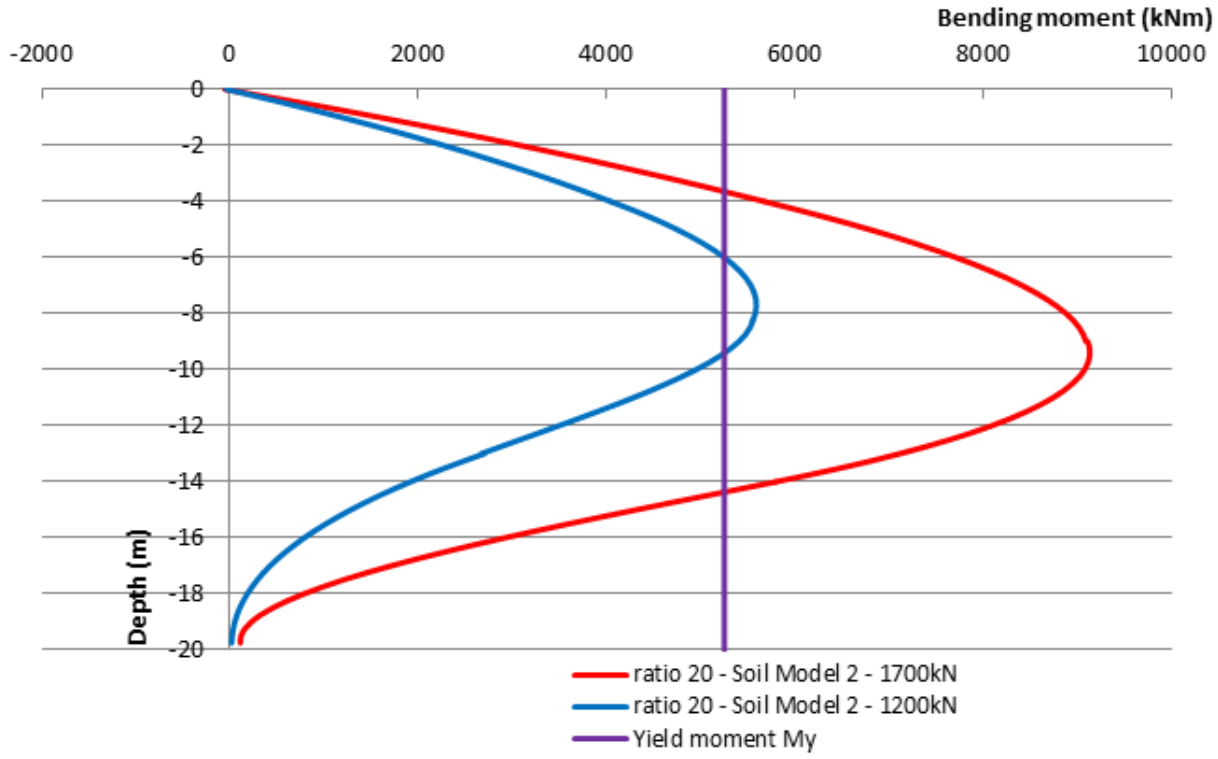

Figure 60 - Soil Model 2: bending moment of the laterally loaded piles for L/D-ratio 20

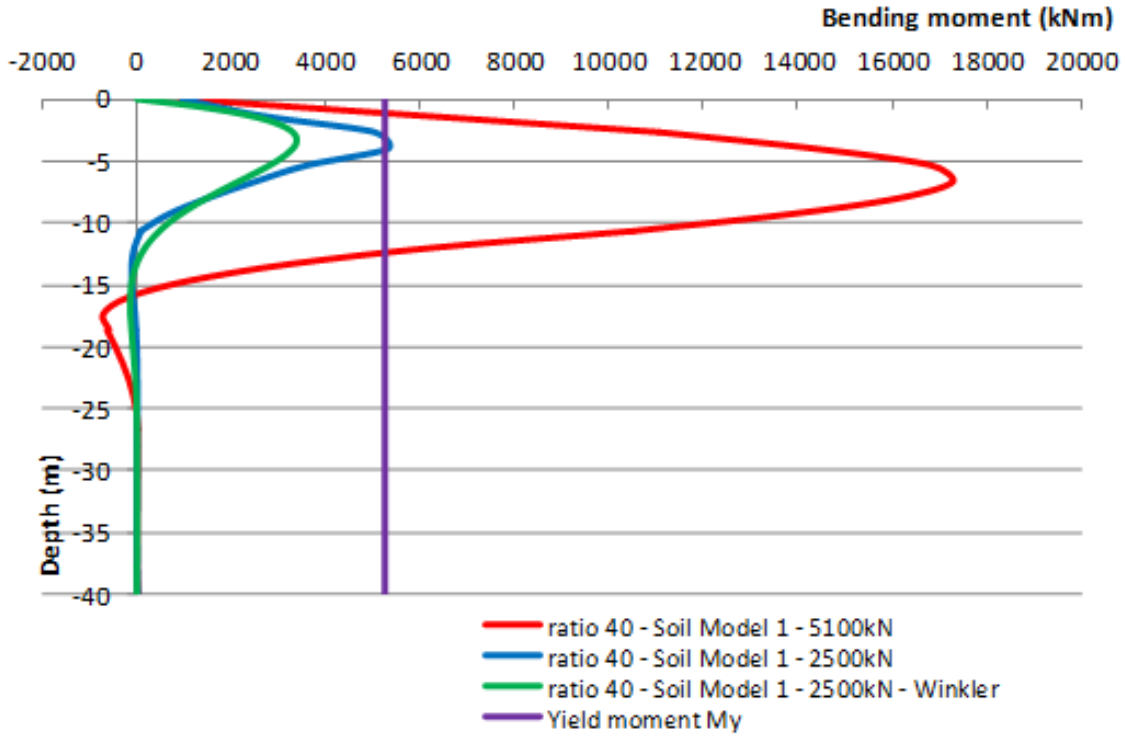

Figure 61 - Soil Model 1: bending moment of the laterally loaded piles for L/D-ratio 40

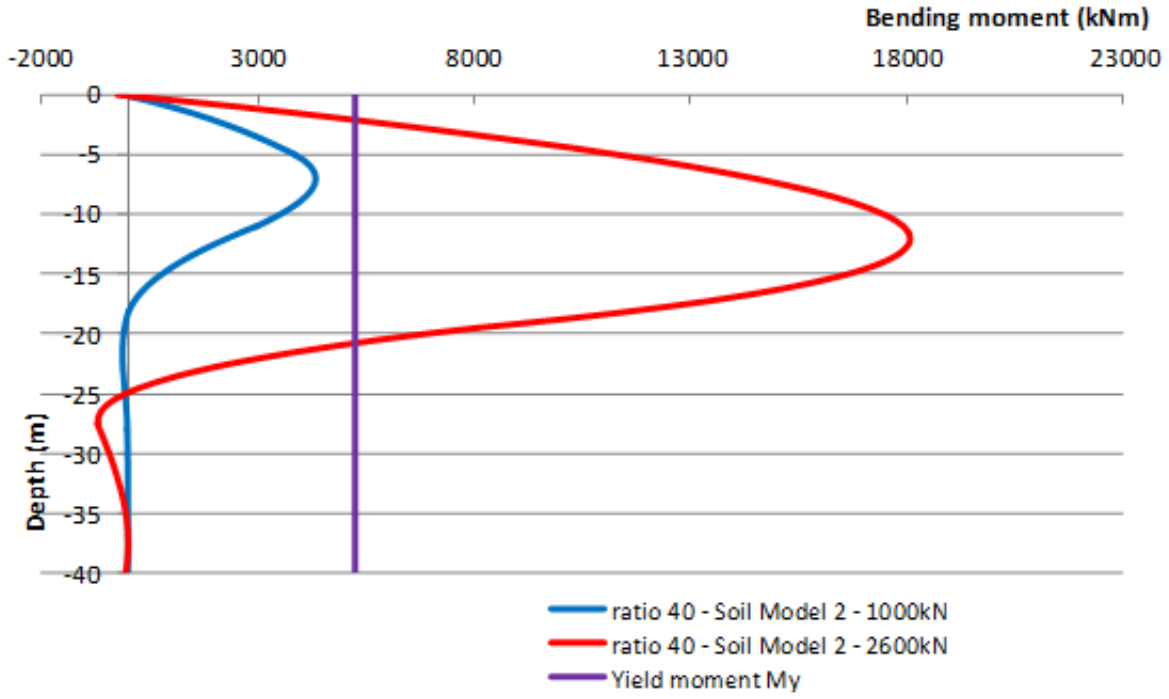

Figure 62 - Soil Model 2: bending moment of the laterally loaded piles for L/D-ratio 40

6.4.4 Soil resistance along the pile

A way to check the limiting pressure along the pile is the method of [31]. This model considers a rigid plastic model of soil and is only allowed for a pile-soil interface with limiting friction and without friction. N_{pl}, the limiting bearing factor for a perfectly rough pile is 11.94 [31].

$$N_{pl} = \frac{Pu}{cu\ d} = 11.94 \qquad (6.3)$$

So the theoretical limiting pressure, P_u, will be 716,4 kN/m. Figure 63 shows the contact pressure of the section of the laterally loaded pile with L/D-ratio 20, 1 m below the soil surface. The sum of these pressures is 693 kN/m. This value divided by the cohesion and the diameter of the pile gives a limiting bearing factor of 11,55 which is near by the theoretical 11.94.

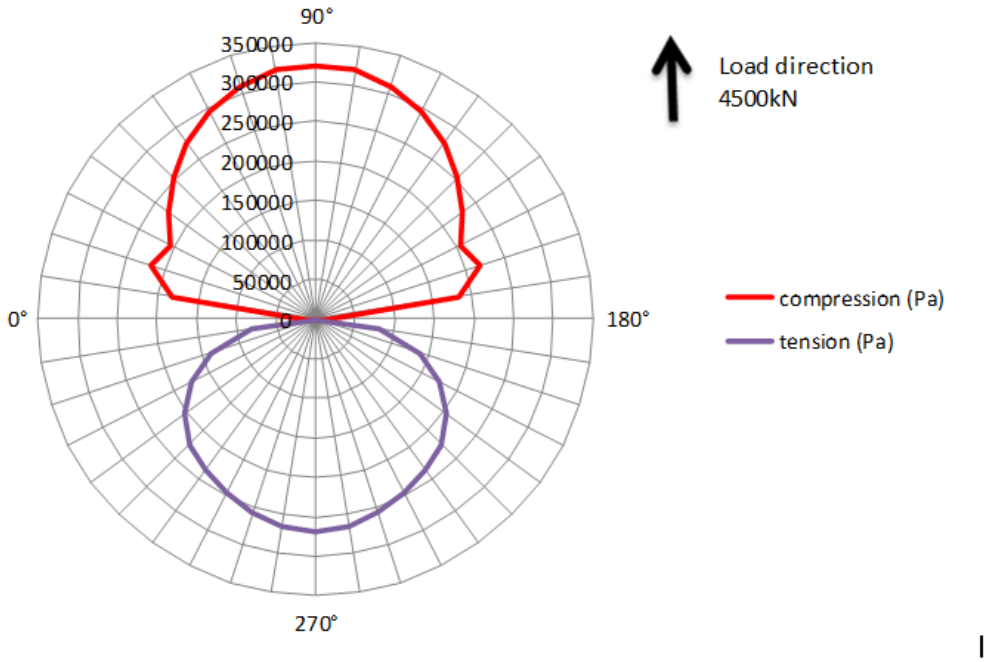

Figure 63 - Soil Model 1: soil resistance at 1 m depth for pile with L/D-ratio 20

In Figure 64 the limiting bearing factors evaluated at 1 meter intervals along the pile with L/D-ratio 20 and Soil Model 1 are presented by the blue curve. Also shown are the distribution of the lateral pressures assumed by Broms and the modified method; these have much lower values than those obtained from the FEA. This discrepancy can be explained by the fact that the Broms and modified method only assume the compression because there should be a gap where the tension is occuring in Figure 63. The lower part with negative limiting bearing factors (below 10 m depth, Figure 64) is ignored in the Broms and modified method for long piles.

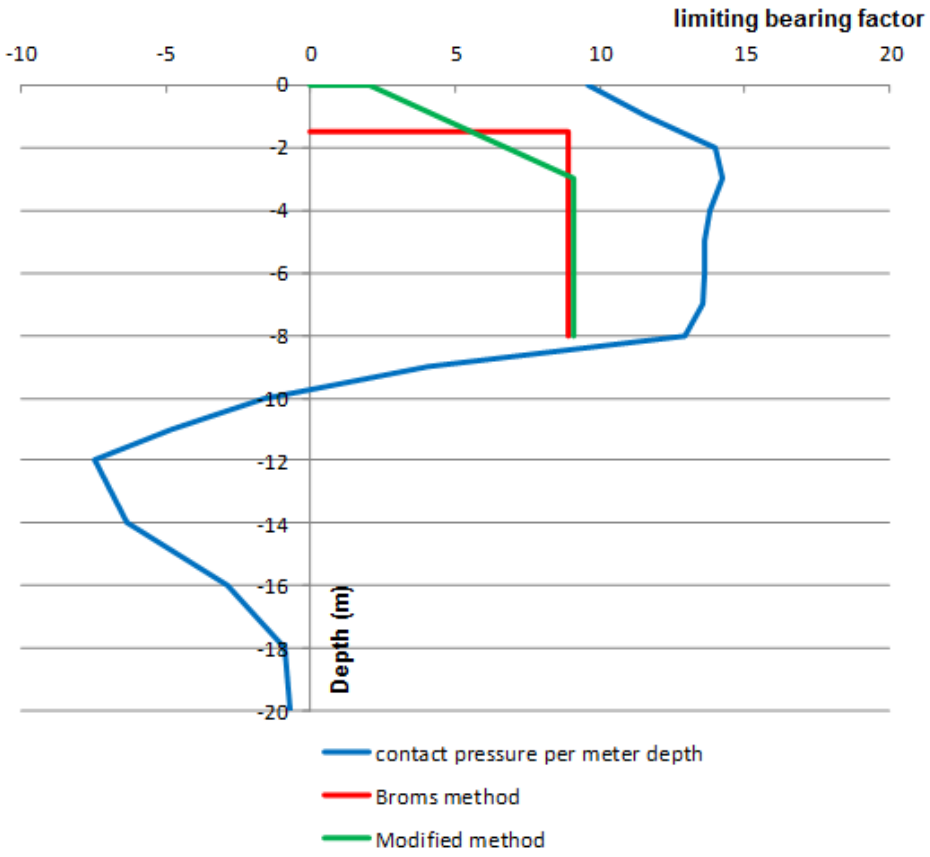

Figure 64 - Soil resistance along the pile from the pile with L/D-ratio 20 and constant cohesion

The reaction modulus k (Chapter 3.3.2.1) can be calculated by the division of the contact pressure, p (kN/m) determined above, by the deflection at the same depth, Table 18.

Table 18 - Soil Model 1: Limiting bearing factor, contact pressure, deflection and reaction modulus of the pile with L/D-ratio 20

Depth (m)	Lim. Bearing factor	p (MN/m)	y (m)	k (MPa)	Average	
0	9,6	575	0,403	1,43	10.3	3.8
1	11,5	693	0,338	2,05		
2	14,0	840	0,274	3,06		
3	14,3	856	0,215	3,98		
4	13,8	827	0,162	5,10		
5	13,6	817	0,116	7,03		
6	13,6	818	0,078	10,47		
7	13,6	814	0,048	16,91		
8	12,9	775	0,026	30,05		
9	4,1	245	0,011	23,23		

There can be seen that the reaction modulus is not constant as was assumed for the calculation of the bending moment profiles, Figure 59 and the deflection profiles, Figure 55. The initial reaction modulus used was 20 MPa (calculations in Appendix B) which is large compared with the reaction moduli referred from the FEA in the upper part of the pile. Two averages were taken, the first over the upper half of the pile, and the second over the upperst 5 m, or 5 pile diameters over which the lateral loading response is most controlled. Below 10 m, the deflection values are very small and the derived k values are considered to be unrealistic.

The equations used to calculate the constant reaction modulus are based on Vesic elastic theory. In this case, there will be plasticity developing which gave a lower effective reaction modulus, Figure 29. In Figure 65 and Figure 66 the deflection and bending moment profiles for these revised reaction moduli are presented, and compared with the initial elastic soultion.

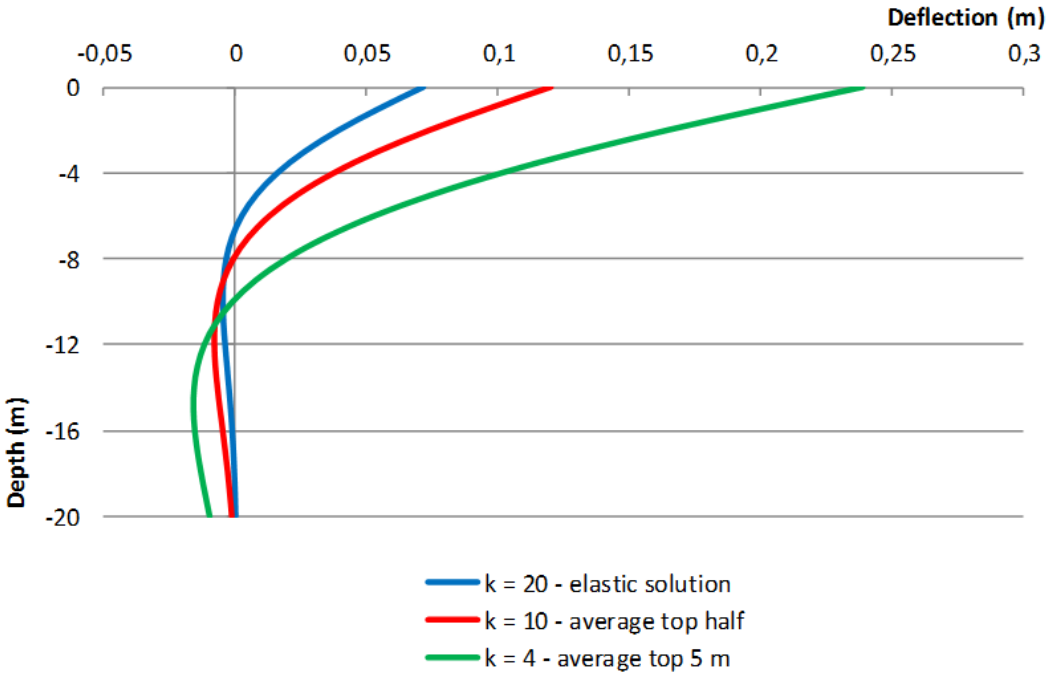

Figure 65 - Deflection curves with different reaction moduli (L/D-ratio 20, Soil Model 1)

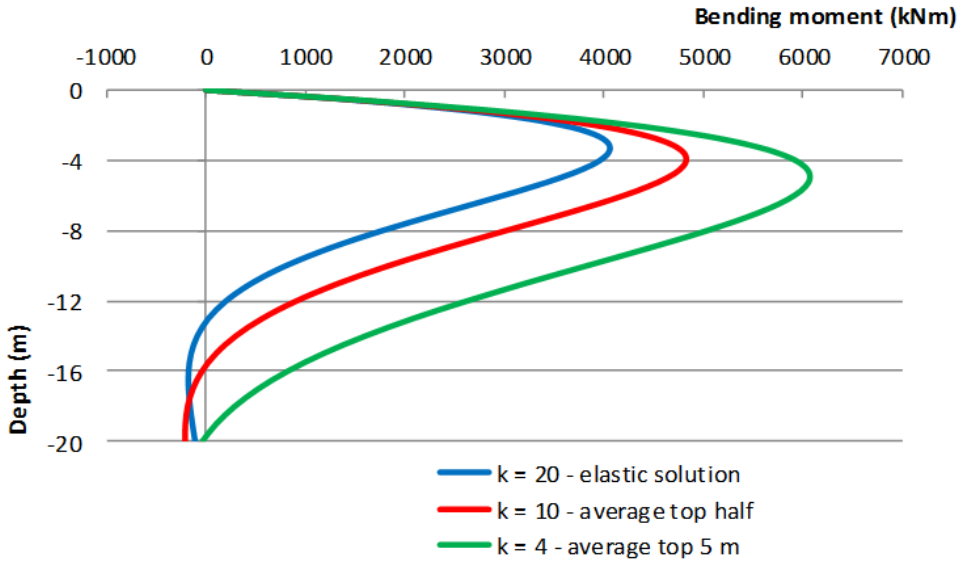

Figure 66 - Bending moments with different reaction moduli (L/D-ratio 20, Soil Model 1)

It can be concluded that the smaller the reaction modulus, the larger the deflections and the bending moment, and the depth to the maximum moment will increase. With these conclusions, it can be declared why the deflections calculated by the Winkler equations were smaller than the deflections of the FEA in Figures 54, 55 and 56. Also the smaller bending moments and the depths of the maximum moments from Figures 57 to 62 can be explained by Figure 66. There was found that the deflection profile calculated with the reaction modulus equal to 10 MPa will be the closest to the deflection profile of the FEA. In contrast, the bending moment profile calculated with a reaction modulus of 4 MPa will be the closest to the bending moment profile of the FEA. This confirms that assuming a constant reaction modulus is not comfortable in term of deflection and bending moment profiles. Also assuming

a non-linear function of the reaction modulus, e.g. load-deflection method, Figure 29, is likely to provide a closer agreement with the FEA.

6.5 Combined loading

Pile anchors with taut leg mooring system are used for the transfer of both axial and lateral loads into the ground. Combining these two loads, the interaction of the horizontal and vertical load-bearing behaviour can be analyzed. In this chapter, the effect of the combined loading of piles in the soil will be identified and quantified.

For piles, the interaction between combined loads is less significant than for shallow foundations. A horizontal load will not affect the vertical capacity a lot and vice versa [35]. That can be declared by the difference in mechanism. The axial loading involves the whole pile shaft interface acting in shear and the base in case of compression loading, while the lateral loading involves compression and shearing of a soil mass perpendicular to the interface over a limited depth. This statement can also be confirmed by the steep curves in Figure 67. In this figure the term Vu defines the ultimate tension load and is used to normalize both axis. Figure 67 shows that the horizontal load resistance is largely unaffected by the axial tension except when the tension is very close to the ultimate value. Further, in design, the design action would be limited to about 55% of the ultimate resistance, so the full ultimate horizontal resistance could be relied on when deriving the design horizontal resistance – noting of course that this may be controlled by yielding of the pile rather than geotechnical failure.

The dotted lines in Figure 67 and Figure 68 represent the interaction diagrams based on failure loads extrapolated from the FEA, as described in Section 6.4.

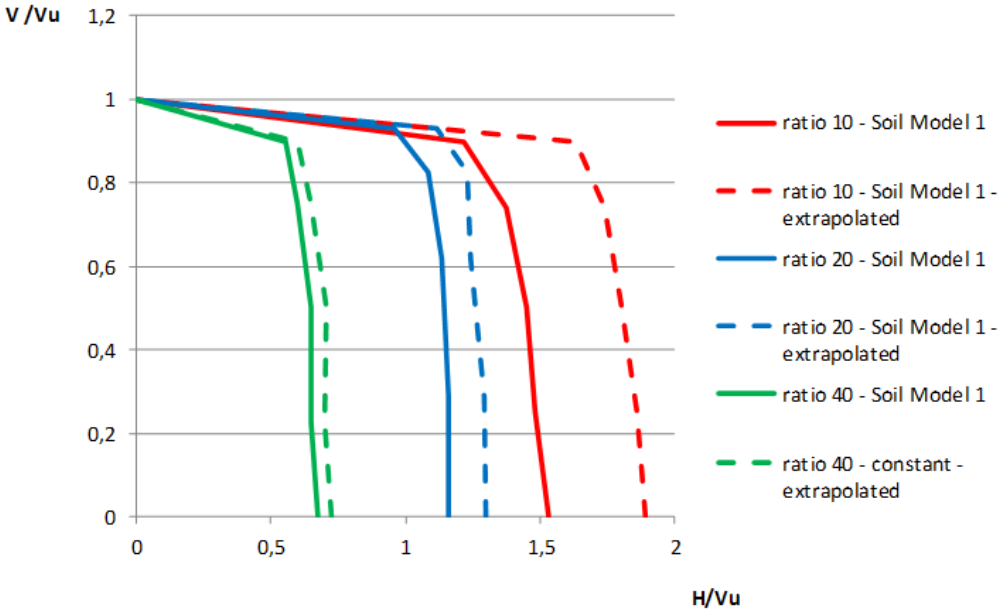

Figure 67 - Soil Model 1: Ultimate load interaction diagram for piles

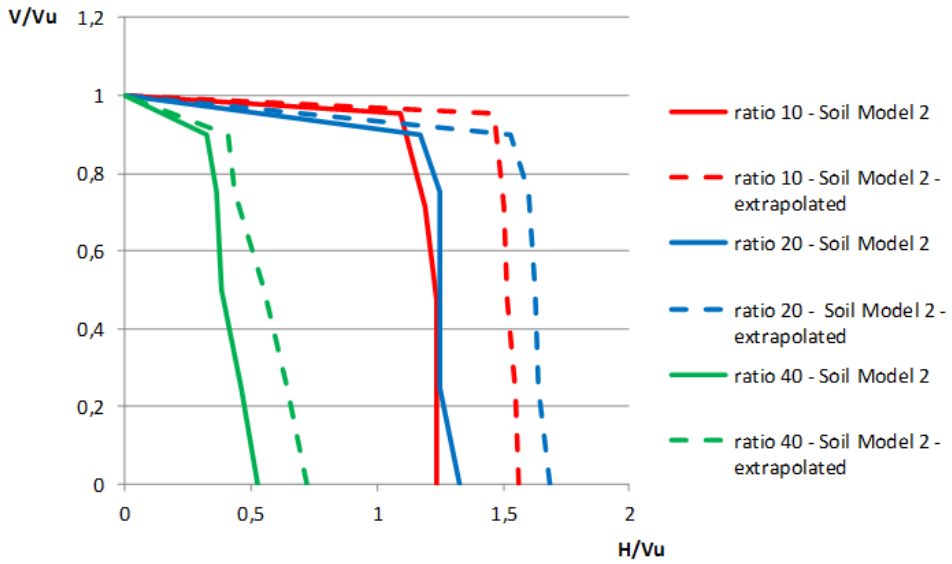

Figure 68 - Soil Model 2: Ultimate load interaction diagram for piles

Further there can be obtained from Figure 67 and Figure 68 that the ultimate lateral load of the pile with a length of 40 m will be less than the ultimate axial load which has a large value due to the large amount of shaft resistance. So the longer the pile, the smaller the amount of lateral resistance relative to the tension resistance. If we apply next to the lateral load, also a tension load at the head of the pile, the ultimate lateral load will not change a lot. However the tension load will have more influence on the 40 m long pile with Soil Model 2 than the pile 40 m long pile with Soil Model 1. This is not the case for the other L/D-ratios.

For the pile with an L/D-ratio of 20 and 10, the ultimate lateral load will be larger than the ultimate vertical load. For the Soil Model 1, the ultimate lateral load of the 10 m long pile will be larger than the ultimate lateral load of the 20 m long pile, relative to the ultimate tension load. In contrast Soil Model 2, where the curves are very close to each other. It is not clear why this discrepancy occurs, so it is recommended to exam these curves in future work.

In Figure 69, the ultimate load interaction curve and the extrapolated curve for the 20 m long pile embedded in a soil with varying undrained shear strength is shown. Besides this, the green curve presents the interaction curve where the combined load mobilizes the yield moment of the pile. The values of this curve are smaller than the other curves because the other curves are based on a pile with elastic behaviour. There can be seen that on the time that the yield moment is reached, the horizontal loads also not affect the tension loads, only a large tension load will decrease the ultimate lateral load.

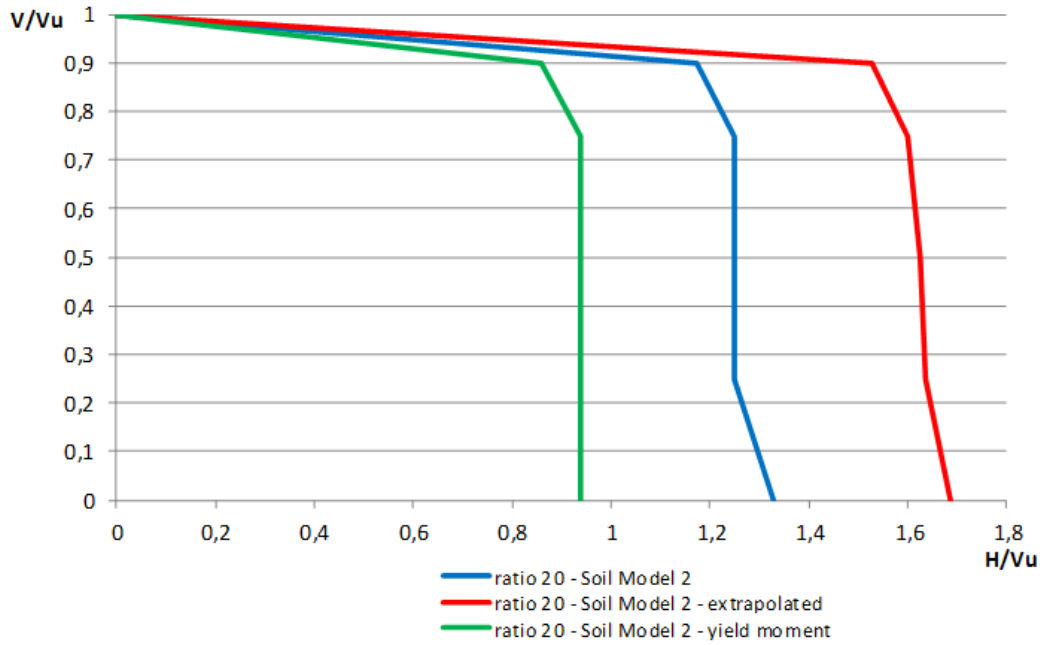

Figure 69- Ultimate load interaction diagram for the piles with L/D-ratio 20 and soil with varying undrained shear strength

A typical evolution of the strain and stress profiles across the pile is shown in Figure 70. The variation of the normal strain, Ɛ over the cross section will be linear in the elastic range, Figure 70(a). As the loading continues increasing, yielding will start and a plastic zone will propagate. With tension and lateral loading applied together, yielding will be reached first on one side of the pile in contrast to the piles loaded with only an axial load or only a lateral load which had the same strain on both sides. The yield moment calculated in Chapter 3.3.2.4 is defined as the moment at the yield stress is reached at the outer fibres of the pile section. But as mentioned, the yielding for combined loadings will be reached earlier, so the calculated yield moment used here will be larger than the bending moment at the stage when yielding starts [44] – therefore, the yield moment line shown in Figure 69 may be inclined with lower ultimate horizontal loads associated with larger axial tensions.

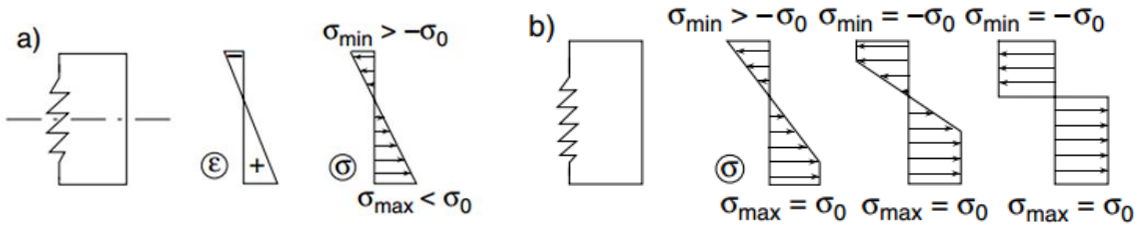

Figure 70 - Strain and stress profiles [44]

The same curves as in Figure 69 are presented in Figure 71 for a pile with L/D-ratio 10 and a soil with constant undrained shear strength (Soil Model 1). There can be concluded that also here the structural yield occurs before the geotechnical failure, however this is a semi-flexible pile. Only for a large tension load is the geotechnical failure reached before the yielding of the pile. For the 10 m long pile

embedded in soil with varying cohesion (Soil Model 2), yielding will occur after the geotechnical failure since the bending moment at the last stage of the elastic pile analysis (Figure 58) is smaller than the yield moment.

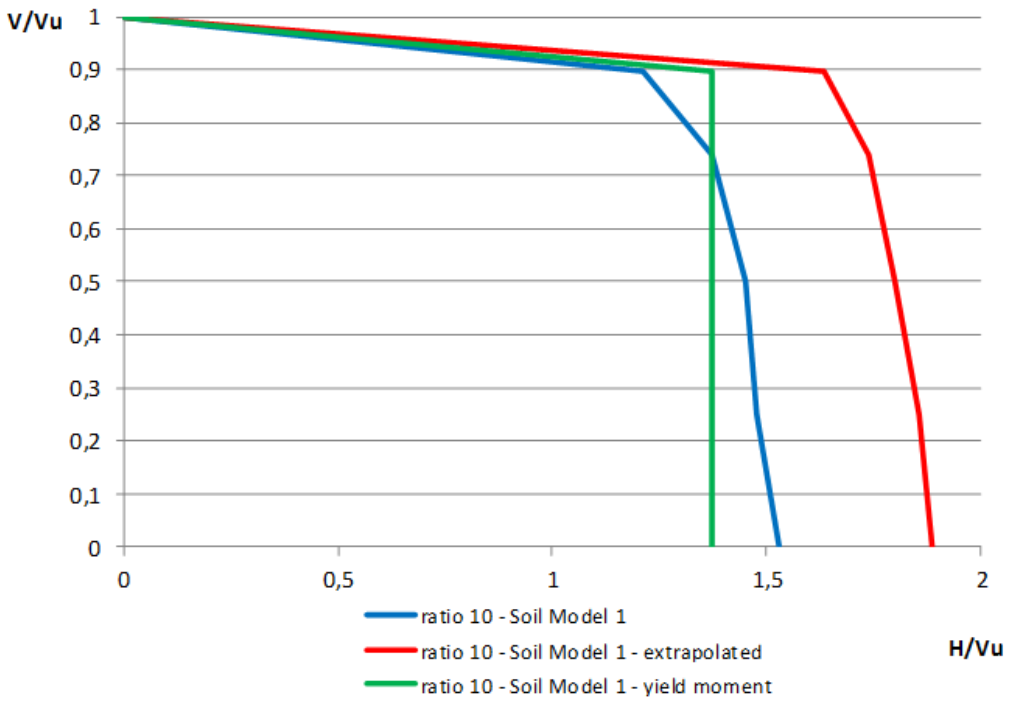

Figure 71 - Ultimate load interaction diagram for the piles with L/D-ratio 10 and soil with constant undrained shear strength

Chapter 7

Conclusions

7.1 Conclusions and Results summary

This thesis has analysed the problem of pile-soil interaction under lateral and combined loadings, the geotechnical modelling with the program Abaqus has been developed progressively, starting with an elastic model and progressing to a simple elasto-plastic model.

After the elastic simulations of the different pile L/D-ratios, some conclusions can be made:

- The results of the 2D models are better while using quadratic elements which will be solved by a second-order interpolation. For the 3D models, linear elements were used, because 3D quadratic elements did not always improve the results compared to the lower order elements and the 2D FEA, and the run time for analysis using these elements was excessive.
- The finer the mesh, the closer the FEA results were to the theoretical values; however this mesh gave also longer run times.

To get good results for the 3D models, a good mesh has to be chosen taking the above conclusions into account.

Subsequently, an elastic pile in a soil modelled as an elastic- perfectly plastic material was considered, more specific the Tresca model was used to simulate the undrained response of a clayey soil.

Firstly, the elastic-plastic models were verified by the load-displacement graphs for piles under axial compression and tension loading. Both the 2D and 3D models gave acceptable results and reached the theoretical ultimate bearing capacity, however the shape of the load-displacement curves were a little bit different.

Subsequently, laterally loaded piles were examined. The ultimate lateral load was calculated by two theoretical models: Broms method and the modified method. The ultimate lateral loads obtained from the FEA were larger than the theoretical predictions because the theoretical solutions account for the moment resistance of the pile section wheras in the FEA, pile yield was not considered. Another aspect that made the ultimate lateral load larger than the theoretical values was that the contact between the pile and soil did not allow a gap to open when the contact was in tension. These two reasons will also explain why the bending moments from the final stage of the elasic pile analysis were larger than the yield moment.

Further, the deflection and bending moment profiles of the FEA of the laterally loaded piles were compared with the Winkler method. The deflections and bending moments obtained from the Winkler equations were smaller than those of the FEA These results can be explained by the reaction modulus, k that is used in the Winkler analysis. The initially used k was based on the elastic (Vesic) theory and was too large to reach the values of the deflection and bending moment profiles of the FEA. The lower k values were due to the development of significant plasticity. Using these lower values of k in the Winkler equations gave better values compared with the FEA. It was notable that

different reaction moduli were used for the deflection profile and the bending moment profile to fit with the FEA profiles which means that the reaction modulus cannot be taken constant.

Finally, combined vertical and horizontal loadings applied at the head of the pile were examined. It was found that the horizontal load reistance was largely unaffected by axial tension loading except when the tension is very close to the ultimate value.

It can also be concluded for the pile with L/D-ratio 10 and Soil Model 1, that structural yield occured before geotechnical failure, however this is a semi-flexible pile. In contrast for the pile with L/D-ratio 10 and Soil Model 2, geotechnical failure occurred and the bending moment at the last stage of the elastic pile analysis was smaller than the yield moment.

The final conclusion is that depending on the relative stiffness of the pile-soil system, the model will fail by geotechnical failure or by yielding of the pile. In a case of doubt, both have to be examined. When combined tension and lateral loads are applied to a pile there is little interaction between one and the other in terms of ultimate resistance. Thus for short, rigid pile, the full ultimate horizontal soil resistance can be relied on when deriving the design horizontal resistance. For long, flexible piles, the lateral resistance is governed by the strength of the pile section. Further there has to be taken some care in using certain methods to simulate the pile-soil interaction at the Ultimate Limit State (ULS). It was shown for the Winkler method that there may be an incompatibility in terms of predicted displacement and bending moment when assuming a constant reaction modulus.

7.2 Future developments

Currently there are few floating wind turbines installed and it is necessary to do a lot of research for these structures. There is much experience designing foundation structures within the oil and gas industry; however, compared to OWTs, these structures are large. So it is very important to examine the difference between the floating wind turbines and the structures used in the oil and gas industry, before using the experience of the oil and gas industry for the floating platforms.

In this thesis only the Tresca model was applied, because severe difficulties were experienced in implementing the Drucker-Prager and the Mohr-Coulomb models. The Tresca model can be used to simulate the behaviour of undrained, clayey soil, but it would be of intrest to simulate other kinds of soils using the Drucker-Prager and Mohr-Coulomb model. In that way the difference between drained and undrained soils, sandy and clayey soils can be examined.

In practice, the optimal attachment point for the anchor chain is below the mudline, part way down the pile. In this thesis, the load was applied at the head of the pile, therefore in future studies it is recommended that analyses are untertaken with loads applied part way down the pile.

This thesis has examined the pile behaviour at failure, i.e. ULS, another topic that can be examined in the future is the SLS. This should be useful to look for a load combination that exceeds a certain deflection or rotation of the pile head.

Finally, it would be of interest to examine the ultimate load interaction diagrams further to confirm why the curves of the piles with L/D-ratio 10 and 20 with the Soil Model 2 are near each other in contrast to those of the Soil Model 1.

References

[1] REN21. (2014). *Renewables 2014 – Global status report* (1st ed.). Retrieved from REN21 website: http://www.ren21.net/portals/0/documents/resources/gsr/2014/gsr2014_full%20report_low%20res.pdf

[2] Schaumann, P., Lochte-Holtgreven, S., & Steppeler, S. (2011). Special fatigue aspects in support structures of offshore wind turbines. Besondere Aspekte hinsichtlich der Materialermüdung bei Tragstrukturen von Offshore-Windenergieanlagen. *Materialwissenschaft und Werkstofftechnik, 42*(12), 1075-1081. doi: 10.1002/mawe.201100913

[3] *Implementation of a 2MW Deep Offshore Wind Demonstration Project*. (2013, July). Paper presented at The WindFloat Project- Public Session of edp, Apúlia.

[4] European Wind Energy Association. (2015, January). *The European offshore wind industry – key trends and statistics 2014* (1st ed.). Retrieved from EWEA website: http://www.ewea.org/fileadmin/files/library/publications/statistics/EWEA-European-Offshore-Statistics-2014.pdf

[5] Wikipedia [Online], http://en.wikipedia.org/wiki/Wind_turbine_design [Accessed 11 10 2012].

[6] Malhotra, S. (2011). *Selection, design and construction of offshore wind turbine foundations*: INTECH Open Access Publisher. Det Norske Veritas and Wind Energy Department, R. N. L. (2002). "Guidelines for Design of Wind Turbines." 394.

[7] DNV-OS-C101(2004). Design of Offshore Steel Structures, General (LRFD Method): Det Norske Veritas

[8] Veritas, N. (2007, April). *Environmental conditions and environmental loads*. Det Norske Veritas.

[9] Bhattacharya, S., Nikitas, N., Garnsey, J., Alexander, N., Cox, J., Lombardi, D., . . . Nash, D. (2013). Observed dynamic soil–structure interaction in scale testing of offshore wind turbine foundations. *Soil Dynamics and Earthquake Engineering, 54*, 47-60.

[10] Williams, A. (2011, May 3). *A Buoyant Future for Floating Wind Turbines?* Retrieved from http://www.renewableenergyworld.com/rea/news/article/2011/05/a-buoyant-future-for-floating-wind-turbines

[11] ORECCA. (2011). *WP3 Technologies stat of the art* (Final version). Retrieved from ORECCA website: http://www.orecca.eu/c/document_library/get_file?uuid=144f87d6-c41a-4a04-8742-7ebdc88f5a5c&groupId=10129

[12] Chandrasekaran, S., & Jain, A. K. (2002). Triangular Configuration Tension Leg Platform behaviour under random sea wave loads. *Ocean Engineering, 29*(15), 1895-1928. doi: http://dx.doi.org/10.1016/S0029-8018(01)00111-1

[13] Butterfield, C. P., Musial, W., Jonkman, J., Sclavounos, P., & Wayman, L. (2007). *Engineering challenges for floating offshore wind turbines*: National Renewable Energy Laboratory Golden, CO, USA.

[14] Cichon, M. (2011, June 21). *DeepCwind tirelessly developing floting offshore wind.* Retrieved from http://www.renewableenergyworld.com/rea/news/article/2011/06/deepcwind-project-tirelessly-developing-floating-offshore-wind

[15] Sclavounos, P., Lee, S., DiPietro, J., Potenza, G., Caramuscio, P., & De Michele, G. (2010). *Floating offshore wind turbines: tension leg platform and taught leg buoy concepts supporting 3-5 MW wind turbines.* Paper presented at the European wind energy conference EWEC.
[16] Di Emidio, G. (2014). *Offshore foundations.* Ugent, laboratory of geotechnics.
[17] Vryhof anchors. (2010). *Anchor Manual 2010 – The Guide to Anchoring.* (4rd ed.). Yssel, The Netherlands. Retrieved from http://www.vryhof.com/anchor_manual.pdf
[18] Gomes, P. (2014). *Offshore Foundations: Technologies, Design and Application.* [Thesis]. Technico Lisboa, Civil Engineering.
[19] Gaudin, C., O'loughlin, C., Randolph, M., & Lowmass, A. (2006). Influence of the installation process on the performance of suction embedded plate anchors. *Géotechnique, 56*(6), 381-391.
[20] Richardson, M. D. (2008). *Dynamically installed anchors for floating offshore structures.* PhD Thesis, The University of Western Australia.
[21] Musial, W., Butterfield, S., & Boone, A. (2004). Feasibility of floating platform systems for wind turbines. Paper presented at the 23rd ASME Wind Energy Symposium, Reno, NV.
[22] O'Loughlin, C., Randolph, M., & Richardson, M. (2004). *Experimental and theoretical studies of deep penetrating anchors.* Paper presented at the Offshore Technology Conference.
[23] Raie, M. S. (2009). A computational procedure for simulation of torpedo anchor installation, set-up and pull-out.
[24] Reese, L. C., & Van Impe, W. F. (2000). Single piles and pile groups under lateral loading: CRC Press.
[25] Helwany, S. (2007). Applied soil mechanics with ABAQUS applications: John Wiley & Sons.
[26] Veritas, N. (2005, october). *Geotechnical design and installation of suction anchors in clay*. Det Norske Veritas.
[27] Danson, E. (2005). Geotechnical & geophysical investigations for offshore and nearshore developments.
[28] Manual Abaqus 6.14
[29] STROMBLAD, N. Modelling of Soil and Structure Interaction Subsea.
[30] Bowles, J. E. (1988). Foundation analysis and design.
[31] Fleming, K., Weltman, A., Randolph, M., & Elson, K. (2008). Piling engineering: CRC press.
[32] Broms, B. B. (1964). Lateral resistance of pile in cohesive soils.
[33] Minik, D. (2010). [Master thesis] Finite Element Analysis of Compact Reinforced Compsite substructure to a bucket foundation and offshore wind turbines.
[34] Chin, F. (1972). *The inverse slope as a prediction of ultimate bearing capacity of piles.* Paper presented at the Proceedings of the 3rd southeast Asian conference on soil engineering, Hong Kong.
[35] Randolph, M., & Gourvenec, S. (2011). *Offshore geotechnical engineering:* CRC Press.
[36] Spagnoli, G., &Weixler, L. (2013). *Drilling technologies for offshore foundation engineering.* Paper presented at the ASME 2013 32nd international conference on ocean, offshore and arctic engineering.
[37] Vinckier, D.(2013). Geotechniek I [syllabus]. University of Ghent, Construction department.
[38] Poulos, H. G., & Davis, E. H. (1980). Pile foundation analysis and design.
[39] *Soil elastic Young's modulus.* (2013) Retrieved from http://www.geotechdata.info/parameter/soil-young's-modulus.html

[40] Randolph, M., Cassidy, M., Gouvenec, S., & Erbrich, C. (2005). *Challenges of offshore geotechnical engineering.* Paper presented at the Proceedings of the international Conference on Soil Mechanics and Geotechnical Engineering.

[41] Achmus, M., &Thieken, K. (2010). On the behaviour of piles in non-cohesive soil under combined horizontal and vertical loading. *Acta Geotechnica,* 5(3), 199-210.

[42] Pacific Marine Group. (2015) *Installation of grouted screw mooring system.*Retreived from http://www.pacificmarinegroup.com

[43] DNV-OS-J101(2011). Design of Offshore Wind Turbine Structures, General (LRFD Method): Det Norske Veritas

[44] Jirásek, M., & Bazant, Z.P. (2002). *Inelastic analysis of structures.* John Wiley & Sons.

[45] Yanguas Miñambres, Ó. (2012). Assessment of current offshore wind support structures concepts: challenges and technological requirements by 2020.

[46] Bond, A., & Harris, A. (2008). *Decoding Eurocode 7*. CRC Press.

Appendix

A. Ultimate bearing capacity: axially loaded pile anchor

A.1 Compression

A.1.1 Pile base resistance

Soil Model 1: constant cohesion

The first model with the Tresca failure criterion has a constant cohesion of 60 kPa. As explained in Chapter 3.3.1.1 the pile base resistance will be nine times the cohesion.

$$q_u = 9\ c_u = 9\ s_u$$

$$P_{pu} = A_p\ q_u$$

The values of the pile base resistance are the same for every L/D-ratio since the pile base resistance is independent of the length of the pile.

L/D-ratio 10:

$q_u = 9\ c = 9\ s_u = 9 * 60\text{kPa} = 540\ \text{kPa}$

$P_{pu} = A_p\ q_u = \frac{\pi * D^2}{4} * q_u = \frac{\pi * (1m)^2}{4} * 540\ \text{kPa} = 424\ \text{kN}$

L/D-ratio 20: $P_{pu} = 424\ \text{kN}$

L/D-ratio 40: $P_{pu} = 424\ \text{kN}$

Soil model 2: varying cohesion

Model 2 has a cohesion increasing with the depth, Table 13. The following equation will be used to calculate the pile base resistance:

$$q_u = 9\ c = 9\ s_u$$

$$P_{pu} = A_p\ q_u$$

The applied cohesion in the equation is the cohesion beneath the pile point.

L/D-ratio 10:

$q_u = 9\ c = 9\ s_u = 9 * 23.75\text{kPa} = 214\ \text{kPa}$

$P_{pu} = A_p\ q_u = \frac{\pi * D^2}{4} * q_u = \frac{\pi * (1m)^2}{4} * 213.75\ \text{kPa} = 168\ \text{kN}$

L/D-ratio 20:

$q_u = 9\ c = 9\ s_u = 9 * 38.75\text{kPa} = 349\ \text{kPa}$

$P_{pu} = A_p\ q_u = \frac{\pi * D^2}{4} * q_u = \frac{\pi * (1m)^2}{4} * 213.75\ \text{kPa} = 274\ \text{kN}$

L/D-ratio 40:

$q_u = 9\ c = 9\ s_u = 9 * 68.75\ kPa = 619\ kPa$

$P_{pu} = A_p\ q_u = \frac{\pi * D^2}{4} * q_u = \frac{\pi * (1m)^2}{4} * 213.75\ kPa = 486\ kN$

A.1.2 Shaft resistance

Soil Model 1: constant cohesion

In the Tresca model, the soil strength is described by the undrained shear strength, s_u or c_u. The general equation to calculate the shaft resistance is equation 3.7.

$$\tau = s_u = c_u$$

$$P_{si} = \sum(P * (\Delta L) * f_s) = \sum(P * (\Delta L) * s_u)$$

L/D-ratio 10:

$P_{si} = \sum(P * (\Delta L) * f_s) = \pi * 1m * 10m * 60\ kPa = 1884.96\ kN$

L/D-ratio 20:

$P_{si} = \sum(P * (\Delta L) * f_s) = \pi * 1m * 20m * 60\ kPa = 3769.91\ kN$

L/D-ratio 40:

$P_{si} = \sum(P * (\Delta L) * f_s) = \pi * 1m * 40m * 60\ kPa = 7539.82\ kN$

Soil Model 2: varying cohesion

For these models, the same equation is used. However, the cohesion is not constant anymore, so the unit skin friction will be different every five meter, Table 13.

$$P_{si} = \sum(P * (\Delta L) * f_s) = \sum(P * (\Delta L) * s_u)$$

L/D-ratio 10:

$P_{si} = \sum(P * (\Delta L) * f_s) = \pi * 1m * 5m * 8.75kPa + \pi * 1m * 5m * 16.25kPa = 392.70\ kN$

L/D-ratio 20:

$P_{si} = \sum(P * (\Delta L) * f_s) = \pi * 1m * 5m * 8.75kPa + \pi * 1m * 5m * 16.25kPa + \pi * 1m * 5m * 23.75kPa + \pi * 1m * 5m * 31.25kPa = 1256.64\ kN$

L/D-ratio 40:

$P_{si} = \sum(P * (\Delta L) * f_s) = \pi * 1m * 5m * 8.75kPa + \pi * 1m * 5m * 16.25kPa + \pi * 1m * 5m * 23.75kPa + \pi * 1m * 5m * 31.25kPa + \pi * 1m * 5m * 38.75kPa + \pi * 1m * 5m * 46.25kPa + \pi * 1m * 5m * 53.75kPa + \pi * 1m * 5m * 61.25kPa = 4398.23\ kN$

A.1.3 Total compression resistance

Soil Model 1

The following equation gives the total compression resistance:

$$P_u = P_{pu} + P_{si}$$

L/D-ratio 10:

$P_u = P_{pu} + P_{si}$ = 424.12 kN + 1884.96 kN = 2309.08kN

L/D-ratio 20:

$P_u = P_{pu} + P_{si}$ = 424.12 kN + 3769.91 kN = 4194.03kN

L/D-ratio 40:

$P_u = P_{pu} + P_{si}$ = 424.12 kN + 7539.82 kN = 7963.94kN

Soil Model 2

For the varying cohesion the same equation is used:

L/D-ratio 10:

$P_u = P_{pu} + P_{si}$ = 167.88 kN + 392.70 kN = 560.58 kN

L/D-ratio 20:

$P_u = P_{pu} + P_{si}$ = 273.91 kN + 1256.64 kN = 1530.55 kN

L/D-ratio 40:

$P_u = P_{pu} + P_{si}$ = 485.97 kN + 4398.23 kN = 4884.20 kN

A.2 Tension

A.2.1 Shaft resistance

See Chapter A.1.2 of this Appendix

A.2.2 Weight of the pile

As the model used in this study was purely cohesive (strength independent of confining stress), it was not necessary to define an initial stress field nor apply gravity body forces, and thus the pile has no weight. Since the weight of the pile is included in the ultimate tension resistance, the weight will be calculated with equation 3.11.

$$W_P = \rho * \pi * r^2 * L * g$$

L/D-ratio 10:

$W_P = \rho * \pi * r^2 * L * g$ = 1458 kg/m³ * π * (0.5m)² * 10m * 9.81 = 112,34 kN

L/D-ratio 20:

$W_P = \rho * \pi * r^2 * L * g = 1458\ kg/m^3 * \pi * (0.5m)^2 * 20m * 9.81 = 224{,}67\ kN$

L/D-ratio 40:

$W_P = \rho * \pi * r^2 * L * g = 1458\ kg/m^3 * \pi * (0.5m)^2 * 40m * 9.81 = 449{,}34\ kN$

A.2.3 Total bearing capacity

The total bearing capacity is given by:

$$T_u = W_p + P_{si}$$

The results obtained from Abaqus include only the shaft resistance. So they should be equal to the results given in Chapter A.1.2 shaft bearing capacity.
Below, there are the theoretical results.

Soil Model 1:

L/D-ratio 10:

$T_u = W_p + P_{si} = 112.34\ kN + 1884.96\ kN = 1997.30\ kN$

L/D-ratio 20:

$T_u = W_p + P_{si} = 224.67\ kN + 3769.91\ kN = 3994.58\ kN$

L/D-ratio 40:

$T_u = W_p + P_{si} = 449.34\ kN + 7539.82\ kN = 7989.16\ kN$

Soil Model 2:

L/D-ratio 10:

$T_u = W_p + P_{si} = 112.36\ kN + 392.7\ kN = 505.06\ kN$

L/D-ratio 20:

$T_u = W_p + P_{si} = 224.67\ kN + 1256.64\ kN = 1481.31\ kN$

L/D-ratio 40:

$T_u = W_p + P_{si} = 449.34\ kN + 4398.23\ kN = 4847.57\ kN$

B.Ultimate static bearing capacity: lateral loaded pile anchor

B.1 Winkler method

The classic Winkler equation determines if the piles with length 10 m, 20 m and 40 m has to be considered as a rigid, semi-flexible or long pile. More information about this method is in Chapter 3.3.2.4 of the thesis. Firstly, the reaction modulus of soil, k will be calculated by equation 3.14 for both the soil with constant k and for soil with increasing k with the depth. After, the λL-parameter will be determined by equation 3.15 for model 1 and the ηL- parameter will be calculated with equation 3.16.

B.1.1 Soil Model 1

For L/D-ratio 10:

$$k = 0.65 \sqrt[12]{\frac{E\,B^4}{E_p I_p}} * \frac{E}{(1-\nu^2)} = \sqrt[4]{\frac{40 * 1^4}{1.55 * 10^9}} * \frac{40}{(1-0.2^2)} = 19.97\text{MPa}$$

$$\lambda L = \sqrt[4]{\frac{k\,L^4}{4E_p I_p}} = \sqrt[4]{\frac{19.97 * 10^4}{4 * 1.55 * 10^9}} = 2.38$$

For L/D-ratio 20:

$$\lambda L = \sqrt[4]{\frac{k\,L^4}{4E_p I_p}} = \sqrt[4]{\frac{19.97 * 20^4}{4 * 1.55 * 10^9}} = 4.76$$

For L/D-ratio 40:

$$\lambda L = \sqrt[4]{\frac{k\,L^4}{4E_p I_p}} = \sqrt[4]{\frac{19.97 * 40^4}{4 * 1.55 * 10^9}} = 9.52$$

The conclusion is that the pile with L/D-ratio 10 can be considered as a semi-flexible pile. In contrast, the piles with a length of 20m and 40m can be considered as long piles.

B.1.2 Soil Model 2

For L/D-ratio 10, the following values are calculated by equation 3.14 and 3.16.

Depth (m)	k (MPa)	n_h(Pa/m)	η (m^{-1})	ηL
2,5	1,82	173507	0,162	1,62
7,5	3,55			

For L/D-ratio 20:

Depth (m)	k (MPa)	n_h (Pa/m)	η (m^{-1})	ηL
2,5	1,82	539540	0,203	4,07
7,5	3,55			
12,5	5,36			
17,5	7,21			

For L/D-ratio 40:

Depth (m)	k (MPa)	n_h (Pa/m)	η (m^{-1})	ηL
2,5	1,82	1313359	0,243	9,72
7,5	3,55			
12,5	5,36			
17,5	7,21			
22,5	9,10			
27,5	11,03			
32,5	12,98			
37,5	14,95			

The conclusion is that the pile with a length of 10 m has to be considered as a semi-flexible pile. The piles with L/D-ratio 20 and 40 are defined as long, flexible piles.

B.2 Broms method

B.2.1 By equation

The Broms method supposes the following limiting pressure, shear and bending moment for a short free-headed pile in a soil with constant ultimate shear strength:

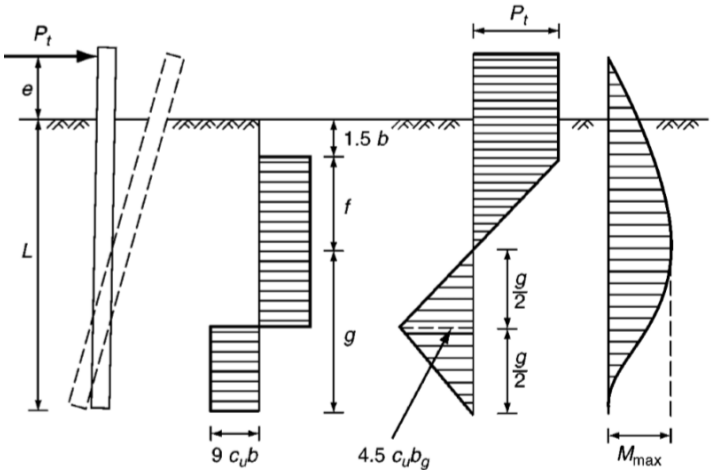

Figure B1 - The soil resistance, the shear and the moment of a short free-headed pile embedded in cohesive soil (Broms method). [11]

To calculate the lateral bearing capacity, the following equation has to be solved:

$$M_{max}^{pos} = \frac{4.5\ cu\ b\ g^2}{2} = P_t\ (e + 1.5b + 0.5f)$$

$$\frac{4.5\ cu\ b\ (L - 1.5b - \frac{Pt}{9\ b\ cu})^2}{2} = P_t\ (e + 1.5b + 0.5\ \frac{Pt}{9\ b\ cu})$$

Firstly the lateral bearing capacity will be calculated for an L/D-ratio 20, the pile will be considered as a short pile. Than the following parameters are needed to solve the equation:

Parameter	value
c_u	60kPa
b	1 m
e	0 m
L	20 m

L/D-ratio 20:

$$\frac{4.5\ cu\ b\ (L - 1.5b - \frac{Pt}{9\ b\ cu})^2}{2} = P_t\ (e + 1.5b + 0.5\ \frac{Pt}{9\ b\ cu})$$

$$\frac{4.5 * 60\ kPa * 1\ m\ (20\ m - 1.5 * 1\ m - \frac{Pt}{9 * 1m * 60kPa})^2}{2} = P_t\ (0\ m + 1.5 * 1\ m + 0.5\ \frac{Pt}{9 * 1m * 60kPa})$$

$$\frac{4.5 * 60\ kPa * 1\ m\ (20\ m - 1.5 * 1\ m - \frac{Pt}{9 * 1m * 60kPa})^2}{2} = P_t\ (0\ m + 1.5 * 1\ m + 0.5\ \frac{Pt}{9 * 1m * 60kPa})$$

$$135\ \ (18.5m - 0.00185\ Pt)^2 = Pt\ (1.5 + 9.259 * 10^{-4}\ Pt)$$

$$0.000463\ Pt^2 + 10.741\ Pt - 46203.75 = 0$$

$$Pt = 3709\ kN$$

L/D-ratio 10: Pt = 1512 kN

L/D-ratio 40: Pt = 8158 kN

The maximum moment is:

L/D-ratio 20:

$$M_{max}^{pos} = P_t\ (e + 1.5b + 0.5f)$$

$$= P_t\ (e + 1.5b + 0.5\ \frac{Pt}{9\ b\ cu})$$

$$= 3708.72kN\ (0\ m + 1.5 * 1\ m + 0.5\ \frac{3708.72kN}{9 * 1m * 60\ kPa})$$

$$= 18299\ kNm$$

L/D-ratio 10: M_{max}^{pos} = 4386 kNm

L/D-ratio 40: M_{max}^{pos} = 73868 kNm

To decide if the pile has to be considered as a short or long pile, the yield moment has to be calculated. Therefore the parameters of the hollow steel pile will be taken into account.

Parameter	value
fy	355MPa
d2	1 m
d1	0.96 m

$$M_\gamma = f_y S_e = f_y \frac{\pi\,(d_2^4 - d_1^4)}{32\,d_2} = 355\text{MPa}\ \frac{\pi\,((1m)^4 - (0.96m)^4)}{32 * 1m} = 5251\ \text{kNm}$$

Since the maximum moment of the short pile for L/D-ratio 10 is smaller than the yield moment of the long pile, the short-pile equation has to be considered. For the L/D-ratios 20 and 40, the long-pile equations count as predicted with the Winkler method.

The Broms method supposes the following limiting pressure, shear and bending moment for a long free-headed pile:

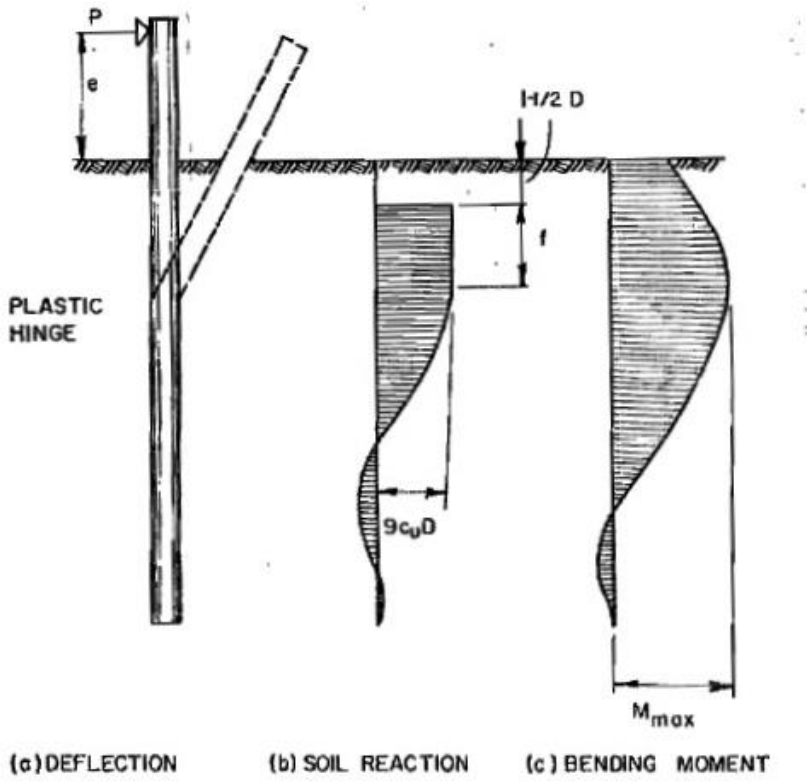

Figure B2 - The deflection, soil reaction and bending moment for long laterally loaded, free-headed piles in cohesive soils (Broms method) [19]

The ultimate lateral load for L/D-ratios 20 and 40 has to be calculated:

$$5250.58\ kNm = P_t\ (\ 0m + 1.5*1\ m + 0.5\ \frac{Pt}{9*1m*60kPa})$$

$$9.259 *10^{-4}\ Pt^2 + 1.5\ Pt - 5250.58 = 0$$

$$Pt = 1705\ kN$$

B.2.2 By graph

The ultimate bearing capacity for short piles can be derived on the following graph:

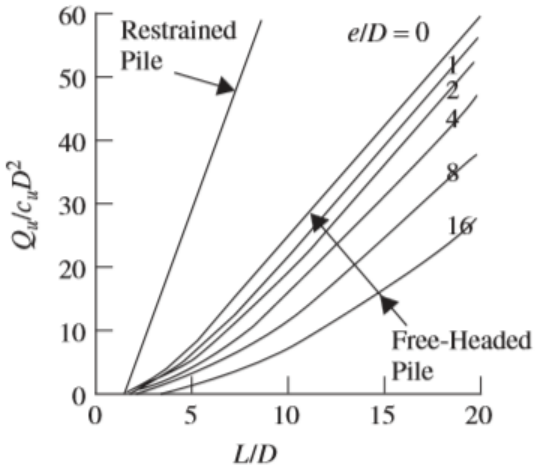

Figure B3 - Broms method solution for free-headed short piles embedded in cohesive soil. [13]

With L/D-ratio 20, e/D-ratio 0 and a free-headed pile, the value for Q_u/c_uD^2 is equal to 60. The limit bearing capacity can be obtained from:

$$\frac{Qu}{cu\ D^2} = 25$$

$$Q_u = 60 * c_u\ D^2 = 25 * 60kPa * (1m)^2 = 1500\ kN$$

The calculated ultimate bearing capacity for short piles was 1513 kN which is close to 1500 kN obtained by the graphs.

For the long piles, the bearing capacity is length-independent and can be derived from the graph beneath:

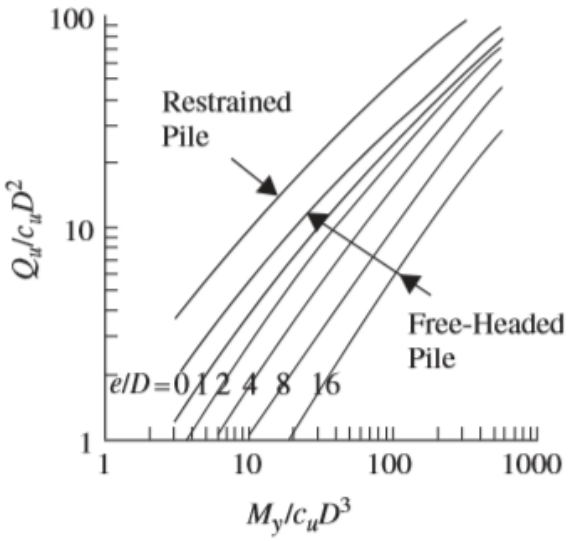

Figure B4 - Broms method solution for free-headed long piles embedded in cohesive soil. [13]

The $M\gamma/c_uD^3$-ratio is equal to:

$$\frac{Mg}{cu\ D^3} = \frac{5250.58\ kNm}{60\ kPa*(1m)^3} = 87.51$$

For e/D-ratio 0 and a free-headed pile, the value for Q_u/c_uD^2 is equal to 60. The limit bearing capacity can be obtained from:

$$\frac{Qu}{cu\ D^2} = 30$$

$$Q_u = 30 * c_u\ D^2 = 30 * 60kPa * (1m)^2 = 1800\ kN$$

The calculated ultimate bearing capacity for long piles was 1705 kN which is close to 1800 kN obtained by the graphs.

B.2.3 Conclusion

If h is the depth with zero deflection, the results obtained by the equations are:

L/D	10	20	40
Type	Short	Long	Long
Bearing capacity	1512 kN	1705 kN	1705 kN
Maximum moment	4386 kNm	5251 kNm	5251 kNm
h	7.15 m	4.66 m	4.66 m

B.3 Modified method

B.3.1 By equations

In the modified method, the profile of the limiting pressure is defined in another way than the profile of the Broms method, Figure 35. The explanation of the method is mentioned in 3.3.2.4. The following parameters have to be applied in the equation:

Parameter	value
cu	60kPa
D	1 m
e	0 m

For a short pile, the following equations have to be considered. The distance h can be smaller than 3D or larger than 3D. In this case, h will be larger than 3D.

The horizontal equilibrium for L/D-ratio 10:

$$H_f - P_{bc} = P_{ab}$$

$$H_f + 9c_u x = 16.5c_u + 9c_u y$$

$$H_f + 9c_u (L-3-y) = 16.5c_u + 9c_u y$$

$$H_f = -46.5\, c_u + 18\, c_u y$$

The moment equilibrium for L/D-ratio 10:

$$H_f (3+y) - 6\, c_u (y+1.5) - 10.5\, c_u (y+1) - 4.5\, c_u y^2 = 4.5\, c_u x^2 = 4.5\, c_u (7-y)^2$$

$$9\, c_u y^2 + 54\, c_u y - 379.5\, c_u = 0$$

$$y = 4.15\text{m}$$

$$x = L-3-y = 2.85\text{m}$$

$$H_f = 1692\ \text{kN}$$

$$M_{max} = 2193\ \text{kNm}$$

For L/D-ratio 20:

$H_f = 3884$ kN

$M_{max} = 9146$ kNm

This moment is larger than the yield moment, so the pile with a length of 20m has to be considered as a long pile. The soil resistance for long piles in a cohesive soil is shown in Figure B5.

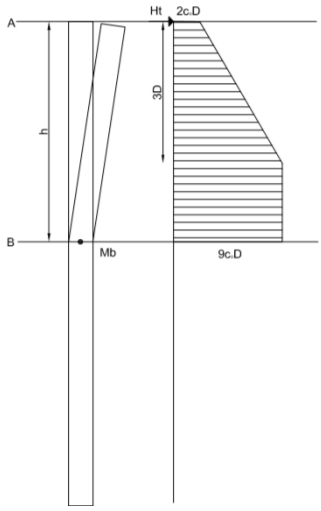

Figure B5 - The deflection and soil reaction for long laterally loaded, free-headed pile in cohesive soils (modified method) [19]

Also for long piles, there has to be considered two different cases. In the first case, h is smaller than 3D and in the second case, h is larger than 3D. For this example, the second option gives the solution.

The horizontal equilibrium is:

$$H_f = 16.5c_u + (h-3) * 9c_u = -10.5c_u + 9hc_u$$

The moment equilibrium is:

$$H_f * h - 6c_u * (h - 1.5) - 10.5c_u\ (h- 2) - \frac{9cu\ (h-3)^2}{2} = M_Y$$

$$(-10.5c_u + 9hc_u) * h - 6c_u * (h - 1.5) - 10.5c_u\ (h- 2) - \frac{9cu\ (h-3)^2}{2} = M_Y$$

$$4.5c_uh^2 - 10.5c_u = 5250.58kNm$$

$$h = 4.67m$$

$$Hf = -10.5c_u + 9hc_u = 1892\ kN$$

B.3.2 Conclusion

The results obtained by the equations are:

L/D	10	20	40
Type	Short	Long	Long
Bearing capacity	1692kN	1891.8kN	1891.8kN
Maximum moment	2193.08 kNm	5250.58 kNm	5250.58 kNm
h	7.15m	4.67m	4.67m

B.4 Conclusion

Comparison of the lateral resistance between Broms method and the modified method:

L/D-ratio	Broms method (kN)	Modified method (kN)
10	1512	1692
20	1705	1892
40	1705	1892